



## ATLAS Note

GROUP-2017-XX

15th March 2021



1

# 2 WZ + Heavy Flavor Production in pp collisions 3 at $\sqrt{s} = 13$ TeV

4

The ATLAS Collaboration

5

A measurement of WZ produced with an associated heavy flavor jet is performed using 140  
6  $\text{fb}^{-1}$  of proton-proton collision data at  $\sqrt{s} = 13$  TeV from the ATLAS experiment at the  
7 LHC. The measurement is performed in the fully leptonic decay mode,  $\text{WZ} \rightarrow \ell\bar{\nu}\ell\bar{\nu}$ . The  
8 cross-section of  $\text{WZ} + b\text{-jets}$  is measured to be  $X \pm X \pm X$ , while the cross-section of  $\text{WZ} +$   
9 charm is measured as  $X$ , with a correlation of  $X$  between the two processes.

10

© 2021 CERN for the benefit of the ATLAS Collaboration.

Reproduction of this article or parts of it is allowed as specified in the CC-BY-4.0 license.

# 11 Contents

12	<b>1 Changes and outstanding items</b>	<b>4</b>
13	1.1 Changelog	4
14	1.1.1 Changes relative to v5	4
15	1.1.2 Changes relative to v4	4
16	1.1.3 Changes relative to v3	4
17	1.1.4 Changes relative to v2	5
18	1.1.5 Changes relative to v1	5
19	1.2 Outstanding Items	6
20	<b>2 Executive Summary</b>	<b>7</b>
21	<b>3 Data and Monte Carlo Samples</b>	<b>8</b>
22	3.1 Data Samples	8
23	3.2 Monte Carlo Samples	9
24	<b>4 Object Reconstruction</b>	<b>10</b>
25	4.1 Trigger	10
26	4.2 Light leptons	11
27	4.3 Jets	12
28	4.4 B-tagged Jets	12
29	4.5 Missing transverse energy	13
30	<b>5 Event Selection and Signal Region Definitions</b>	<b>13</b>
31	5.1 Event Preselection	13
32	5.2 Fit Regions	16
33	5.3 Non-Prompt Lepton Estimation	31
34	5.3.1 $t\bar{t}$ Validation	31
35	5.3.2 Z+jets Validation	35
36	<b>6 tZ Separation Multivariate Analysis</b>	<b>39</b>
37	6.1 Top Mass Reconstruction	40
38	6.2 tZ BDT	40
39	<b>7 Systematic Uncertainties</b>	<b>44</b>
40	<b>8 Results</b>	<b>51</b>
41	8.1 1-jet Results	53
42	8.2 2-jet Results	58
43	<b>9 Conclusion</b>	<b>63</b>

44	<b>Appendices</b>	<b>66</b>
45	.1 tZ Interference Studies	66
46	.2 Alternate tZ Inclusive Fit	70
47	.3 DSID list	74

48 **List of contributions**

49

50 **1 Changes and outstanding items**

51 **1.1 Changelog**

52 This is version 6

53 **1.1.1 Changes relative to v5**

- 54 • added list of DSIDs to an appendix  
55 • included systematics on jet migrations  
56 • Updated results section to include simultaneous fit over 1-jet and 2-jet bins, describe  
57 unfolding procedure  
58 • Updated other sections to account for this change

59 **1.1.2 Changes relative to v4**

- 60 • Fixed various typos, clarified wording  
61 • Expanded info about JER uncertainties, electron systematics, theory uncertainties  
62 • removed a table on lepton selection, included information in the text instead  
63 • Plotted lepton Pt Z and W for Zjet CR, rather than lep 1 and 2  
64 • fixed binning in kinematic plots  
65 • Included prefit and postfit yield tables  
66 • added signal modelling systematics  
67 • included alternate fit studies with tZ included in signal

68 **1.1.3 Changes relative to v3**

- 69 • Merged introduction into executive summary, including unblinding details and list of  
70 SRs/CRs used  
71 • listed ptag used (p4133), and release (AB 21.2.127)  
72 • Included table reftab:xsecUnc listing x-sec uncertainties used  
73 • Removed selection criteria listed in table ?? (QMisID, AmbiguityType) that were removed  
74 from the analysis

- 75     • specified variable used to make truth jet flavor determination (HadronConeExclTruthLa-  
 76       belID)
- 77     • fixed bug in MtLepMet calculation, updated selection/fits to account for this
- 78     • Included plots of MtLepMet and PtZ, swapped lep 1 and 2  $p_T$  plots for lep W and lep Z  
 79       plots
- 80     • updated tZ BDT training to reduce overfitting, updated plots to include error bars, feature  
 81       importance
- 82     • updated table 7 to clarify selection, fix the tZ\_BDT cut used
- 83     • replace a few broken ntuples which included large weight events
- 84     • include DL1r distribution for Z+jets and  $t\bar{t}$  VRs
- 85     • Expanded section on fakes, included information on derived scale factors from VRs.
- 86     • Changed the kinematic plots to include  $p_T(Z)$  and  $m_T(W)$ , list lepton  $p_T$  based on W and  
 87       Z candidates.

88 **1.1.4 Changes relative to v2**

- 89     • Added alternate VBS samples to include missing b-jet diagrams
- 90     • Included a section on tZ interference effects, ??.
- 91     • Updated to reflect changes for 2018, including the move to PFlow jets, DL1r, updated  
 92       trigger, and updated AnalysisBase version (now 21.2.127)
- 93     • Revised fit regions, using separate 1-jet and 2-jet fits, with all 2-j regions included
- 94     • updated plots for tZ BDT, added details about the model
- 95     • Included truth jet information

96 **1.1.5 Changes relative to v1**

- 97     • Added GRL list
- 98     • Fixed latex issue in line 92, typo in line 172
- 99     • Added tables 5 and ??, summarizing the event and object selection
- 100     • Added table 2, which includes the DSID of samples used
- 101     • Included reference to WZ inclusive paper in introduction

102 **1.2 Outstanding Items**

- 103     • Complete interference studies, apply any interference effects observed as a systematic  
104     • Update results section with additional studies, possibly including:  
105         – Truth jet migration studies  
106         – Simultaneous fit over 1j and 2j  
107         – Impact of allowing tZ to float  
108     • Unblind, update plots and fits to include data  
109     • Add cross-section, significance once unblinded

## 110 2 Executive Summary

111 The production of  $WZ$  in association with a heavy flavor jet represents an important background  
 112 for many major analyses. This includes any process with leptons and b-jets in the final state,  
 113 such as  $t\bar{t}H$ ,  $t\bar{t}W$ , and  $t\bar{t}Z$ . While precise measurements have been made of  $WZ$  production  
 114 [1],  $WZ +$  heavy flavor remains poorly understood. This is largely because the QCD processes  
 115 involved in the production of the b-jet make it difficult to simulate accurately. This introduces a  
 116 large uncertainty for analyses that include this process as a background.

117 Motivated by its relevance to the  $t\bar{t}H$  multilepton analysis, we perform a study of the fully  
 118 leptonic decay mode of this channel; that is, events where both the W and Z decay leptonically.  
 119 Because  $WZ$  has no associated jets at leading order, while the major backgrounds for this channel  
 120 tend to have high jet multiplicity, events with more than two jets are rejected. This gives a final  
 121 state signature of three leptons and one or two jets.

122 Events that meet this selection criteria are sorted into pseudo-continuous b-tagging regions based  
 123 on the DL1r b-tag score of their associated jets. This is done to separate  $WZ +$  b-jet events from  
 124  $WZ +$  charm and  $WZ +$  light jets. These regions are fit to data in order make a more accurate  
 125 estimate of the contribution of  $WZ +$  heavy-flavor, where heavy-flavor jets include b-jets and  
 126 charm jets. The full Run-2 dataset collected by the ATLAS detector, representing  $139 \text{ fb}^{-1}$  of  
 127 data from pp collisions at  $\sqrt{s} = 13 \text{ TeV}$ , is used for this study.

128 All backgrounds are accounted for using Monte Carlo, with the simulation of non-prompt lepton  
 129 backgrounds -  $Z+jets$  and  $t\bar{t}$  - validated using non-prompt Validation Regions.

130 Section 3 details the data and Monte Carlo (MC) samples used in the analysis. The reconstruction  
 131 of various physics objects is described in section 4. Section 5 describes the event selection applied  
 132 to these samples, along the definitions of the various regions used in the fit. The multivariate  
 133 analysis techniques used to separate the  $tZ$  background from  $WZ +$  heavy flavor are described in  
 134 section 6. Section 7 describes the various sources of systematic uncertainties considered in the  
 135 fit. Finally, the results of the analysis are summarized in section 8, followed by a brief conclusion  
 136 in section 9.

137 The analysis aims to report a cross-section measurement of  $WZ+b$  and  $WZ+charm$ , along with  
 138 their correlations, for both 1-jet and 2-jet exclusive regions. The proposed fiducial region for  
 139 these measurements includes events with three leptons, where the invariant mass of at least one  
 140 opposite charge, same flavor lepton pair falls within  $10 \text{ GeV}$  of  $91.2 \text{ GeV}$ , with 1 or 2 associated  
 141 jets. An alternate version of the measurement is included in the appendix, which considers  $tZ$  as  
 142 part of the  $WZ+b$  signal.

143 The current state of the analysis shows blinded results for the full Run 2 dataset. Regions  
 144 containing  $>5\%$   $WZ+b$  events are blinded, and results are from Asimov, MC only fits. Expected  
 145 significance and cross-section numbers are reported.

---

### <sup>146</sup> 3 Data and Monte Carlo Samples

<sup>147</sup> Both data and Monte Carlo samples used in this analysis were prepared in the `xAOD` format,  
<sup>148</sup> which was used to produce a `DxAOD` sample in the `HIGG8D1` derivation framework. The `HIGG8D1`  
<sup>149</sup> framework is designed for the  $t\bar{t}H$  multi-lepton analysis, which targets events with multiple  
<sup>150</sup> leptons as well as tau hadrons. This framework skims the dataset to remove unneeded variables  
<sup>151</sup> as well as entire events. Events are removed from the derivations that do not meet the following  
<sup>152</sup> selection:

- <sup>153</sup> • at least two light leptons within a range  $|\eta| < 2.6$ , with leading lepton  $p_T > 15$  GeV and  
<sup>154</sup> subleading lepton  $p_T > 5$  GeV
- <sup>155</sup> • at least one light lepton with  $p_T > 15$  GeV within a range  $|\eta| < 2.6$ , and at least two hadronic  
<sup>156</sup> taus with  $p_T > 15$  GeV.

<sup>157</sup> Samples were then generated from these `HIGG8D1` derivations with p-tag of p4134 using Ana-  
<sup>158</sup> lysisBase version 21.2.127 modified to include custom variables..

#### <sup>159</sup> 3.1 Data Samples

<sup>160</sup> The study uses a sample of proton-proton collision data collected by the ATLAS detector from  
<sup>161</sup> 2015 through 2018 at an energy of  $\sqrt{s} = 13$  TeV, which represents an integrated luminosity of  
<sup>162</sup>  $139 \text{ fb}^{-1}$ . This data set was collected with a bunch crossing rate of 25 ns. All data used in this  
<sup>163</sup> analysis was verified by data quality checks, having been included in the following Good Run  
<sup>164</sup> Lists:

- <sup>165</sup> • `data15_13TeV.periodAllYear_DetStatus-v79-repro20-02_DQDefects-00-02-02`  
<sup>166</sup>   `_PHYS_StandardGRL_All_Good_25ns.xml`
- <sup>167</sup> • `data16_13TeV.periodAllYear_DetStatus-v88-pro20-21_DQDefects-00-02-04`  
<sup>168</sup>   `_PHYS_StandardGRL_All_Good_25ns.xml`
- <sup>169</sup> • `data17_13TeV.periodAllYear_DetStatus-v97-pro21-13_Unknown_PHYS_StandardGRL`  
<sup>170</sup>   `_All_Good_25ns_Triggerno17e33prim.xml`
- <sup>171</sup> • `data18_13TeV.periodAllYear_DetStatus-v102-pro22-04_Unknown_PHYS_StandardGRL`  
<sup>172</sup>   `_All_Good_25ns_Triggerno17e33prim.xml`

<sup>173</sup> Runs included from the AllYear period containers are included.

---

### <sup>174</sup> 3.2 Monte Carlo Samples

<sup>175</sup> Several different generators were used to produce Monte Carlo simulations of the signal and  
<sup>176</sup> background processes. For all samples, the response of the ATLAS detector is simulated using  
<sup>177</sup> Geant4. The WZ signal samples are simulated using Sherpa 2.2.2 [2]. Specific information  
<sup>178</sup> about the Monte Carlo samples being used can be found in Table 1. A list of the specific samples  
<sup>179</sup> used by data set ID is shown in Table 2.

Table 1: The configurations used for event generation of signal and background processes, including the event generator, matrix element (ME) order, parton shower algorithm, and parton distribution function (PDF).

Process	Event generator	ME order	Parton Shower	PDF
WZ, VV	SHERPA 2.2.2	MEPS NLO	SHERPA	CT10
tZ	MG5_AMC	LO	PYTHIA 6	CTEQ6L1
t̄tW	MG5_AMC (SHERPA 2.1.1)	NLO (LO multileg)	PYTHIA 8 (SHERPA)	NNPDF 3.0 NLO (NNPDF 3.0 NLO)
t̄t(Z/γ* → ll)	MG5_AMC	NLO	PYTHIA 8	NNPDF 3.0 NLO
t̄tH	MG5_AMC (MG5_AMC)	NLO (NLO)	PYTHIA 8 (HERWIG++)	NNPDF 3.0 NLO [3] (CT10 [4])
tHqb	MG5_AMC	LO	PYTHIA 8	CT10
tHW	MG5_AMC (SHERPA 2.1.1)	NLO (LO multileg)	HERWIG++ (SHERPA)	CT10 (NNPDF 3.0 NLO)
tWZ	MG5_AMC	NLO	PYTHIA 8	NNPDF 2.3 LO
t̄t̄t, t̄t̄t̄t̄	MG5_AMC	LO	PYTHIA 8	NNPDF 2.3 LO
t̄tW+W-	MG5_AMC	LO	PYTHIA 8	NNPDF 2.3 LO
t̄t	POWHEG-BOX v2 [5]	NLO	PYTHIA 8	NNPDF 3.0 NLO
t̄t̄γ	MG5_AMC	LO	PYTHIA 8	NNPDF 2.3 LO
s-, t-channel, Wt single top	POWHEG-BOX v1 [6]	NLO	PYTHIA 6	CT10
qqVV, VVV				
Z → l+l-	SHERPA 2.2.1	MEPS NLO	SHERPA	NNPDF 3.0 NLO

Sample	DSID
WZ	364253, 364739-42
VV	364250, 364254, 364255, 363355-60, 364890
t̄W	410155
t̄Z	410156, 410157, 410218-20
low mass t̄Z	410276-8
Rare Top	410397, 410398, 410399
single Top	410658-9, 410644-5
three Top	304014
four Top	410080
t̄WW	410081
Z + jets	364100-41
low mass Z + jets	364198-215
W + jets	364156-97
Vγ	364500-35
tZ	410560
tW	410013-4
WtZ	410408
VVV	364242-9
VH	342284-5
WtH	341998
t̄tγ	410389
t̄t	410470
t̄tH	345873-5, 346343-5

Table 2: List of Monte Carlo samples by data set ID used in the analysis.

## 180 4 Object Reconstruction

181 All regions defined in this analysis share a common lepton, jet, and overall event preselection.  
 182 The selection applied to each physics object is detailed here; the event preselection, and the  
 183 selection used to define the various fit regions, is described in Section 5.

### 184 4.1 Trigger

185 Events are required to be selected by dilepton triggers, as summarized in Table 3.

Dilepton triggers (2015)	
$\mu\mu$ (asymm.)	HLT_mu18_mu8noL1
$ee$ (symm.)	HLT_2e12_lhloose_L12EM10VH
$e\mu, \mu e$ ( $\sim$ symm.)	HLT_e17_lhloose_mu14
Dilepton triggers (2016)	
$\mu\mu$ (asymm.)	HLT_mu22_mu8noL1
$ee$ (symm.)	HLT_2e17_lhvloose_nod0
$e\mu, \mu e$ ( $\sim$ symm.)	HLT_e17_lhloose_nod0_mu14
Dilepton triggers (2017)	
$\mu\mu$ (asymm.)	HLT_mu22_mu8noL1
$ee$ (symm.)	HLT_2e24_lhvloose_nod0
$e\mu, \mu e$ ( $\sim$ symm.)	HLT_e17_lhloose_nod0_mu14
Dilepton triggers (2018)	
$\mu\mu$ (asymm.)	HLT_mu22_mu8noL1
$ee$ (symm.)	HLT_2e24_lhvloose_nod0
$e\mu, \mu e$ ( $\sim$ symm.)	HLT_e17_lhloose_nod0_mu14

Table 3: List of lowest  $p_T$ -threshold, un-prescaled dilepton triggers used for 2015-2018 data taking.186 **4.2 Light leptons**

- 187 Electron candidates are reconstructed from energy clusters in the electromagnetic calorimeter  
 188 that are associated with charged particle tracks reconstructed in the inner detector [7]. Electron  
 189 candidates are required to have  $p_T > 10$  GeV and  $|\eta_{\text{cluster}}| < 2.47$ . Muon candidates are  
 190 reconstructed by combining inner detector tracks with track segments or full tracks in the muon  
 191 spectrometer [8]. Muon candidates are required to have  $p_T > 10$  GeV and  $|\eta| < 2.5$ . Candidates  
 192 in the transition region between different electromagnetic calorimeter components,  $1.37 <$   
 193  $|\eta_{\text{cluster}}| < 1.52$ , are rejected. A multivariate likelihood discriminant combining shower shape  
 194 and track information is used to distinguish real electrons from hadronic showers (fake electrons).  
 195 To further reduce the non-prompt electron contribution, the track is required to be consistent  
 196 with originating from the primary vertex; requirements are imposed on the transverse impact  
 197 parameter significance ( $|d_0|/\sigma_{d_0} < 5$ ) and the longitudinal impact parameter ( $|\Delta z_0 \sin \theta_\ell| < 0.5$   
 198 mm).
- 199 Muon candidates are reconstructed by combining inner detector tracks with track segments or  
 200 full tracks in the muon spectrometer [8]. Muon candidates are required to have  $p_T > 10$  GeV  
 201 and  $|\eta| < 2.5$ . The longitudinal impact parameter is the same for both electrons and muons, while  
 202 muons are required to pass a slightly tighter transverse impact parameter,  $|d_0|/\sigma_{d_0} < 3$ .

203 All leptons are required to be isolated, as defined through the standard `isolationFixedCutLoose`  
 204 working point supported by combined performance groups. Leptons are additionally required to  
 205 pass a non-prompt BDT selection described in detail in [9]. Optimized working points and scale  
 206 factors for this BDT are taken from that analysis.

207 **4.3 Jets**

208 Jets are reconstructed from calibrated topological clusters built from energy deposits in the  
 209 calorimeters [10], using the anti- $k_t$  algorithm with a radius parameter  $R = 0.4$ . Jets with energy  
 210 contributions likely arising from noise or detector effects are removed from consideration [11],  
 211 and only jets satisfying  $p_T > 25$  GeV and  $|\eta| < 2.5$  are used in this analysis. For jets with  
 212  $p_T < 60$  GeV and  $|\eta| < 2.4$ , a jet-track association algorithm is used to confirm that the jet  
 213 originates from the selected primary vertex, in order to reject jets arising from pileup collisions  
 214 [12].

215 **4.4 B-tagged Jets**

216 In order to make a measurement of  $WZ +$  heavy flavor it is necessary to distinguish these events  
 217 from  $WZ +$  light jets. For this purpose, the DL1r b-tagging algorithm is used to distinguish  
 218 heavy flavor jets from lighter ones. The DL1r algorithm uses jet kinematics, particularly jet  
 219 vertex information, as input for a neural network which assigns each jet a score designed to  
 220 reflect how likely that jet is to have originated from a b-quark.

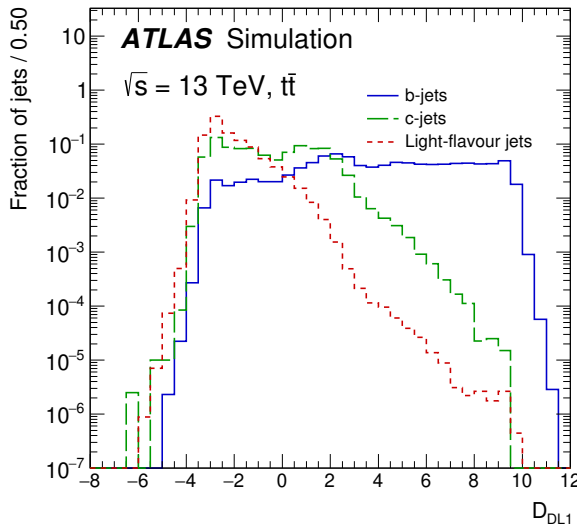


Figure 1: Output distribution of the DL1r algorithm for b-jets, charm jets, and light jets

221 From the output of the BDT, working points (WPs) are developed based on the efficiency of truth  
 222 b-jets at particular values of the DL1r algorithm. The working points used in this analysis are  
 223 summarized in Table 4.

WP	none	loose	medium	tight	tightest
b eff.	-	85%	77%	70%	60%

Table 4: B-tagging Working Points by tightness and b-jet efficiency

224 A tighter WP will accept fewer b-jets, but reject a higher fraction of charm and light jets.  
 225 Generally, analyses that include b-jets will use a fixed working point, for example, requiring that  
 226 a jet pass the 70% threshold. By instead treating these working point as bins, e.g. events with  
 227 jets that fall between the 85% and 77% WPs fall into one bin, while events with jets passing the  
 228 60% WP fall into another, and looking at the full psuedo-continuous DL1r spectrum of the jets,  
 229 additional information can be gained. The psuedo-continuous b-tag spectrum is used in this case  
 230 to separate out WZ + b, WZ + charm, and WZ + light.

#### 231 4.5 Missing transverse energy

232 Missing transverse momentum ( $E_T^{\text{miss}}$ ) is used as part of the event selection. The missing  
 233 transverse momentum vector is defined as the inverse of the sum of the transverse momenta of  
 234 all reconstructed physics objects as well as remaining unclustered energy, the latter of which is  
 235 estimated from low- $p_T$  tracks associated with the primary vertex but not assigned to a hard object,  
 236 with object definitions taken from [13]. Light leptons considered in the  $E_T^{\text{miss}}$  reconstruction are  
 237 required to have  $p_T > 10 \text{ GeV}$ , while jets are required to have  $p_T > 20 \text{ GeV}$ .

### 238 5 Event Selection and Signal Region Definitions

239 Event are required to pass a preselection described in Section 5.1 and summarized in Table 5.  
 240 Those that pass this preselection are divided into various fit regions described in Section 5.2,  
 241 based on the number of jets in the event, and the b-tag score of those jets.

#### 242 5.1 Event Preselection

243 Events are required to include exactly three reconstructed light leptons passing the requirement  
 244 described in 4.2, which have a total charge of  $\pm 1$ . As the opposite sign lepton is found to be  
 245 prompt the vast majority of the time [9], it is required to be loose and isolated, as defined though  
 246 the standard `isolationFixedCutLoose` working point supported by combined performance

247 groups. The same sign leptons are required to be very tightly isolated, as per the recommended  
 248 `isolationFixedCutTight`.

249 The leptons are ordered in the analysis code as 0, 1, and 2. Lepton 0 is the lepton whose charge  
 250 is opposite the other two. Lepton 1 is the lepton closest to the opposite charge lepton, i.e. the  
 251 smallest  $\Delta R$ , leaving lepton 2 as the lepton further from the opposite charge lepton. Lepton 0  
 252 is required to have  $p_T > 10$  GeV, while the same sign leptons, 1 and 2, are required to have  
 253  $p_T > 20$  GeV to reduce the contribution of non-prompt leptons.

254 The invariant mass of at least one pair of opposite sign, same flavor leptons is required to fall  
 255 within 10 GeV of the mass of the Z boson, 91.2 GeV. Events where one of the opposite sign pairs  
 256 have an invariant mass less than 12 GeV are rejected in order to suppress low mass resonances.

257 An additional requirement is placed on the missing transverse energy,  $E_T^{\text{miss}} > 20$  GeV, and the  
 258 transverse mass of the W candidate,  $m(E_T^{\text{miss}} + l_{\text{other}}) > 30$  GeV, where  $E_T^{\text{miss}}$  is the missing  
 259 transverse energy, and  $l_{\text{other}}$  is the lepton not included in the Z-candidate.

260 Events are required to have one or two reconstructed jets passing the selection described in  
 261 Section 4.3. Events with more than two jets are rejected in order to reduce the contribution of  
 262 backgrounds such as  $t\bar{t}Z$  and  $t\bar{t}W$ , which tend to have higher jet multiplicity.

Event Selection
Exactly three leptons with charge $\pm 1$
Two tight Iso, tight ID same-charge leptons with $p_T > 20$ GeV
One loose Iso, medium ID opposite charge lepton with $p_T > 10$ GeV
$m(l^+l^-)$ within 10 GeV of 91.2 GeV
Transverse mass of W-candidate, $m_T(E_T^{\text{miss}} + \text{lep}_{\text{other}}) > 30$ GeV
Missing transverse energy, $E_T^{\text{miss}} > 20$ GeV
One or two jets with $p_T > 25$ GeV

Table 5: Summary of the selection applied to events for inclusion in the fit

263 The event yields in the preselection region for both data and Monte Carlo are summarized in  
 264 Table 5.1, which shows good agreement between data and Monte Carlo, and demonstrates that  
 265 this region consists primarily of WZ events. The WZ events are split into WZ + b, WZ + c, and  
 266 WZ + l based on the truth flavor of the associated jet in the event. Specifically, this determination  
 267 is made based on the `HadronConeExclTruthLabelID` of the jet, as recommended by the b-  
 268 tagging working group [14]. In this ordering b-jet supersedes charm, which supersedes light. That  
 269 is, WZ + l events contain no charm and no b jets at truth level, WZ + c contain at least one truth  
 270 charm and no b-jets, and WZ + b contains at least one truth b-jet.

Process	Events
WZ + b	$167.6 \pm 6.5$
WZ + c	$1080 \pm 40$
WZ + l	$7220 \pm 310$
Other VV	$850 \pm 140$
t̄tW	$16.8 \pm 2.3$
t̄tZ	$115 \pm 17$
rare Top	$2.2 \pm 0.1$
Single top	$0.10 \pm 0.45$
Three top	$0.01 \pm 0.01$
Four top	$0.02 \pm 0.01$
t̄tWW	$0.23 \pm 0.05$
Z + jets	$600 \pm 260$
V + $\gamma$	$37 \pm 54$
tZ	$190 \pm 70$
tW	$5.5 \pm 1.2$
WtZ	$25.8 \pm 1.1$
VVV	$26.2 \pm 0.9$
VH	$94 \pm 7$
t̄t	$108.68 \pm 8$
t̄tH	$4.3 \pm 0.5$
Total	$10600 \pm 530$
Data	10574

Table 6: Event yields in the preselection region at  $139.0 \text{ fb}^{-1}$ 

<sup>271</sup> Here Other VV represents diboson processes other than WZ, and consists predominantly of  
<sup>272</sup>  $ZZ \rightarrow ll\bar{l}\bar{l}$  events where one of the leptons is not reconstructed.

<sup>273</sup> Simulations are further validated by comparing the kinematic distributions of the Monte Carlo  
<sup>274</sup> with data, which are shown in Figure 2. Here, bins with 5% or more WZ+b are blinded.

### WZ Fit Region - Inclusive

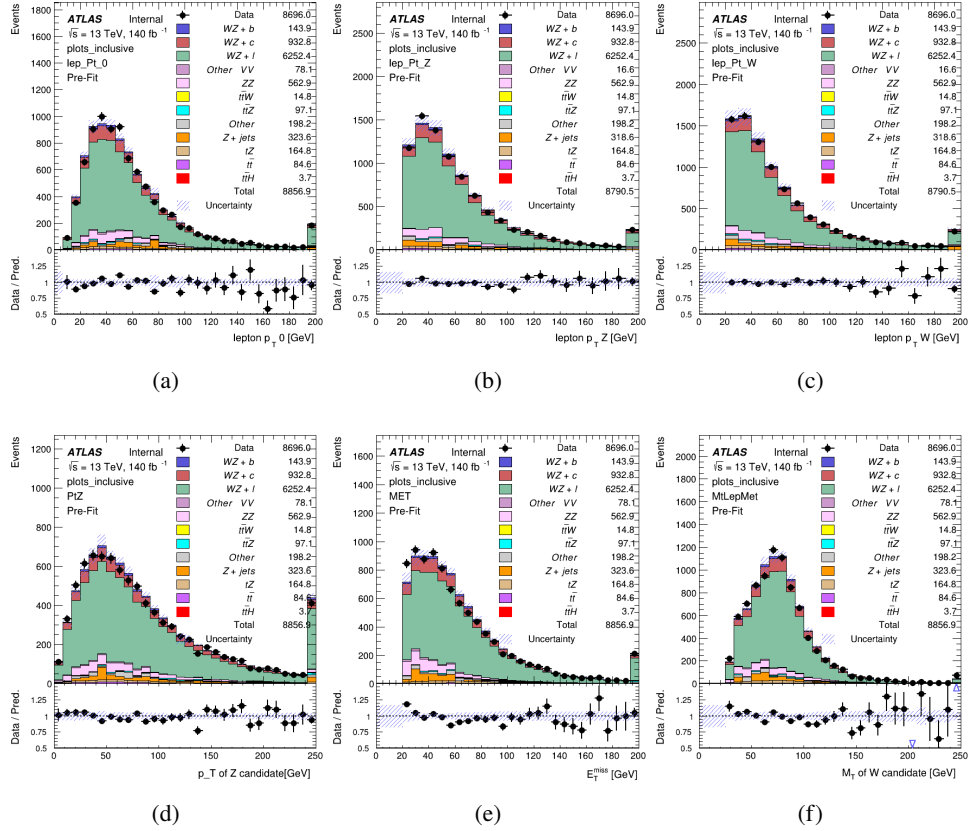


Figure 2: Comparisons between the data and MC distributions in the preselection region for (a) the  $p_T$  of the opposite sign lepton, (b) the  $p_T$  of the other lepton from the Z candidate, (c) the  $p_T$  of the lepton from the W candidate, (d) the  $p_T$  of the Z candidate, (e) the  $E_T^{\text{miss}}$ , and (f) the  $M_T$  of the W candidate.

## 5.2 Fit Regions

Once preselection has been applied, the remaining events are categorized into one of twelve orthogonal regions. The regions used in the fit are summarized in Table 7.

Table 7: A list of the regions used in the fit and the selection used for each.

Region	Selection
1j, <85%	$N_{\text{jets}} = 1, n\text{Jets\_DL1r\_85} = 0$
1j, 85%-77%	$N_{\text{jets}} = 1, n\text{Jets\_DL1r\_85} = 1, n\text{Jets\_DL1r\_77}=0$
1j, 77%-70%	$N_{\text{jets}} = 1, n\text{Jets\_DL1r\_77} = 1, n\text{Jets\_DL1r\_70}=0$
1j, 70%-60%	$N_{\text{jets}} = 1, n\text{Jets\_DL1r\_70} = 1, n\text{Jets\_DL1r\_60}=0$
1j, >60%	$N_{\text{jets}} = 1, n\text{Jets\_DL1r\_60} = 1, tZ \text{ BDT} > 0.725$
1j tZ CR	$N_{\text{jets}} = 1, n\text{Jets\_DL1r\_60} = 1, tZ \text{ BDT} < 0.725$
2j, <85%	$N_{\text{jets}} = 2, n\text{Jets\_DL1r\_85} = 0$
2j, 85%-77%	$N_{\text{jets}} = 2, n\text{Jets\_DL1r\_85} >= 1, n\text{Jets\_DL1r\_77}=0$
2j, 77%-70%	$N_{\text{jets}} = 2, n\text{Jets\_DL1r\_77} >= 1, n\text{Jets\_DL1r\_70}=0$
2j, 70%-60%	$N_{\text{jets}} = 2, n\text{Jets\_DL1r\_70} >= 1, n\text{Jets\_DL1r\_60}=0$
2j, >60%	$N_{\text{jets}} = 2, n\text{Jets\_DL1r\_60} >= 1, tZ \text{ BDT} > 0.725$
2j tZ CR	$N_{\text{jets}} = 2, n\text{Jets\_DL1r\_60} >= 1, tZ \text{ BDT} < 0.725$

278 The working points discussed in Section 4.4 are used to separate events into fit regions based on  
 279 the highest working point reached by a jet in each event. Because the background composition  
 280 differs significantly based on the number of b-jets, events are further subdivided into 1 jet and 2  
 281 jet regions in order to minimize the impact of background uncertainties.

282 An additional tZ control region is created based on the BDT described in Section 6. The region  
 283 with 1-jet passing the 60% working point is split in two - a signal enriched region of events with  
 284 a BDT score greater than 0.03, and a tZ control region including events with less than 0.03. This  
 285 cutoff is arrived at by performing an Asimov fit with a variety of cutoffs, and selecting the value  
 286 that produces the highest significance for the measurement of WZ + b.

287 The modeling in each region is validated by comparing data and MC predictions for various  
 288 kinematic distributions. These plot are shown in Figures 3-16.

## WZ Fit Region - 1j Inclusive

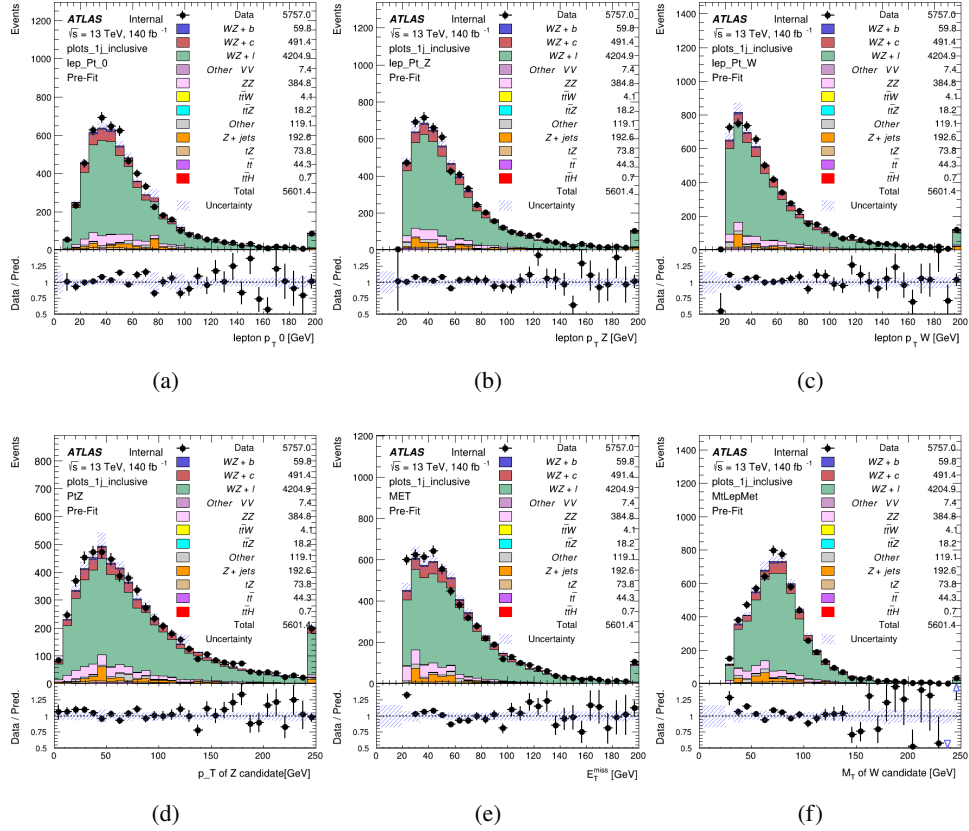


Figure 3: Comparisons between the data and MC distributions in the preselection region for (a) the  $p_T$  of the opposite sign lepton, (b) the  $p_T$  of the other lepton from the Z candidate, (c) the  $p_T$  of the lepton from the W candidate, (d) the  $p_T$  of the Z candidate, (e) the  $E_T^{\text{miss}}$ , and (f) the  $m_T$  of the W candidate.

## WZ Fit Region - 1j &lt; 85% WP

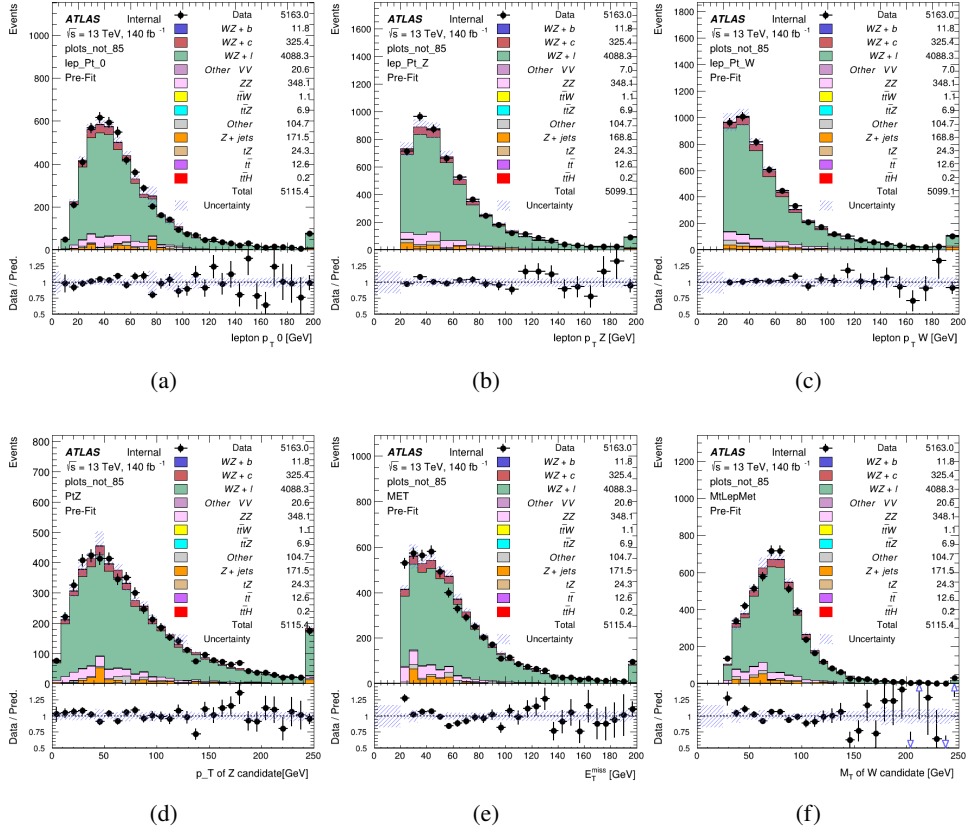


Figure 4: Comparisons between the data and MC distributions in the preselection region for (a) the  $p_T$  of the opposite sign lepton, (b) the  $p_T$  of the other lepton from the  $Z$  candidate, (c) the  $p_T$  of the lepton from the  $W$  candidate, (d) the  $p_T$  of the  $Z$  candidate, (e) the  $E_T^{\text{miss}}$ , and (f) the  $m_T$  of the  $W$  candidate.

## WZ Fit Region - 1j 77-85% WP

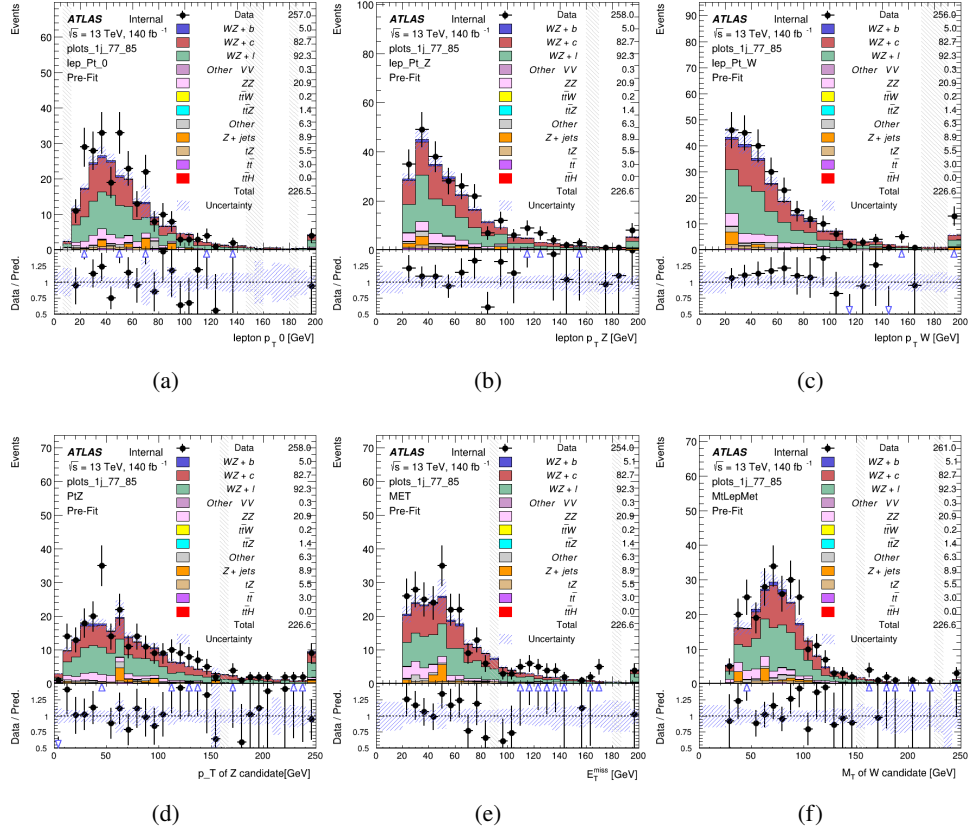


Figure 5: Comparisons between the data and MC distributions in the preselection region for (a) the  $p_T$  of the opposite sign lepton, (b) the  $p_T$  of the other lepton from the Z candidate, (c) the  $p_T$  of the lepton from the W candidate, (d) the  $p_T$  of the Z candidate, (e) the  $E_T^{\text{miss}}$ , and (f) the  $m_T$  of the W candidate.

## WZ Fit Region - 1j 70-77% WP

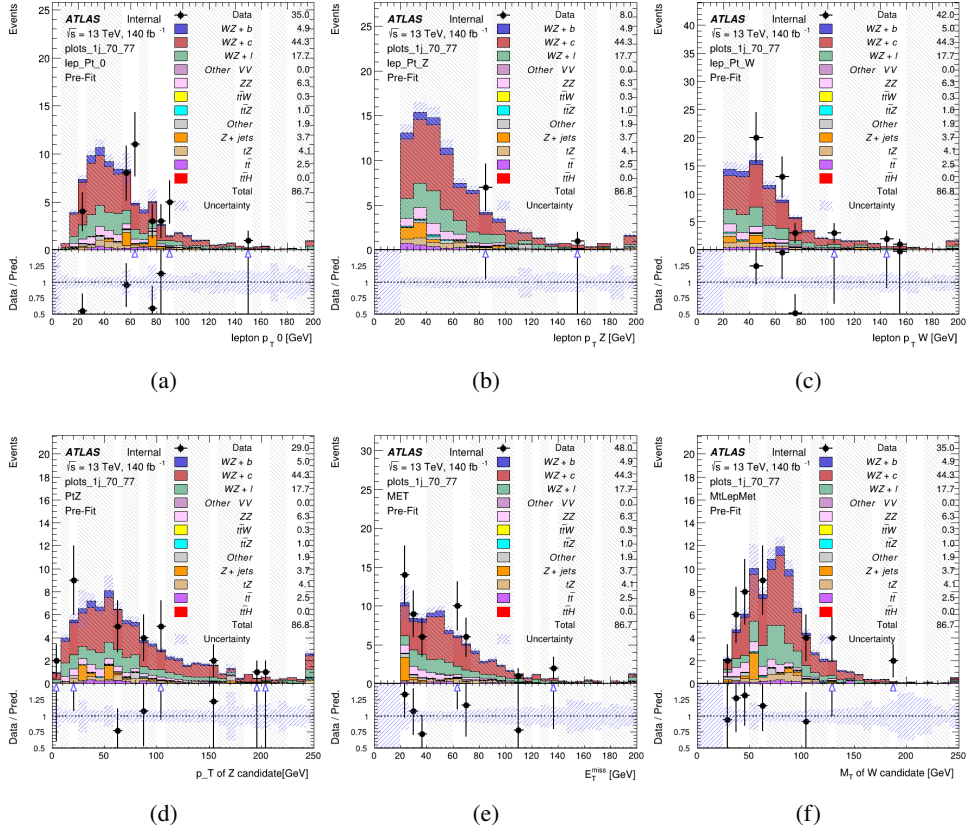


Figure 6: Comparisons between the data and MC distributions in the preselection region for (a) the  $p_T$  of the opposite sign lepton, (b) the  $p_T$  of the other lepton from the  $Z$  candidate, (c) the  $p_T$  of the lepton from the  $W$  candidate, (d) the  $p_T$  of the  $Z$  candidate, (e) the  $E_T^{\text{miss}}$ , and (f) the  $m_T$  of the  $W$  candidate.

## WZ Fit Region - 1j 60-70% WP

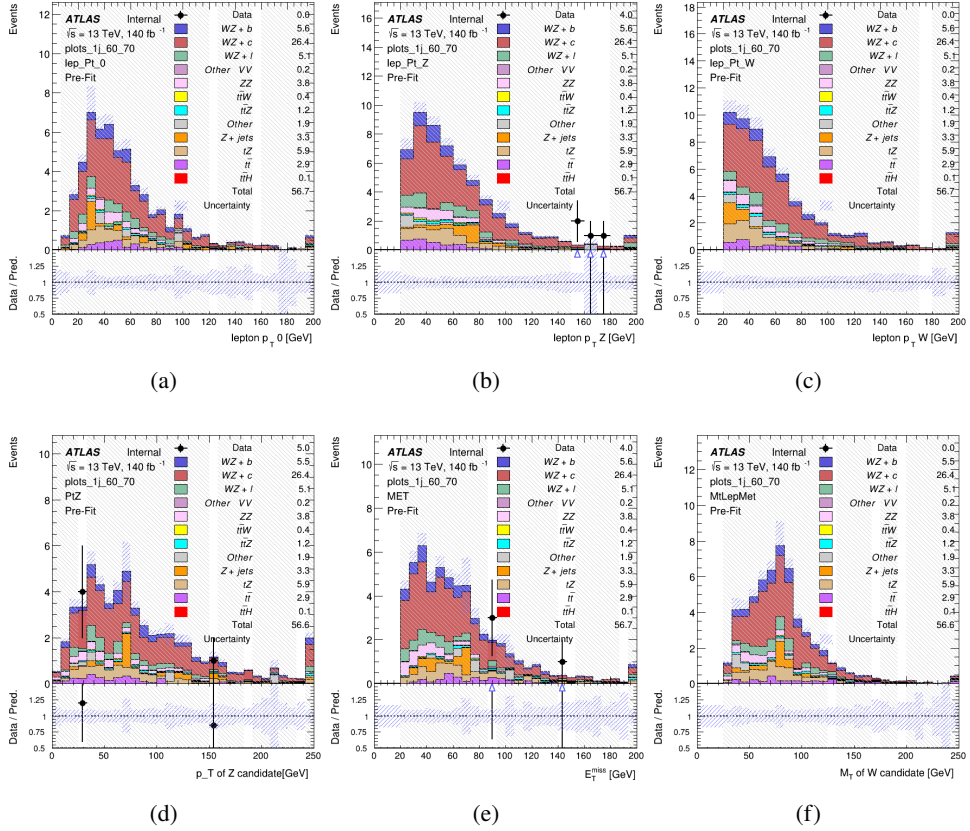


Figure 7: Comparisons between the data and MC distributions in the preselection region for (a) the  $p_T$  of the opposite sign lepton, (b) the  $p_T$  of the other lepton from the  $Z$  candidate, (c) the  $p_T$  of the lepton from the  $W$  candidate, (d) the  $p_T$  of the  $Z$  candidate, (e) the  $E_T^{\text{miss}}$ , and (f) the  $m_T$  of the  $W$  candidate.

## WZ Fit Region - 1j 60% WP

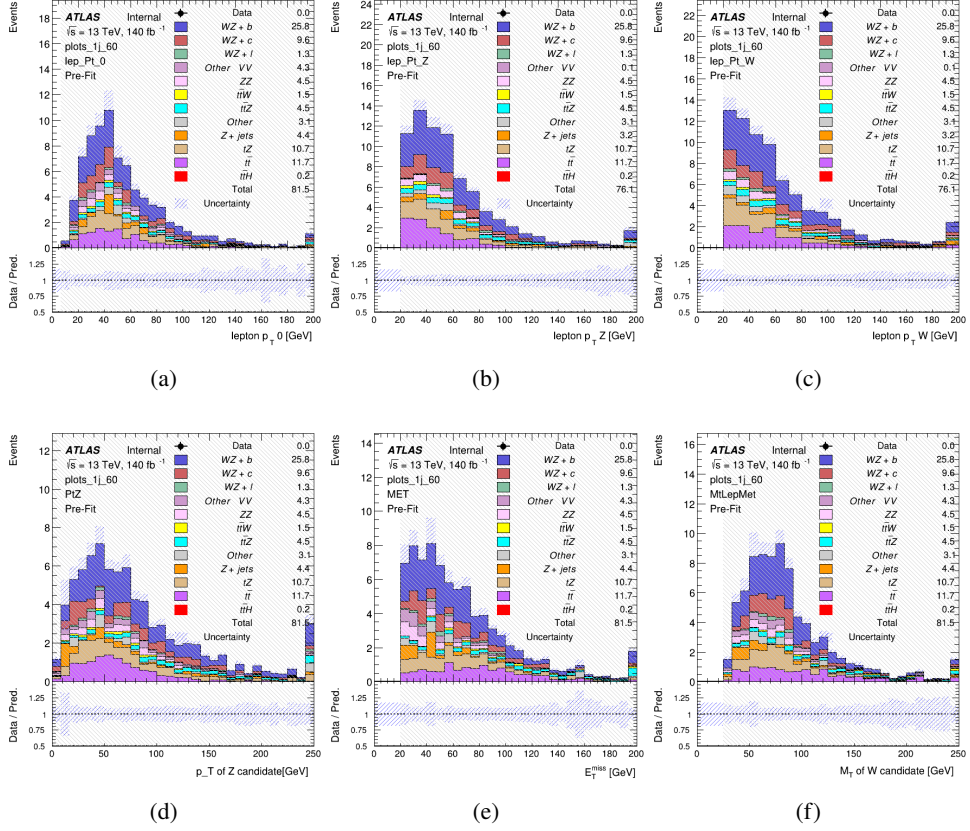


Figure 8: Comparisons between the data and MC distributions in the preselection region for (a) the  $p_T$  of the opposite sign lepton, (b) the  $p_T$  of the other lepton from the Z candidate, (c) the  $p_T$  of the lepton from the W candidate, (d) the  $p_T$  of the Z candidate, (e) the  $E_T^{\text{miss}}$ , and (f) the  $m_T$  of the W candidate.

## WZ Fit Region - tZ-CR

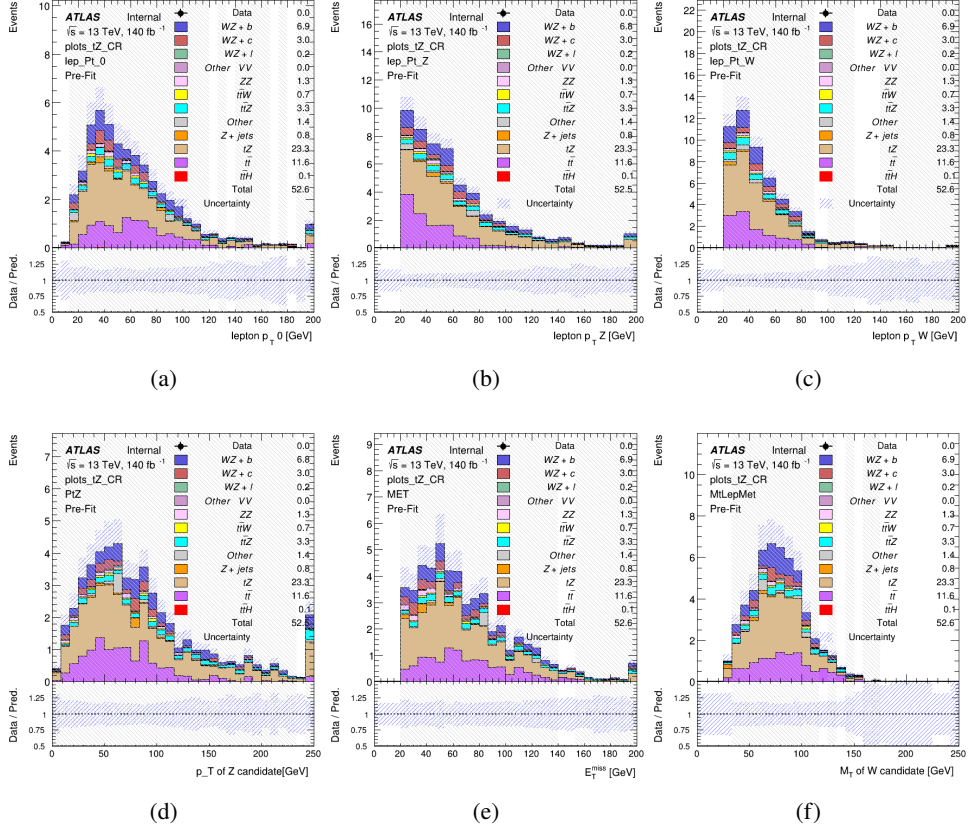


Figure 9: Comparisons between the data and MC distributions in the preselection region for (a) the  $p_T$  of the opposite sign lepton, (b) the  $p_T$  of the other lepton from the Z candidate, (c) the  $p_T$  of the lepton from the W candidate, (d) the  $p_T$  of the Z candidate, (e) the  $E_T^{\text{miss}}$ , and (f) the  $m_T$  of the W candidate.

### WZ Fit Region - 2j Inclusive

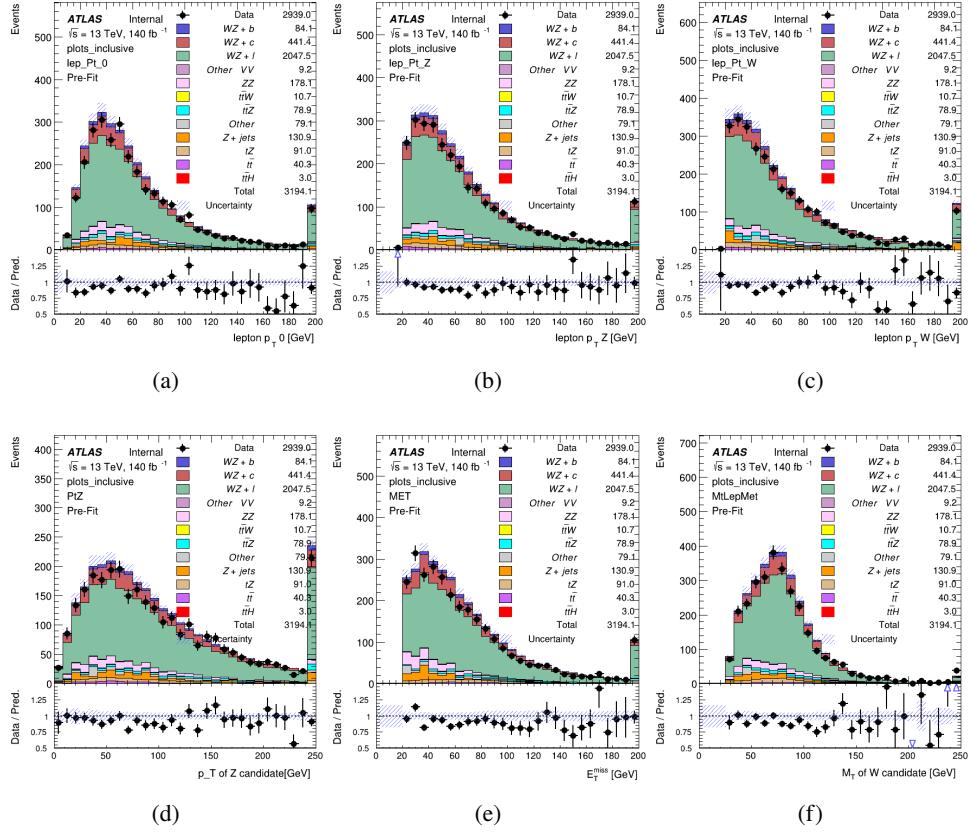


Figure 10: Comparisons between the data and MC distributions in the preselection region for (a) the  $p_T$  of the opposite sign lepton, (b) the  $p_T$  of the other lepton from the Z candidate, (c) the  $p_T$  of the lepton from the W candidate, (d) the  $p_T$  of the Z candidate, (e) the  $E_T^{\text{miss}}$ , and (f) the  $M_T$  of the W candidate.

## WZ Fit Region - 2j &lt; 85% WP

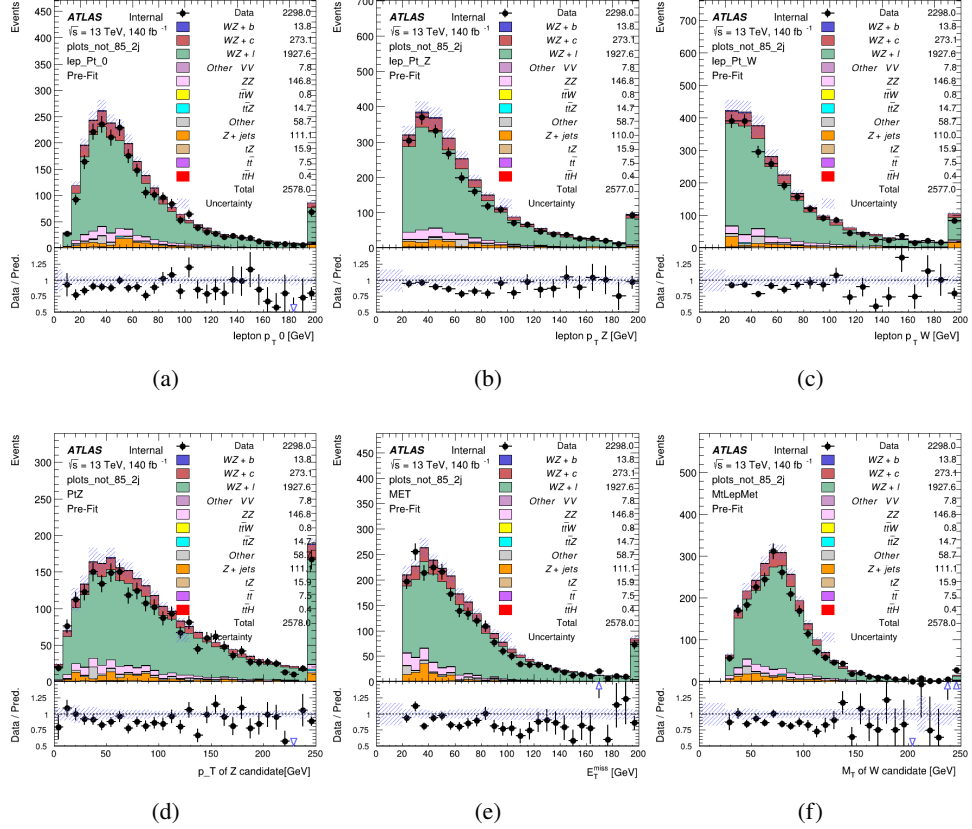


Figure 11: Comparisons between the data and MC distributions in the preselection region for (a) the  $p_T$  of the opposite sign lepton, (b) the  $p_T$  of the other lepton from the Z candidate, (c) the  $p_T$  of the lepton from the W candidate, (d) the  $p_T$  of the Z candidate, (e) the  $E_T^{\text{miss}}$ , and (f) the  $m_T$  of the W candidate.

## WZ Fit Region - 2j 77-85% WP

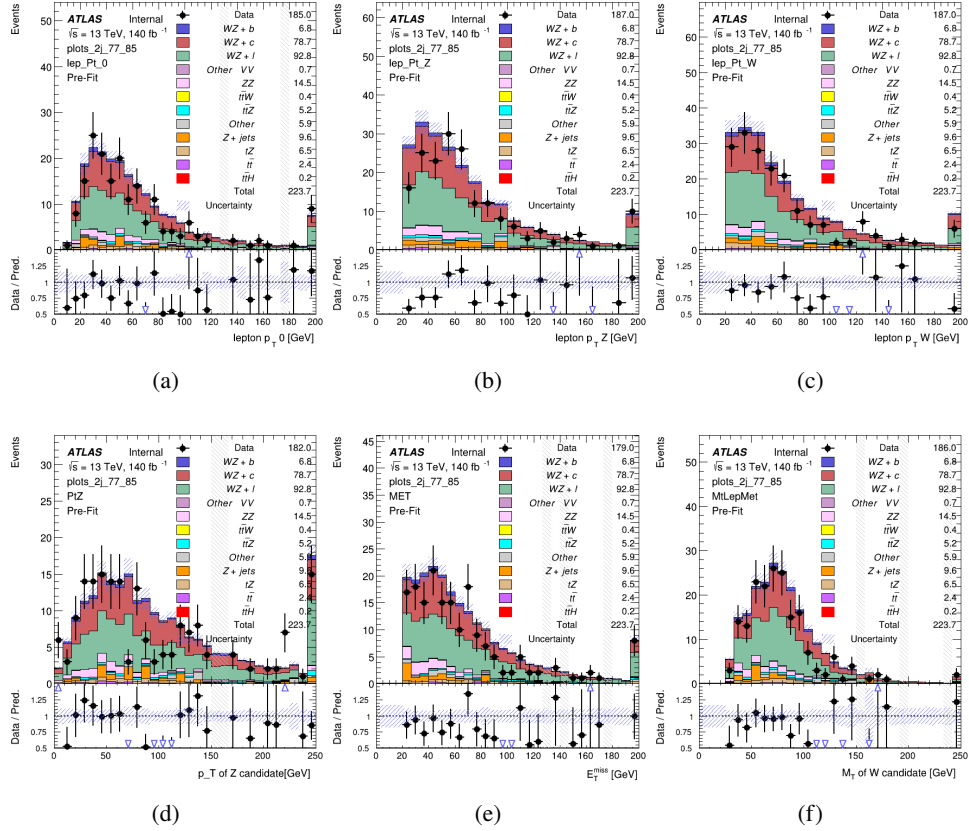


Figure 12: Comparisons between the data and MC distributions in the preselection region for (a) the  $p_T$  of the opposite sign lepton, (b) the  $p_T$  of the other lepton from the Z candidate, (c) the  $p_T$  of the lepton from the W candidate, (d) the  $p_T$  of the Z candidate, (e) the  $E_T^{\text{miss}}$ , and (f) the  $m_T$  of the W candidate.

## WZ Fit Region - 2j 70-77% WP

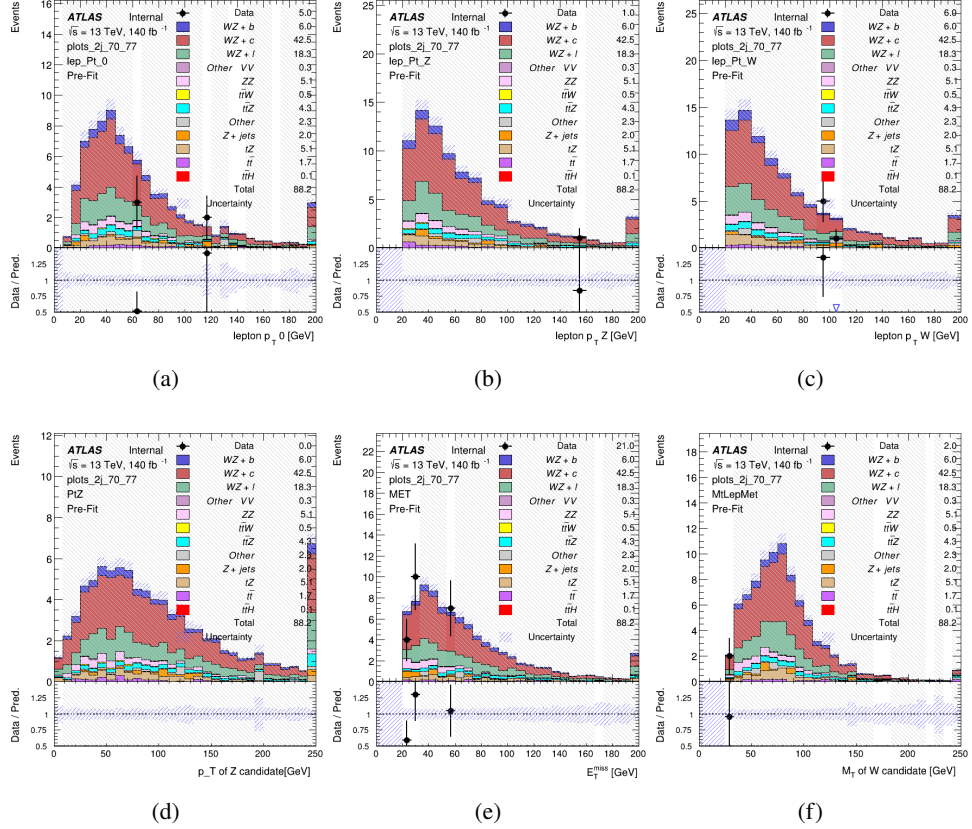


Figure 13: Comparisons between the data and MC distributions in the preselection region for (a) the  $p_T$  of the opposite sign lepton, (b) the  $p_T$  of the other lepton from the Z candidate, (c) the  $p_T$  of the lepton from the W candidate, (d) the  $p_T$  of the Z candidate, (e) the  $E_T^{\text{miss}}$ , and (f) the  $m_T$  of the W candidate.

## WZ Fit Region - 2j 60-70% WP

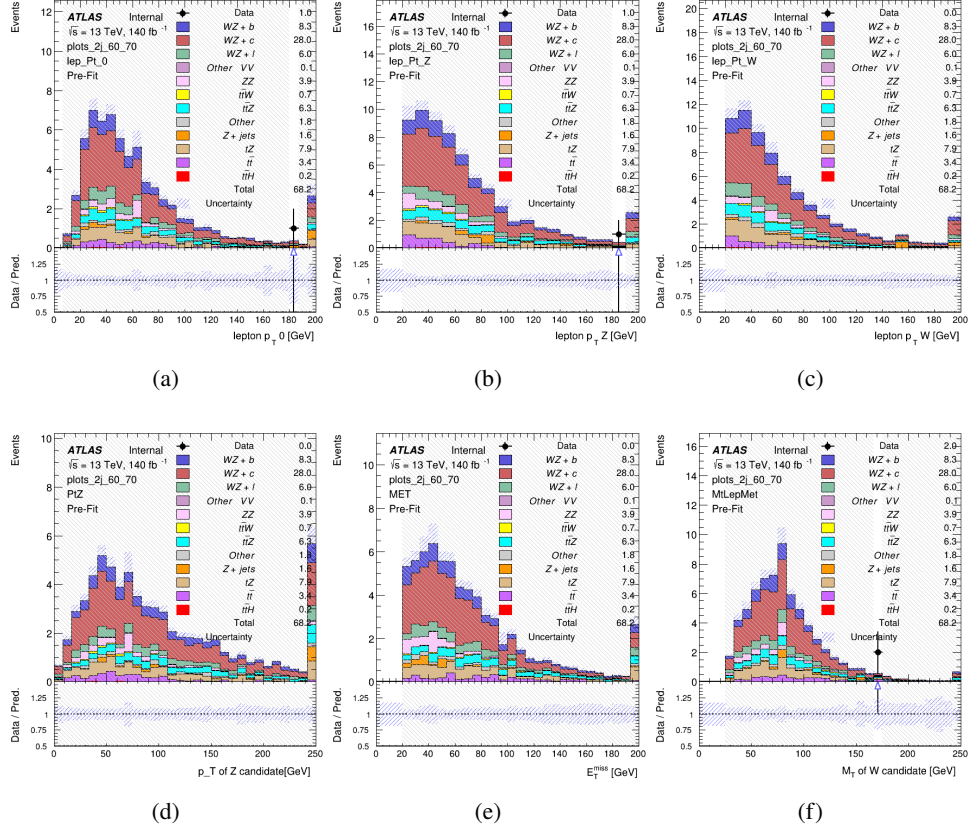


Figure 14: Comparisons between the data and MC distributions in the preselection region for (a) the  $p_T$  of the opposite sign lepton, (b) the  $p_T$  of the other lepton from the Z candidate, (c) the  $p_T$  of the lepton from the W candidate, (d) the  $p_T$  of the Z candidate, (e) the  $E_T^{\text{miss}}$ , and (f) the  $m_T$  of the W candidate.

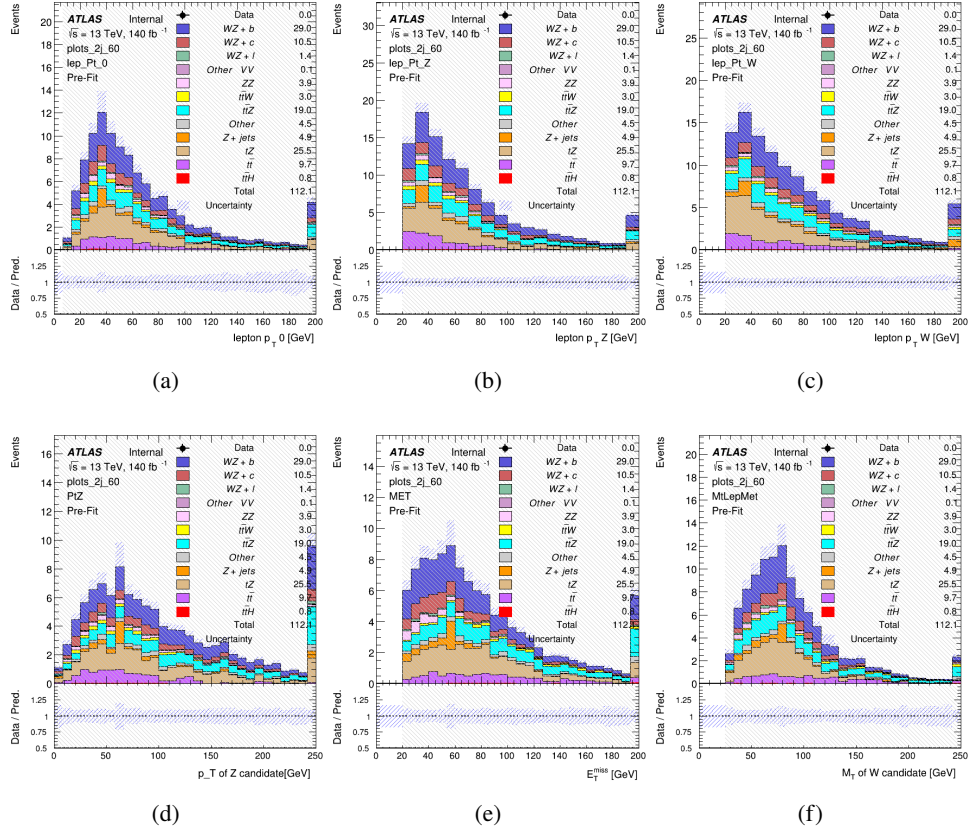
**WZ Fit Region - 2j 60% WP**

Figure 15: Comparisons between the data and MC distributions in the preselection region for (a) the  $p_T$  of the opposite sign lepton, (b) the  $p_T$  of the other lepton from the Z candidate, (c) the  $p_T$  of the lepton from the W candidate, (d) the  $p_T$  of the Z candidate, (e) the  $E_T^{\text{miss}}$ , and (f) the  $m_T$  of the W candidate.

## WZ Fit Region - tZ-CR-2j

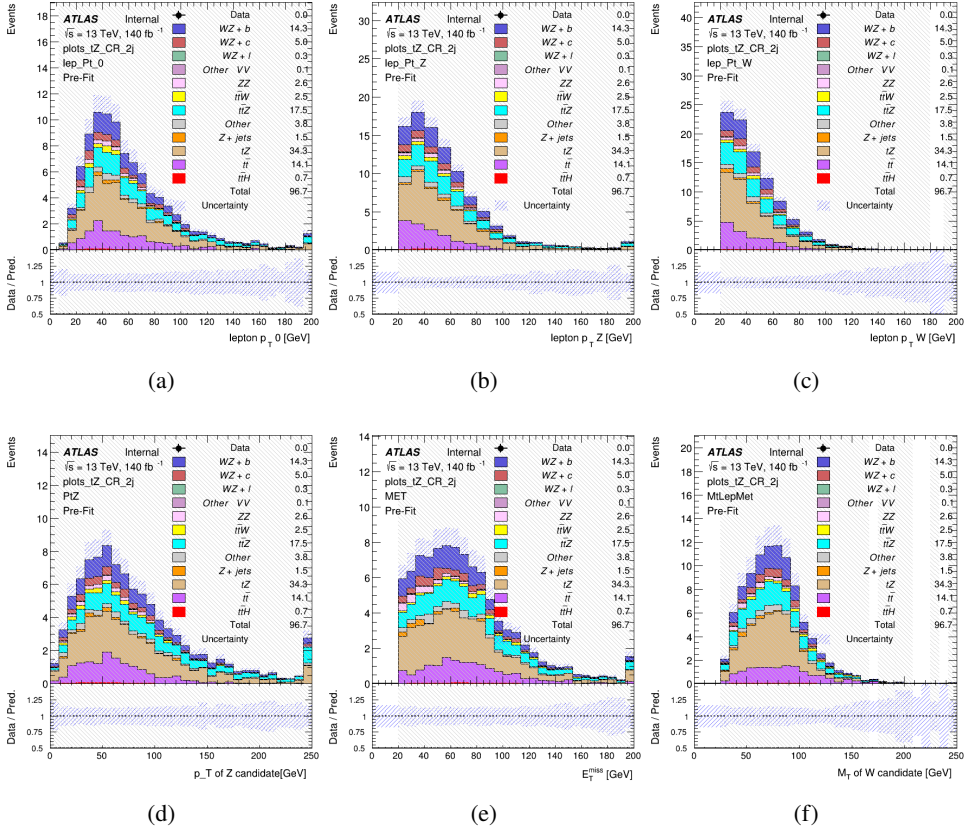


Figure 16: Comparisons between the data and MC distributions in the preselection region for (a) the  $p_T$  of the opposite sign lepton, (b) the  $p_T$  of the other lepton from the  $Z$  candidate, (c) the  $p_T$  of the lepton from the  $W$  candidate, (d) the  $p_T$  of the  $Z$  candidate, (e) the  $E_T^{\text{miss}}$ , and (f) the  $m_T$  of the  $W$  candidate.

### 289 5.3 Non-Prompt Lepton Estimation

290 Two processes act as sources of non-prompt leptons appear in the analysis:  $t\bar{t}$  and  $Z+jet$   
291 production both produce two prompt leptons, and each contribute to the 3l region when an  
292 additional non-prompt lepton appears in the event. The contribution of these processes is  
293 estimated with Monte Carlo simulations, which are validated using enriched validation regions.

#### 294 5.3.1 $t\bar{t}$ Validation

295  $t\bar{t}$  events can produce two prompt leptons from the decay of each of the tops. These top decays  
296 produce two b-quarks, the decay of which can produce additional non-prompt leptons, which  
297 occasionally pass the event preselection. In order to validate that the Monte Carlo accurately

298 simulates this process accurately, the MC prediction in a non-prompt  $t\bar{t}$  enriched validation  
299 region is compared to data.

300 The  $t\bar{t}$  validation region is similar to the preselection region - three leptons meeting the criteria  
301 described in Section 5 are required, and the requirements on  $E_T^{\text{miss}}$  remain the same. However,  
302 the selection requiring a lepton pair form a Z-candidate are reversed. Events where the invariant  
303 mass of any two opposite sign, same flavor leptons falls within 10 GeV of 91.2 GeV are rejected.  
304 This ensures the  $t\bar{t}$  validation region is orthogonal to the preselection region.

305 Further, because the jet multiplicity of  $t\bar{t}$  events tends to be higher than WZ, the number of jets  
306 in each event is required to be greater than 1. As b-jets are almost invariably produced from top  
307 decays, at least one b-tagged jet passing the 70% DL1r WP in each event is required. Various  
308 kinematic plots of this region are shown in Figure 17.

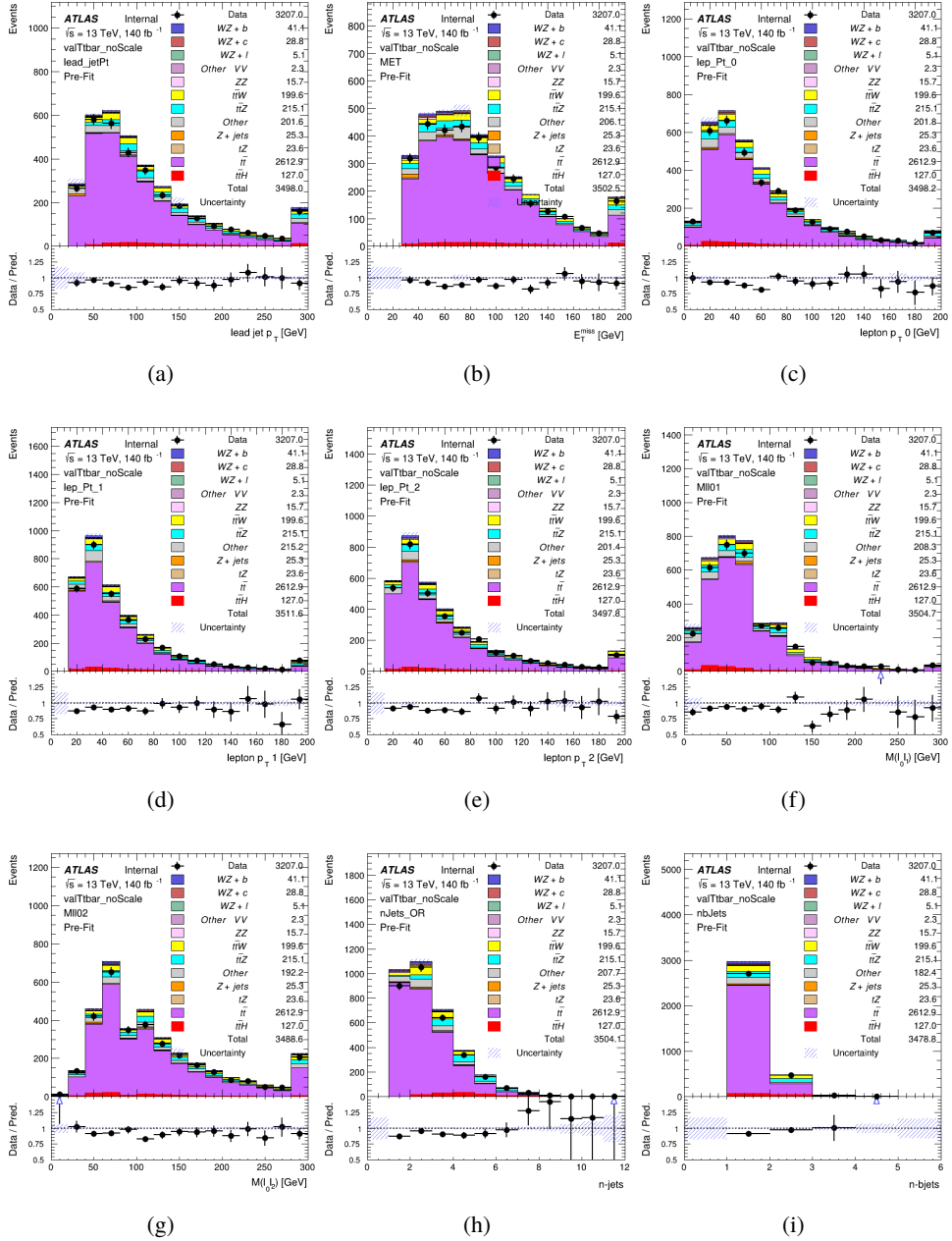


Figure 17: Comparisons between the data and MC distributions in the  $t\bar{t}$  validation region for (a) the  $p_T$  of the leading jet, (b) the missing transverse energy, (c) the  $p_T$  of lepton 0, (d)  $p_T$  of lepton 1, (e)  $p_T$  of lepton 2, (f) the invariant mass of leptons 0 and 1, (g) the invariant mass of leptons 0 and 2, (h) the number of jets, (i) the number of b-tagged jets.

309 The shape of each distribution agrees quite well between data and MC, with a constant offset  
 310 between the two. This is accounted for by applying a constant correction factor of 0.883 to the  $t\bar{t}$

311 MC prediction. Plots showing the kinematics of the  $t\bar{t}$  VR after this correction factor has been  
 312 applied are shown in Figure 18.

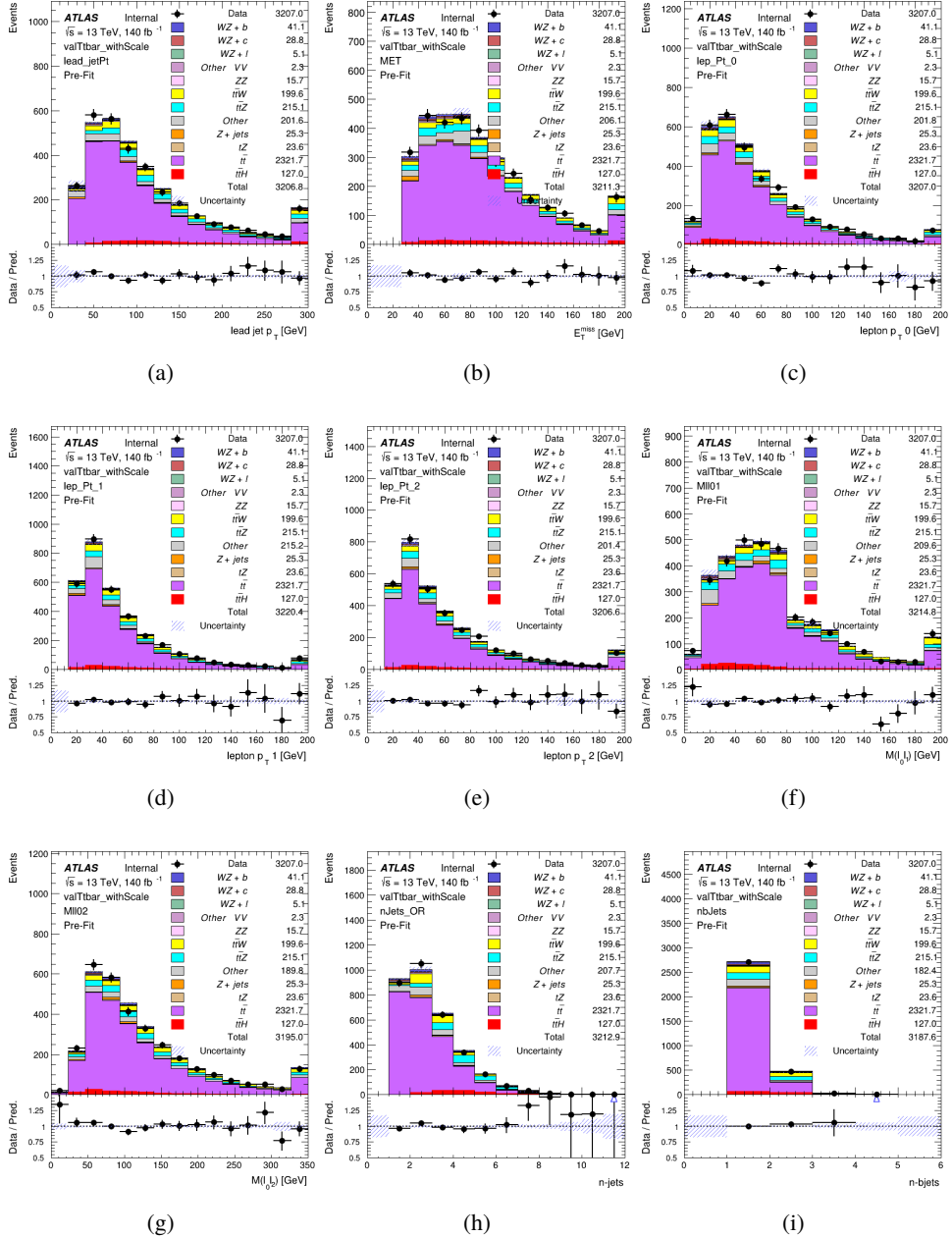


Figure 18: Comparisons between the data and MC distributions in the  $t\bar{t}$  validation region after the correction factor has been applied for (a) the  $p_T$  of the leading jet, (b) the missing transverse energy, (c) the  $p_T$  of lepton 0, (d)  $p_T$  of lepton 1, (e)  $p_T$  of lepton 2, (f) the invariant mass of leptons 0 and 1, (g) the invariant mass of leptons 0 and 2, (h) the number of jets, (i) the number of b-tagged jets.

313 The modeling is further validated by looking at the yield in the  $t\bar{t}$  VR for each DL1r WP, giving  
 314 a clearer correspondence to the signal regions used in the fit. Each region shown in Figure 22  
 315 requires one or more jets pass the listed WP, with no jets passing the next highest WP.

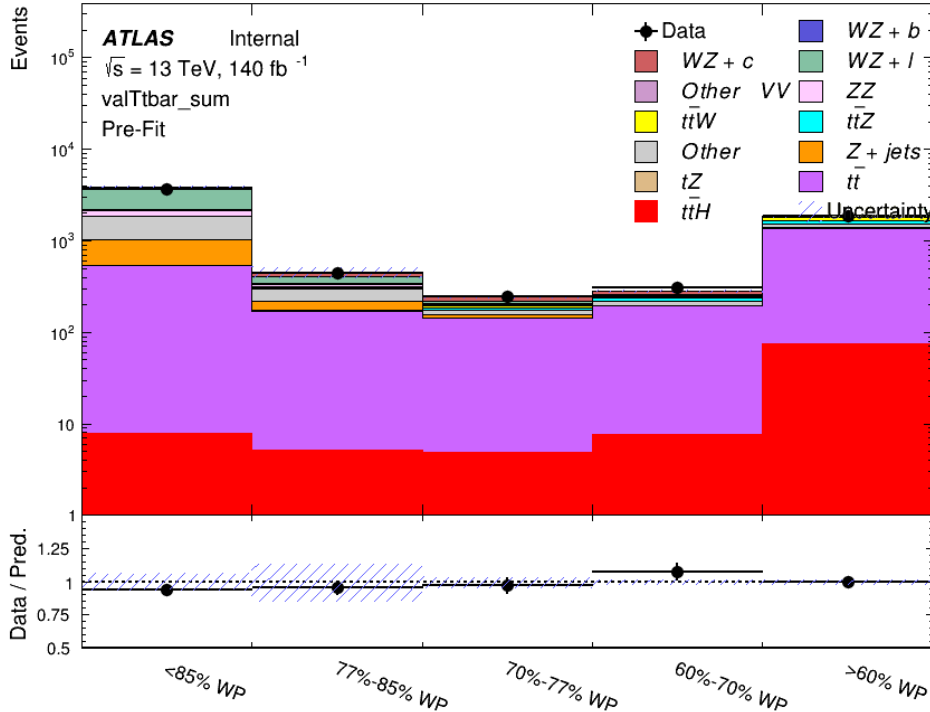


Figure 19: Data and MC comparisons for each DL1r WP for both 1-jet and 2-jet regions, after the  $t\bar{t}$  VR selection and correction factor have been applied

316 As data and MC are found to agree within 10% for each of these working points, a 10% systematic  
 317 uncertainty on the  $t\bar{t}$  prediction is included for the analysis.

### 318 5.3.2 Z+jets Validation

319 Similar to  $t\bar{t}$ , a non-prompt Z+jets validation region is produced in order to validate the MC  
 320 predictions. The lepton requirements remain the same as the preselection region. Because no  
 321 neutrinos are present for this process, the  $E_T^{\text{miss}}$  cut is reversed, requiring  $E_T^{\text{miss}} < 30 \text{ GeV}$ . This  
 322 also ensures this validation region is orthogonal to the preselection region. Further, the number  
 323 of jets in each event is required to be greater than or equal to one. Various kinematic plots of this  
 324 region are shown below. The general agreement between data and MC in each of these suggests  
 325 that the non-prompt contribution of Z+jets is well modeled by Monte Carlo.

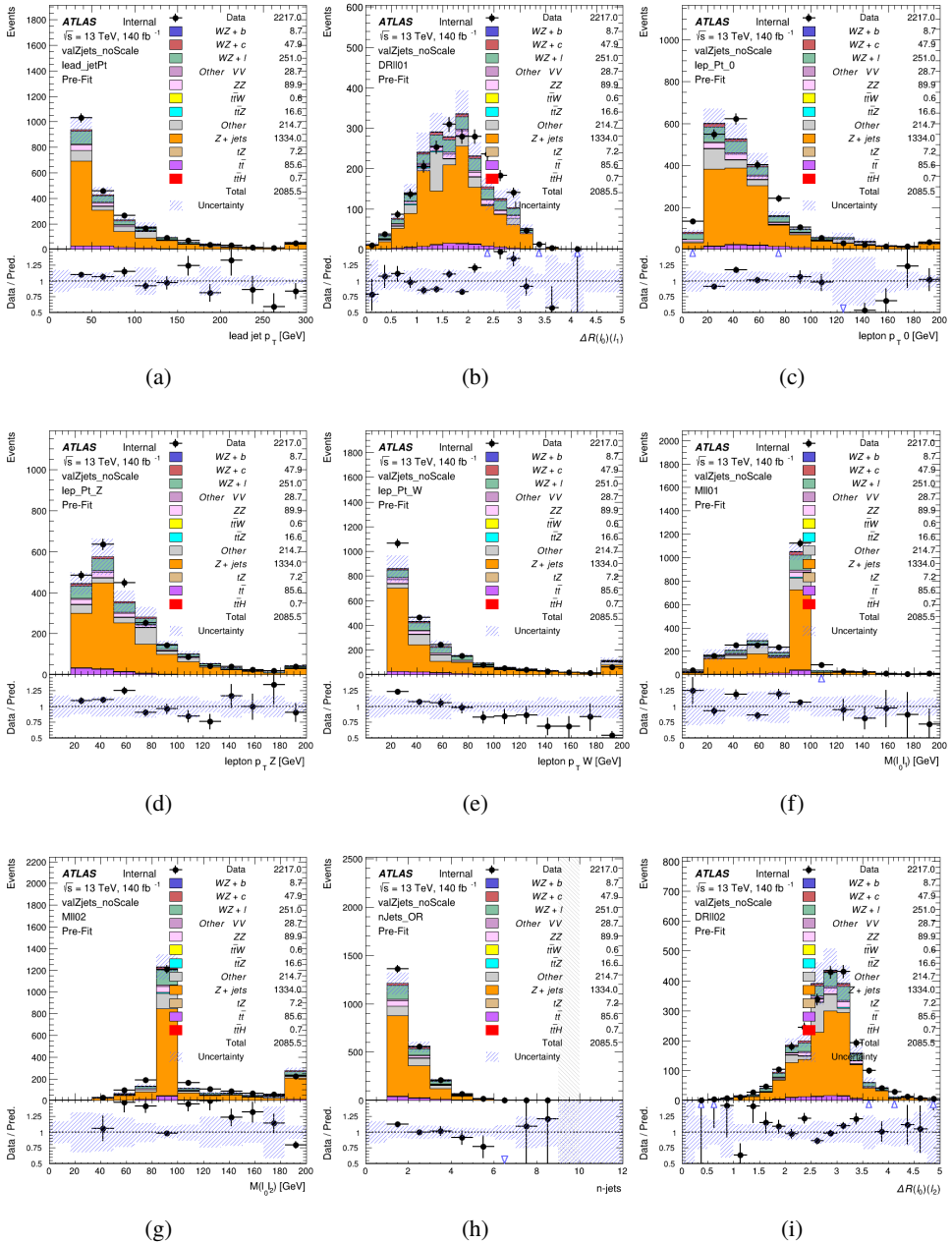


Figure 20: Comparisons between the data and MC distributions in the  $Z+jets$  validation region for (a) the  $p_T$  of the leading jet, (b)  $\Delta R$  between leptons 0 and 1, (c) the  $p_T$  of lepton 0, (d)  $p_T$  of SS lepton from the  $Z$  candidate, (e)  $p_T$  of the SS lepton from the  $W$  candidate, (f) the invariant mass of leptons 0 and 1, (g) the invariant mass of leptons 0 and 2, (h) the number of jets, (i)  $\Delta R$  between leptons 0 and 2. Includes only statistical uncertainties

326 While there is general agreement between data and MC within statistical uncertainty, the shape

327 of the  $p_T$  spectrum of the lepton from the  $W$  is found to differ. To account for this discrepancy,  
328 a variable correction factor is applied to  $Z+jets$ .  $\chi^2$  minimization of the lepton 2  $p_T$  spectrum is  
329 performed to derive a correction factor of  $1.53 - 6.6 * 10^{-6}(lep\_Pt\_W)$ . Kinematic plots of the  
330  $Z + jets$  validation region after this correction factor has been applied are shown in Figure 21.

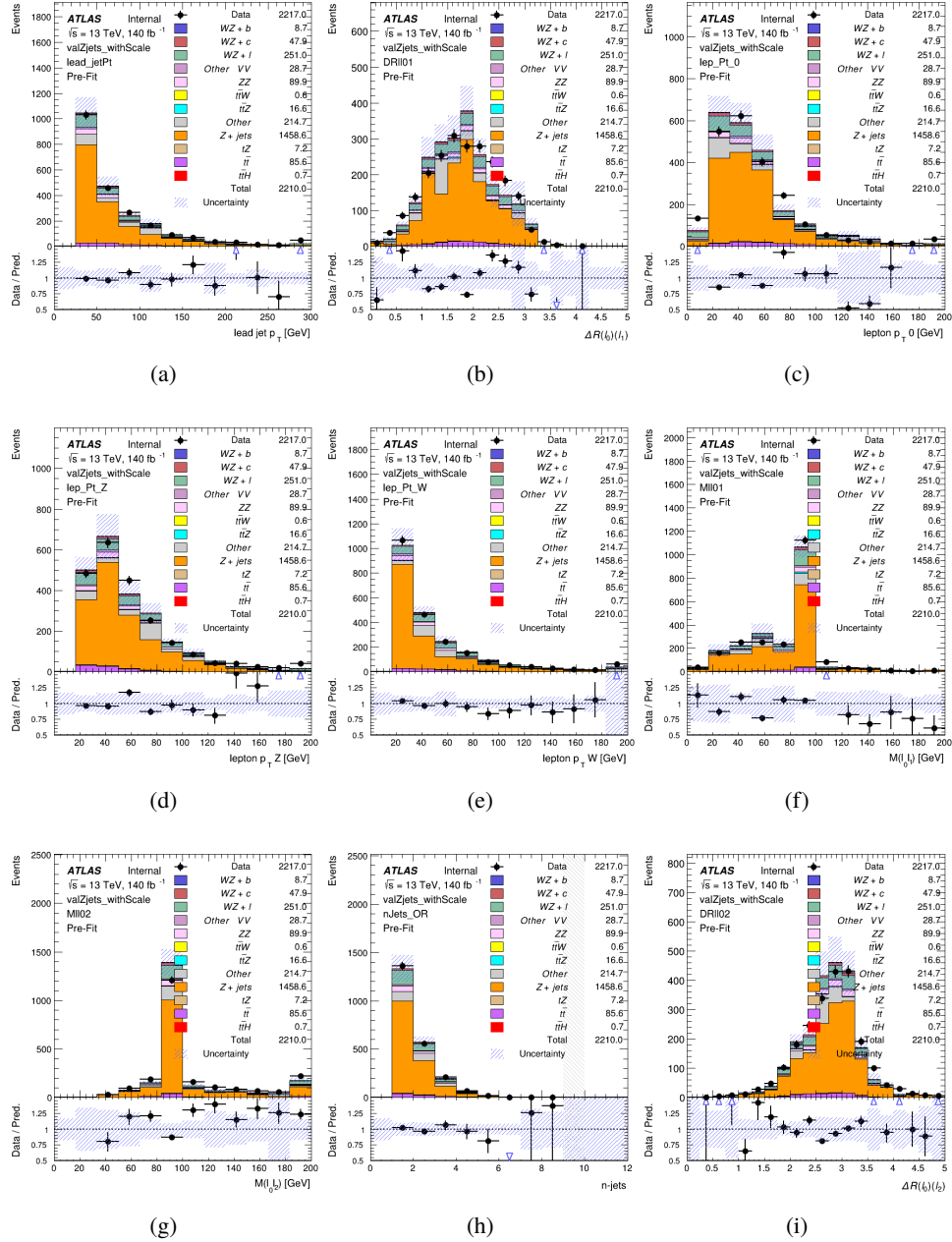


Figure 21: Comparisons between the data and MC distributions in the Z+jets validation region after the correction factor has been applied for (a) the  $p_T$  of the leading jet, (b)  $\Delta R$  between leptons 0 and 1, (c) the  $p_T$  of lepton 0, (d)  $p_T$  of SS lepton from the Z candidate, (e)  $p_T$  of the SS lepton from the W candidate, (f) the invariant mass of leptons 0 and 1, (g) the invariant mass of leptons 0 and 2, (h) the number of jets, (i)  $\Delta R$  between leptons 0 and 2

331 The modeling is further validated by looking at the yield in the Z+jets VR for each DL1r WP,

giving a clearer correspondence to the signal regions used in the fit. Each region shown in Figure 22 requires one or more jets pass the listed WP, with no jets passing the next highest WP.

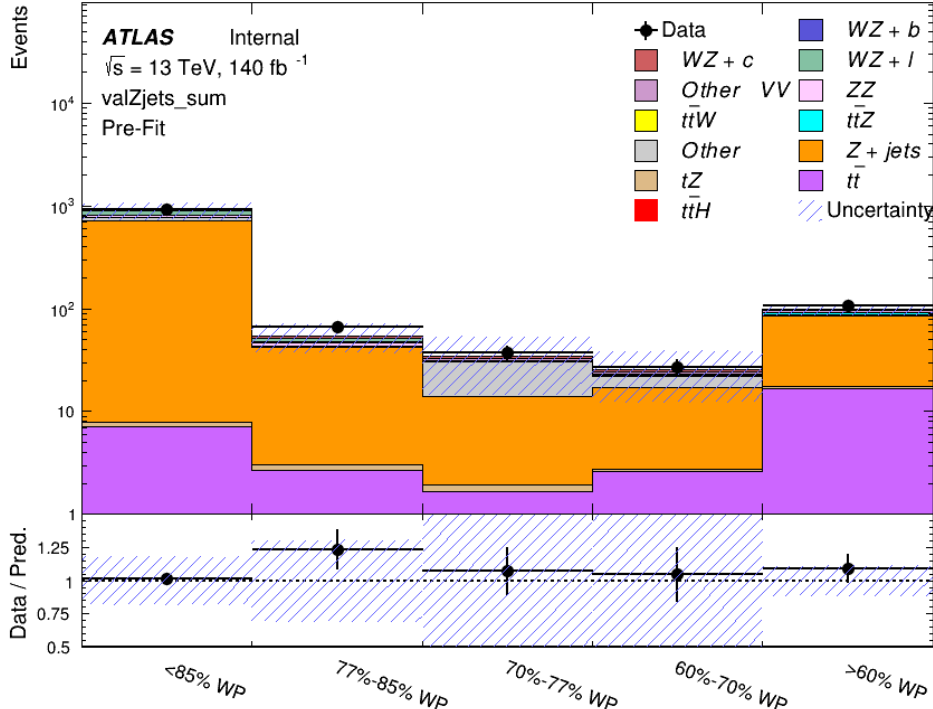


Figure 22: Data and MC comparisons for each DL1r WP for both 1-jet and 2-jet regions, after the Z+jets VR selection and correction factor have been applied

For each of the b-tagging working points considered, the data falls within 20% of the MC prediction once this correction factor has been applied. Therefore, a 20% systematic uncertainty is applied to Z + jets in the analysis.

## 6 tZ Separation Multivariate Analysis

Because tZ produces a final state identical to signal, it represents a predominant background in the most signal enriched regions. That is, the region with one jet passing the 60% DL1r WP. Therefore, a boosted decision tree (BDT) algorithm is trained using TMVA [15] to separate WZ + heavy flavor from tZ.

Separation between tZ and WZ + heavy flavor is achieved in part by reconstructing the invariant mass of the top candidate, which clusters more closely to the top mass for tZ than WZ + heavy flavor.

345 The result of this BDT is used to create a tZ enriched region in the fit, reducing its impact on the  
 346 measurement of WZ + heavy flavor.

347 **6.1 Top Mass Reconstruction**

348 The reconstruction of the top mass follows the procedure described in detail in section 6.1 of  
 349 [16]. The mass of the top quark candidate is reconstructed from the jet, the lepton not included  
 350 in the Z-candidate, and a reconstructed neutrino. In the case that there is one jet in the event,  
 351 there is only possible b-jet candidate. For events with two jets, the jet with the highest DL1r  
 352 score is used.

353 The neutrino from the W decay is expected to be the only source of  $E_T^{\text{miss}}$ . Therefore, the  $E_T$   
 354 and  $\phi$  of the neutrino are taken from the  $E_T^{\text{miss}}$  measurement. This leaves the z-component of  
 355 the neutrino momentum,  $p_{\nu z}$  as the only unknown.

356 This unknown is solved for by taking the combined invariant mass of the lepton and neutrino to  
 357 give the invariant mass of the W boson:

$$358 \quad (p_l + p_\nu)^2 = m_W^2$$

359 Expanding this out into components, this equation gives:

$$360 \quad \sqrt{p_{T\nu}^2 + p_{z\nu}^2} E_l = \frac{m_w^2 - m_l^2}{2} + p_{T\nu}(p_{lx}\cos\phi_\nu + p_{ly}\sin\phi_\nu) + p_{lz}p_{\nu z}$$

361 This equation gives two solutions for  $p_{\nu z}$ . For cases where only one of these solutions is real,  
 362 that is taken as the value of  $p_{\nu z}$ . For instances with two real solutions, the one which is shown  
 363 to be correct in the largest fraction of simulations is taken. For cases when no real solution is  
 364 found, often because of detector effects, the value of  $E_T^{\text{miss}}$  is varied in decreasing increments of  
 365 100 MeV until a real solution is found.

366 The reconstructed top mass distribution for tZ and WZ + b can be seen in figure 23.

367 **6.2 tZ BDT**

368 A Boosted Decision Tree (BDT), specifically XGBoost [17], is used to provide separation between  
 369 tZ and WZ+b. The following kinematic variables are used as inputs:

- 370 • The invariant mass of the reconstructed top candidate
- 371 •  $p_T$  of each of the leptons, jet
- 372 • The invariant mass of each combination of lepton pairs,  $M(l\bar{l})$
- 373 •  $E_T^{\text{miss}}$

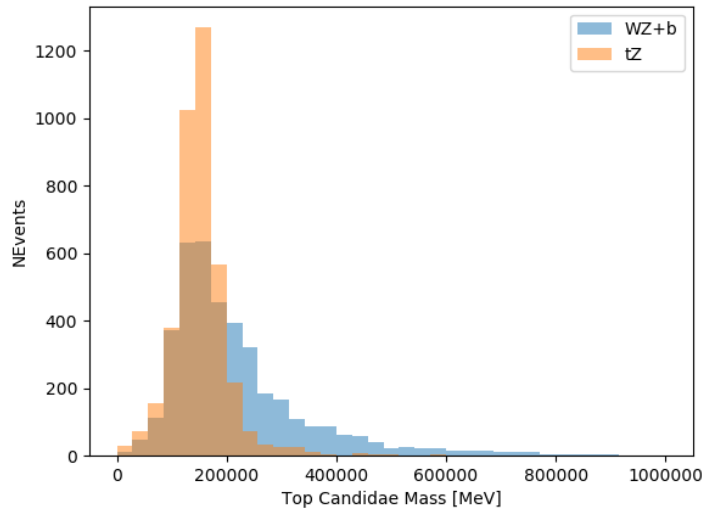


Figure 23: Reconstructed top mass distributions for tZ and WZ + b, measured in MeV.

- 374     • Distance between each combination of leptons,  $\Delta R(ll)$
- 375     • Distance between each lepton and the jet,  $\Delta R(lj)$

376     The training samples included only events meeting the requirements of the 1-jet, >60% region,  
 377     i.e. passing all the selection described in section 5 and having exactly one jet which passes the  
 378     tightest (60%) DL1r working point.

379     The distributions of a few of these features for both signal and background is shown in figure  
 380     24.

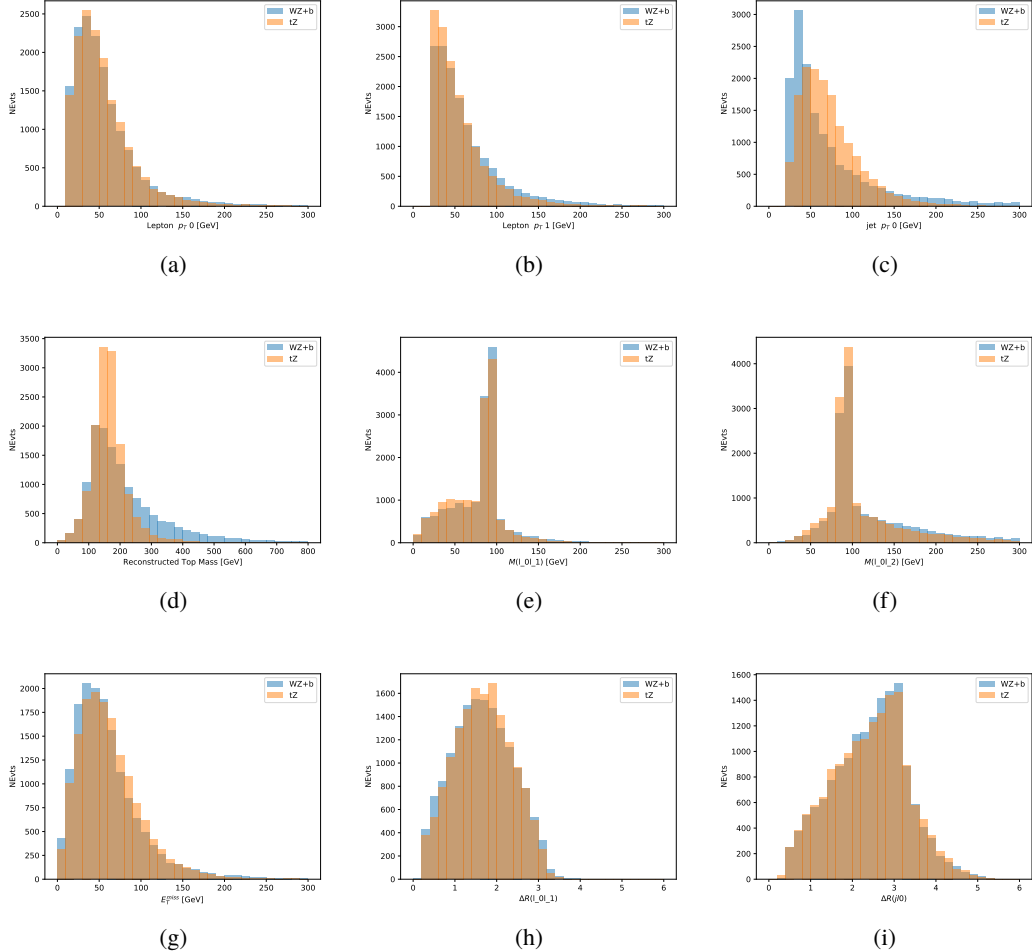


Figure 24: Distribution of input features of the BDT for signal (WZ) and background (tZ). Both are scaled to an equal number of events. (a), (b) and (c) show the  $p_T$  of lepton 0, lepton 1, and the jet, (d) show the reconstructed top mass, (e) and (f) show the invariant mass of leptons 0 and 1, leptons 0 and 2. (g) shows the  $E_T^{\text{miss}}$  of each event. (h) and (i) show the  $\Delta R$  between lepton 0 and lepton 1, and the jet.

381 A sample of 20,000 background (tZ) and signal (WZ+b) Monte Carlo events are used to train  
 382 the BDT. And additional 5,000 events are reserved for testing the model, in order to prevent  
 383 over-fitting. A total of 750 decision trees with a maximum depth of 6 branches are used to build  
 384 the model. These parameters are chosen empirically, by training several models with different  
 385 parameters and selecting the one that gave the best separation for the test sample.

386 The results of the BDT training are shown in figure 25. The output scores for both signal and  
 387 background events is shown on the left. The right shows the receiving operating characteristic  
 388 (ROC) curve that results from the MVA. The ROC curve represents the background rejection  
 389 as a function of signal efficiency, where each point on the curve represents a different response

390 score. The ROC curve of the BDT is compared to the performance of using an optimal set of flat  
 391 selections on the same set of input variables.

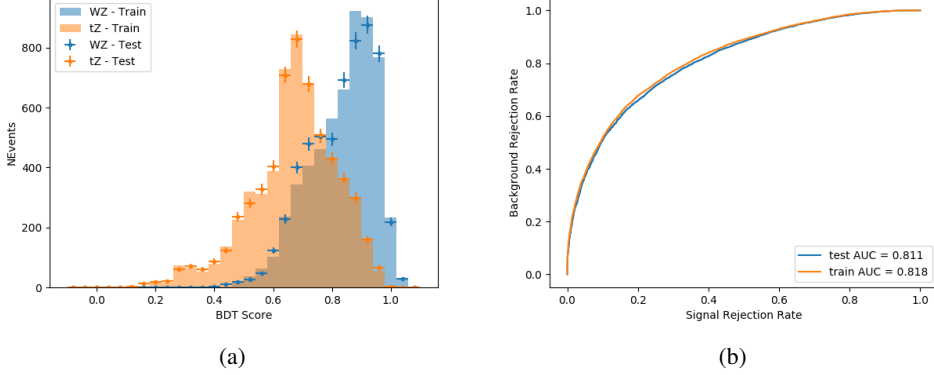


Figure 25: Distribution of the BDT response for signal and background events on the left, the ROC curve for the BDT on the right.

392 The relative important of each input feature in the model, measured by how often they appeared  
 393 in the decision trees, is shown in figure 26.

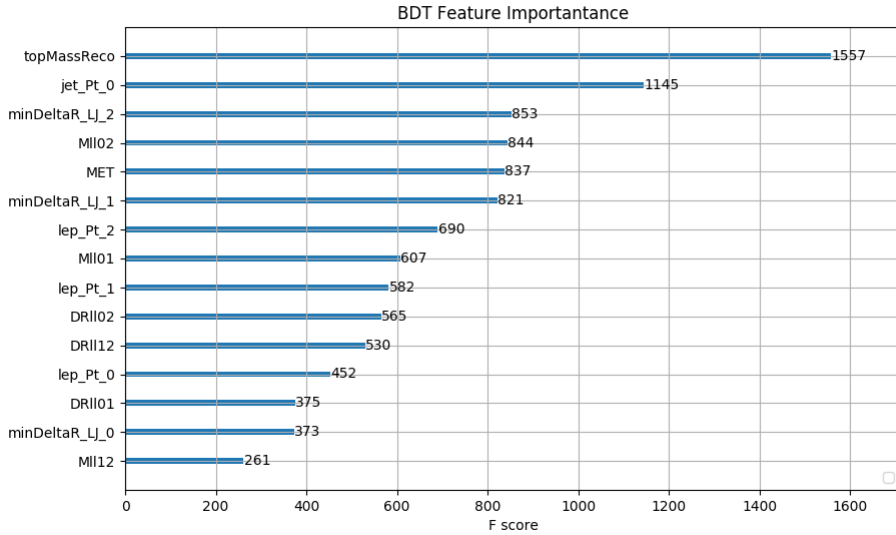


Figure 26: Relative importance of each input feature in the model.

394 These results suggest that some amount of separation can be achieved between these two pro-  
 395 cesses, with a high BDT score selecting a set of events that is pure in  $WZ + b$ . A BDT score

396 of 0.725 is selected as a cutoff, where events with scores higher than this form a signal enriched  
 397 region, and events with scores lower than this form a tZ control region. This cutoff is selected by  
 398 varying the value of this cutoff in stat-only Asimov fits, and selecting the value that minimizes  
 399 the statistical uncertainty on WZ + b.

## 400 7 Systematic Uncertainties

401 The systematic uncertainties that are considered are summarized in Table 8. These are imple-  
 402 mented in the fit either as a normalization factors or as a shape variation or both in the signal  
 403 and background estimations. The numerical impact of each of these uncertainties is outlined in  
 404 Section 8.

Table 8: Sources of systematic uncertainty considered in the analysis.

Systematic uncertainty	Components
Luminosity	1
Pileup reweighting	1
<b>Physics Objects</b>	
Electron	6
Muon	15
Jet energy scale	28
Jet energy resolution	8
Jet vertex fraction	1
Jet flavor tagging	131
$E_T^{\text{miss}}$	3
Total (Experimental)	194
<b>Signal Modeling</b>	
Shape modelling	3
Renormalization and factorization scales	5
nJet Migration	4
<b>Background Modeling</b>	
Cross section	15
Renormalization and factorization scales	12
Total (Signal and background modeling)	35
Total (Overall)	229

405 The uncertainty in the combined integrated luminosity is derived from a calibration of the  
 406 luminosity scale performed for 13 TeV proton-proton collisions [18], [19].

407 The experimental uncertainties are related to the reconstruction and identification of light leptons  
 408 and b-tagging of jets, and to the reconstruction of  $E_T^{\text{miss}}$ . The TOTAL electron ID correlation

409 model is used, corresponding to 1 electron ID systematic. Electron ID is found to be a subleading  
410 systematic that is unconstrained by the fit, making it an appropriate choice for this analysis.

411 The sources which contribute to the uncertainty in the jet energy scale (JES) [20] are decom-  
412 posed into uncorrelated components and treated as independent sources in the analysis. The  
413 CategoryReduction model is used to account for JES uncertainties, which decomposes the uncer-  
414 tainties into 30 nuisance parameters included in the fit. The SimpleJER model is used to account  
415 for jet energy resolution (JER) uncertainties, and 8 JER uncertainty components included as  
416 NPs in the fit.

417 The uncertainties in the b-tagging efficiencies measured in dedicated calibration analyses [21] are  
418 also decomposed into uncorrelated components. The large number of components for b-tagging  
419 is due to the calibration of the distribution of the MVA discriminant.

420 The full list of systematic uncertainties considered in the analysis is summarized in Tables 9, 10  
421 and 11.

422

<b>Experimental Systematics on Leptons and <math>E_T^{\text{miss}}</math></b>			
Type	Description	Systematics Name	Application
<b>Trigger</b>			
Scale Factors	Trigger Efficiency	lepSFTrigTight_MU(EL)_SF_Trigger_STAT(SYST)	Event Weight
<b>Muons</b>			
Efficiencies	Reconstruction and Identification	lepSFObjTight_MU_SF_ID_STAT(SYST)	Event Weight
	Isolation	lepSFObjTight_MU_SF_Isol_STAT(SYST)	Event Weight
	Track To Vertex Association	lepSFObjTight_MU_SF_TTVA_STAT(SYST )	Event Weight
$p_T$ Scale	$p_T$ Scale	MUONS_SCALE	$p_T$ Correction
Resolution	Inner Detector Energy Resolution	MUONS_ID	$p_T$ Correction
	Muon Spectrometer Energy Resolution	MUONS_MS	$p_T$ Correction
<b>Electrons</b>			
Efficiencies	Reconstruction	lepSFObjTight_EL_SF_ID	Event Weight
	Identification	lepSFObjTight_EL_SF_Reco	Event Weight
	Isolation	lepSFObjTight_EL_SF_Isol	Event Weight
Scale Factor	Energy Scale	EG_SCALE_ALL	Energy Correction
Resolution	Energy Resolution	EG_RESOLUTION_ALL	Energy Correction
<b><math>E_T^{\text{miss}}</math></b>			
Soft Tracks Terms	Resolution	MET_SoftTrk_ResoPerp	$p_T$ Correction
	Resolution	MET_SoftTrk_ResoPara	$p_T$ Correction
	Scale	MET_SoftTrk_ScaleUp	$p_T$ Correction
	Scale	MET_SoftTrk_ScaleDown	$p_T$ Correction

Table 9: Summary of experimental systematics considered for leptons and  $E_T^{\text{miss}}$ . Includes type, description, name of systematic as used in the fit, and mode of application. The mode of application indicates the systematic evaluation, e.g. as an overall event re-weighting (Event Weight) or rescaling ( $p_T$  Correction).

Experimental Systematics on Jets			
Type	Origin	Systematics Name	Application
Jet Vertex Tagger		JVT	Event Weight
Energy Scale	Calibration Method	JET_21NP_ JET_EffectiveNP_1-19	$p_T$ Correction $p_T$ Correction
	$\eta$ inter-calibration	JET_EtaIntercalibration_Modelling JET_EtaIntercalibration_NonClosure JET_EtaIntercalibration_TotalStat	$p_T$ Correction $p_T$ Correction $p_T$ Correction
	High $p_T$ jets	JET_SingleParticle_HighPt	$p_T$ Correction
	Pile-Up	JET_Pileup_OffsetNPV JET_Pileup_OffsetMu JET_Pileup_PtTerm JET_Pileup_RhoTopology	$p_T$ Correction $p_T$ Correction $p_T$ Correction $p_T$ Correction
	Non Closure	JET_PunchThrough_MC15	$p_T$ Correction
	Flavour	JET_Flavor_Response JET_BJES_Response JET_Flavor_Composition	$p_T$ Correction $p_T$ Correction $p_T$ Correction
Resolution		JET_JER_SINGLE_NP	Event Weight

Table 10: Jet systematics take into account effects of jets calibration method,  $\eta$  inter-calibration, high  $p_T$  jets, pile-up, and flavor response. They are all diagonalised into effective parameters.

Experimental Systematics on b-tagging		
Type	Origin	Systematic Name
Scale Factors	DL1r b-tagger efficiency on b originated jets in bins of $\eta$	DL1r_Continuous_EventWeight_B0-29
	DL1r b-tagger efficiency on c originated jets in bins of $\eta$	DL1r_Continuous_EventWeight_C0-19
	DL1r b-tagger efficiency on light flavoured originated jets in bins of $\eta$ and $p_T$	DL1r_Continuous_EventWeight_Light0-79
	DL1r b-tagger extrapolation efficiency	DL1r_Continuous_EventWeight_extrapolation DL1r_Continuous_EventWeight_extrapolation_from_charm

Table 11: Summary of experimental systematics to be included for b-tagging of jets in the analysis, using the continuous DL1r tagging algorithm. All of the b-tagging related systematics are applied as event weights. From left: type, description, and the name of systematic used in the fit.

- 423 Theoretical uncertainties applied to MC predictions, including cross section, PDF, and scale  
 424 uncertainties are taken from theory calculations, with the exception of non-prompt and diboson  
 425 backgrounds. The cross-section uncertainty on tZ is taken from [22]. Derivation of the non-  
 426 prompt background uncertainties, Z+jets and tt}, are explained in detail in Section 5.3.  
 427 The other VV + heavy flavor processes (namely VV+b and VV+charm, which primarily consist  
 428 of ZZ events) are also poorly understood, because these processes involve the same physics as  
 429 WZ + heavy flavor, and have also not been measured. Therefore, a conservative 50% uncertainty  
 430 is applied to those samples. While this uncertainty is large, it is found to have little impact on  
 431 the significance of the final result.  
 432 The theory uncertainties applied to the predominate background estimates are summarized in  
 433 Table 12.

Process	X-section [%]
tZ	X-sec: $\pm 15.2$ QCD Scale: $^{+5.2}_{-1.3}$ PDF( $+\alpha_S$ ): $\pm 1.2$
t <bar>t} H (aMC@NLO+Pythia8)</bar>	QCD Scale: $^{+5.8}_{-9.2}$ PDF( $+\alpha_S$ ): $\pm 3.6$
t <bar>t} Z (aMC@NLO+Pythia8)</bar>	QCD Scale: $^{+9.6}_{-11.3}$ PDF( $+\alpha_S$ ): $\pm 4$
t <bar>t} W (aMC@NLO+Pythia8)</bar>	QCD Scale: $^{+12.9}_{-11.5}$ PDF( $+\alpha_S$ ): $\pm 3.4$
VV + b/charm (Sherpa 2.2.1)	$\pm 50$
VV + light (Sherpa 2.2.1)	$\pm 6$
t <bar>t}</bar>	$\pm 10$
Z + jets	$\pm 20$
Others	$\pm 50$

Table 12: Summary of theoretical uncertainties for MC predictions in the analysis.

434 Additional signal uncertainties are estimated by comparing estimates from the nominal Sherpa  
 435 WZ samples with alternate WZ samples generated with Powheg+PYTHIA8 (DSID 361601).  
 436 The shape of the templates used in the fit are compared between these two samples for WZ + b,  
 437 WZ + charm and WZ + light, as shown in Figures 27 and 28. Each of these plots are normalized  
 438 to unity in order to capture differences in shape.

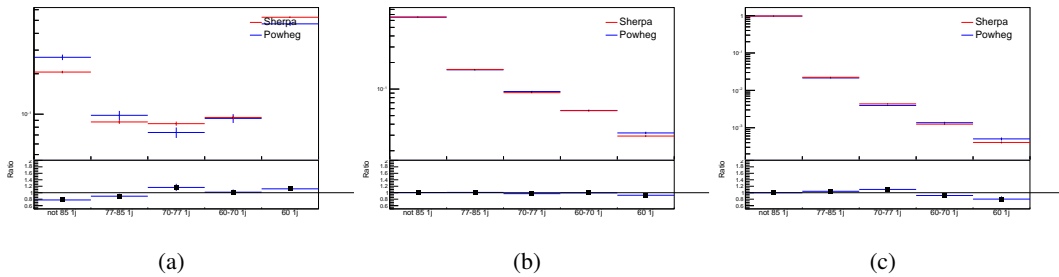


Figure 27: Comparison between Sherpa and Powheg predictions of the distribution of (a) WZ + b, (b) WZ + charm, and (c) WZ + light among the various b-tag WPs used in the 1-jet fit.

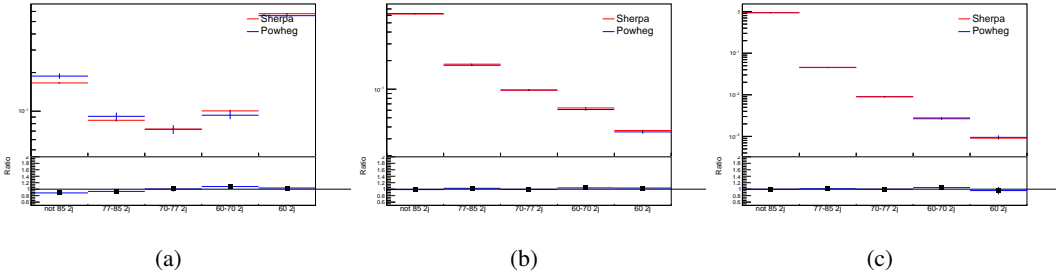


Figure 28: Comparison between Sherpa and Powheg predictions of the distribution of (a) WZ + b, (b) WZ + charm, and (c) WZ + light among the various b-tag WPs used in the 2-jet fit.

439 Separate systematics are included in the fit for WZ + b, WZ + charm and WZ + light, where  
 440 the distribution among each of the fit regions is varied based on the prediction of the Powheg  
 441 sample.

442 A similar approach is taken to account for uncertainties in migrations between the number of  
 443 reco and truth jets. The fraction of events with 1 truth jet which fall into the 1 jet bin versus the  
 444 2 jet bin at reco level is compared for Sherpa and Powheg. The same is done for events with 2  
 445 truth jets. This comparison is shown in figure 29.

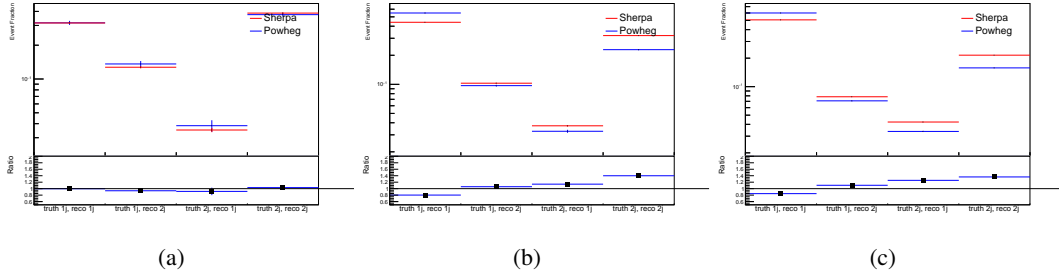


Figure 29: Comparison between Sherpa and Powheg predictions for truth jet migrations between the 1 and 2 jet reco bins for (a) WZ + b, (b) WZ + charm, and (c) WZ + light

446 A systematic is included where events are shifted between the 1-jet and 2-jet regions based on  
 447 the differences between these two shapes. This is done independently for each of the WZ + b,  
 448 WZ + charm, and WZ + light templates.

449 Additional systematics are included to account for the uncertainty in the contamination of 0 jet  
 450 and 3 or more jet events (at truth level) in the 1 and 2 reco jet bins. Because these events fall  
 451 outside the scope of this measurement, these events are included as a background. As such, a  
 452 normalization, rather than a shape, uncertainty is applied for this background.

453 The number of WZ events with 0-jets and  $\geq 3$ -jets in the reconstructed 1-jet and 2-jet regions  
 454 are compared for Sherpa and Powheg, as seen in figure 30. These differences are taken as separate  
 455 normalization systematics on the yield of WZ+0-jet and WZ+ $\geq 3$ -jet events.

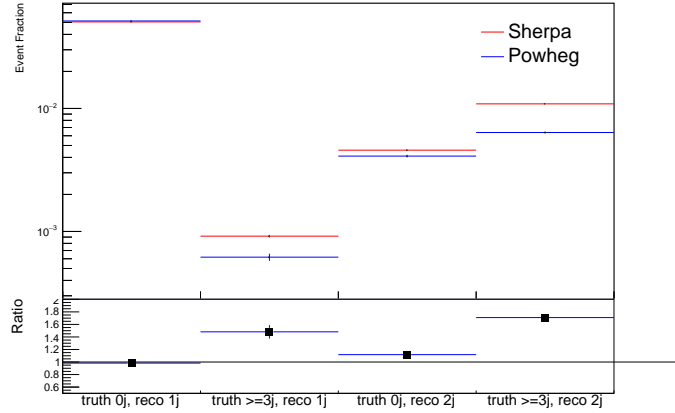


Figure 30: Comparison between Sherpa and Powheg predictions for truth jet migrations between the 1 and 2 jet reco bins

## 456 8 Results

457 A separate maximum-likelihood fit is performed over the various fit regions in order to extract  
 458 the best-fit value of the WZ + b-jet and WZ + charm jet contributions. Separate measurements  
 459 are made for WZ + 1-jet and WZ + 2-jet events. The WZ + b, WZ + charm and WZ + light  
 460 contributions, separated into 1-jet and 2-jet samples at truth level, are allowed to float, with the  
 461 remaining background contributions are held fixed. The result of the fit is used to extract the  
 462 cross-section of WZ + heavy-flavor production.

463 A maximum likelihood fit to data is performed simultaneously in the regions described in Section  
 464 5, summarized in figure 31. The parameters  $\mu_{WZ+b-1-jet}$ ,  $\mu_{WZ+charm1-jet}$ ,  $\mu_{WZ+light-1-jet}$ ,  
 465  $\mu_{WZ+b-2-jet}$ ,  $\mu_{WZ+charm2-jet}$ ,  $\mu_{WZ+light-2-jet}$ , where  $\mu = \sigma_{\text{observed}}/\sigma_{\text{SM}}$ , are extracted from  
 466 the fit. A simultaneous fit is performed over all 1-jet and 2-jet regions.

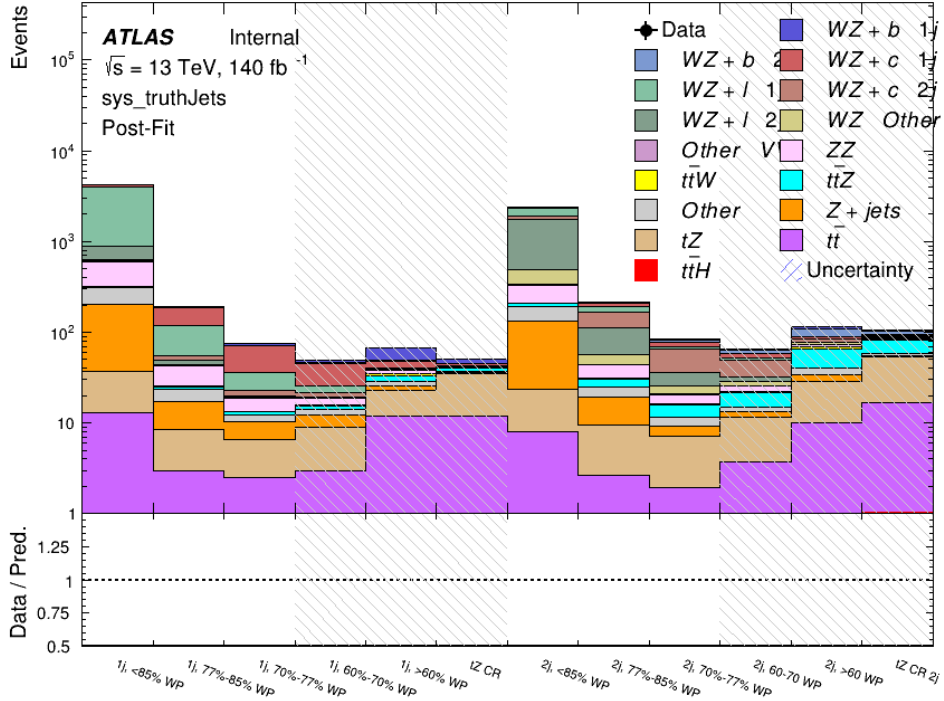


Figure 31: Post-fit summary of the fit regions.

467 **These numbers are preliminary, and need to be updated to account for the latest results.**

468 The Asimov fit for 1-jet events gives an expected  $\mu$  value of  $1.00^{+0.37}_{-0.35}(\text{stat})^{+0.24}_{-0.22}(\text{sys})$  for  $WZ$   
 469 + b. The fitted cross-section modifiers for  $WZ + \text{charm}$  and  $WZ + \text{light}$  are  $1.00 \pm 0.17 \pm 0.15$   
 470 and  $1.00 \pm 0.04 \pm 0.07$ , respectively.

471 The expected cross-section of  $WZ+b$  with 1 associated jet obtained from the fit is  $1.74^{+0.75}_{-0.72}(\text{stat})^{+0.62}_{-0.57}(\text{sys})$   
 472 fb with an expected significance of  $1.8\sigma$ . The expected cross-section of  $WZ + \text{charm}$  is measured  
 473 to be  $14.6 \pm 2.5(\text{stat}) \pm 2.1(\text{sys})$  fb, with a correlation of -0.23.

474 For 2-jet events, the fit gives an expected  $\mu$  value of  $1.00^{+0.34}_{-0.33}(\text{stat})^{+0.29}_{-0.28}(\text{sys})$  for  $WZ + b$ .  
 475 The fitted cross-section modifiers for  $WZ + \text{charm}$  and  $WZ + \text{light}$  are  $1.00 \pm 0.17 \pm 0.15$  and  
 476  $1.00 \pm 0.04 \pm 0.08$ , respectively.

477 The expected  $WZ + b$  cross-section in the 2-jet region is  $2.46^{+0.83}_{-0.81}(\text{stat})^{+0.73}_{-0.68}(\text{sys})$  fb with  
 478 an expected significance of  $2.1\sigma$ . The 2-jet expected cross-section of  $WZ + \text{charm}$  is  $12.7 \pm$   
 479  $2.2(\text{stat}) \pm 2.0(\text{sys})$  fb, and the correlation between  $WZ + \text{charm}$  and  $WZ + b$  is -0.26.

480 While the fit is performed for  $WZ+1\text{-jet}$  and  $WZ+2\text{-jet}$  simultaneously, the detailed results  
 481 below

<sup>482</sup> **8.1 1-jet Results**

<sup>483</sup> **The results of the fit are currently blinded.**

<sup>484</sup> The pre-fit yields in each of the regions used in the fit are shown in Table 8.1.

<sup>485</sup>

Sample	1j, <85% WP	1j, 77%-85% WP	1j, 70%-77% WP	1j, 60%-70% WP	1j, >60% WP	tZ CR
WZ + b - 1j	$8.1 \pm 1.6$	$4.7 \pm 0.5$	$4.6 \pm 0.4$	$5.1 \pm 0.4$	$18.2 \pm 2.4$	$4.8 \pm 0.6$
WZ + c - 1j	$260 \pm 22$	$81 \pm 6$	$43.1 \pm 3.6$	$25.8 \pm 2.6$	$9.4 \pm 1.8$	$2.9 \pm 0.6$
WZ + l - 1j	$3090 \pm 250$	$91 \pm 13$	$17 \pm 3$	$4.9 \pm 1.6$	$1.3 \pm 0.4$	$0.2 \pm 0.1$
WZ + b - 2j	$1.10 \pm 0.37$	$0.44 \pm 0.11$	$0.39 \pm 0.06$	$0.62 \pm 0.14$	$2.1 \pm 0.5$	$0.59 \pm 0.14$
WZ + c - 2j	$21 \pm 5$	$5.6 \pm 1.2$	$3.0 \pm 0.7$	$2.0 \pm 0.5$	$0.70 \pm 0.20$	$0.30 \pm 0.08$
WZ + l - 2j	$250 \pm 60$	$5.7 \pm 1.6$	$0.73 \pm 0.53$	$0.31 \pm 0.15$	$0.07 \pm 0.06$	$0.01 \pm 0.01$
WZ - Other	$13 \pm 5$	$1.4 \pm 0.4$	$0.42 \pm 0.08$	$0.2 \pm 0.01$	$0.30 \pm 0.05$	$0.67 \pm 0.15$
Other VV	$6.2 \pm 0.6$	$0.2 \pm 0.4$	$0.2 \pm 0.04$	$0.07 \pm 0.1$	$0.1 \pm 0.1$	$0.1 \pm 0.2$
ZZ	$336 \pm 26$	$17.8 \pm 2.1$	$4.3 \pm 0.6$	$1.7 \pm 0.5$	$0.36 \pm 0.08$	$0.10 \pm 0.03$
t̄tW	$1.1 \pm 0.2$	$0.2 \pm 0.1$	$0.3 \pm 0.1$	$0.4 \pm 0.1$	$1.5 \pm 0.3$	$0.7 \pm 0.2$
t̄tZ	$6.8 \pm 1.2$	$1.4 \pm 0.3$	$1.0 \pm 0.2$	$1.2 \pm 0.2$	$4.4 \pm 0.8$	$3.2 \pm 0.6$
Z + jets	$169 \pm 38$	$8.9 \pm 1.9$	$3.7 \pm 0.8$	$3.3 \pm 0.7$	$3.2 \pm 0.7$	$0.8 \pm 0.17$
V + $\gamma$	$45 \pm 28$	$1.9 \pm 2.4$	$0.1 \pm 0.1$	$0.02 \pm 0.01$	$1.0 \pm 0.9$	$0.02 \pm 0.03$
tZ	$24.3 \pm 4.3$	$5.5 \pm 1.1$	$4.1 \pm 0.8$	$5.9 \pm 1.1$	$10.7 \pm 2.0$	$23 \pm 4$
tW	$1.4 \pm 0.8$	$0.2 \pm 0.5$	$0.0 \pm 0.2$	$0.7 \pm 0.6$	$0.26 \pm 0.42$	$0.39 \pm 0.41$
WtZ	$2.3 \pm 1.2$	$0.6 \pm 0.3$	$0.3 \pm 0.21$	$0.27 \pm 0.2$	$1.1 \pm 0.7$	$0.6 \pm 0.5$
VVV	$12.4 \pm 0.5$	$0.93 \pm 0.06$	$0.35 \pm 0.03$	$0.13 \pm 0.02$	$0.14 \pm 0.03$	$0.02 \pm 0.01$
VH	$40 \pm 6$	$2.6 \pm 1.4$	$0.9 \pm 0.8$	$0.7 \pm 0.8$	$0.5 \pm 0.6$	$0.0 \pm 0.0$
t̄t	$12.1 \pm 1.6$	$2.9 \pm 0.6$	$2.5 \pm 0.5$	$2.8 \pm 0.5$	$11.2 \pm 1.4$	$10.9 \pm 1.5$
t̄tH	$0.24 \pm 0.03$	$0.05 \pm 0.01$	$0.04 \pm 0.01$	$0.06 \pm 0.01$	$0.20 \pm 0.03$	$0.13 \pm 0.02$
Total	$5010 \pm 260$	$227 \pm 24$	$88 \pm 12$	$57 \pm 8$	$76 \pm 16$	$53 \pm 8$

Table 13: Pre-fit yields in each of the 1-jet fit regions.

<sup>486</sup> The post-fit yields in each region are summarized in Figure 8.1.

<sup>487</sup>

	1j, <85% WP	1j, 77%-85% WP	1j, 70%-77% WP	1j, 60%-70% WP	1j, >60% WP	tZ CR
WZ + b	$8.1 \pm 4.9$	$4.7 \pm 2.0$	$4.6 \pm 2.0$	$5.1 \pm 2.1$	$18 \pm 10$	$5.0 \pm 2.5$
WZ + c	$260 \pm 60$	$80 \pm 14$	$43 \pm 7$	$26 \pm 5$	$9.4 \pm 2.3$	$2.9 \pm 0.7$
WZ + l	$3090 \pm 130$	$90 \pm 11$	$17.3 \pm 2.8$	$4.9 \pm 1.6$	$1.3 \pm 0.4$	$0.23 \pm 0.13$
WZ + b - 2j	$1.10 \pm 0.37$	$0.44 \pm 0.11$	$0.39 \pm 0.06$	$0.62 \pm 0.14$	$2.1 \pm 0.5$	$0.59 \pm 0.14$
WZ + c - 2j	$21 \pm 5$	$5.6 \pm 1.2$	$3.0 \pm 0.7$	$2.0 \pm 0.5$	$0.70 \pm 0.20$	$0.30 \pm 0.08$
WZ + l - 2j	$250 \pm 60$	$5.7 \pm 1.6$	$0.73 \pm 0.53$	$0.31 \pm 0.15$	$0.07 \pm 0.06$	$0.01 \pm 0.01$
WZ - Other	$13 \pm 5$	$1.4 \pm 0.4$	$0.42 \pm 0.08$	$0.2 \pm 0.01$	$0.30 \pm 0.05$	$0.67 \pm 0.15$
Other VV	$6.2 \pm 0.6$	$0.92 \pm 0.07$	$0.02 \pm 0.01$	$0.01 \pm 0.01$	$0.01 \pm 0.01$	$0.01 \pm 0.01$
ZZ	$346 \pm 57$	$19 \pm 5$	$4.3 \pm 0.8$	$2.7 \pm 0.5$	$2.4 \pm 0.1$	$2.1 \pm 0.6$
t̄tW	$1.09 \pm 0.21$	$0.2 \pm 0.1$	$0.1 \pm 0.1$	$0.4 \pm 0.1$	$1.5 \pm 0.3$	$0.1 \pm 0.2$
t̄tZ	$6.8 \pm 1.2$	$1.4 \pm 0.3$	$1.0 \pm 0.2$	$1.2 \pm 0.2$	$4.4 \pm 0.7$	$3.2 \pm 0.5$
rare Top	$0.14 \pm 0.04$	$0.04 \pm 0.02$	$0.04 \pm 0.0$	$0.1 \pm 0.03$	$0.14 \pm 0.04$	$0.15 \pm 0.05$
t̄tWW	$0.04 \pm 0.03$	$0.01 \pm 0.02$	$0.01 \pm 0.01$	$0.01 \pm 0.01$	$0.01 \pm 0.02$	$0.01 \pm 0.01$
Z + jets	$169 \pm 37$	$8.9 \pm 1.9$	$3.7 \pm 0.8$	$3.3 \pm 0.7$	$3.2 \pm 0.7$	$0.8 \pm 0.2$
W + jets	$0.01 \pm 0.01$					
V + $\gamma$	$46 \pm 28$	$1.9 \pm 2.4$	$0.1 \pm 0.1$	$0.0 \pm 0.2$	$1.0 \pm 0.9$	$0.0 \pm 0.0$
tZ	$24 \pm 4$	$5.5 \pm 1.0$	$4.1 \pm 0.8$	$5.9 \pm 1.1$	$10.7 \pm 1.8$	$23.3 \pm 3.7$
tW	$1.37 \pm 0.82$	$0.18 \pm 0.26$	$0.01 \pm 0.12$	$0.67 \pm 0.64$	$0.26 \pm 0.42$	$0.39 \pm 0.41$
WtZ	$2.3 \pm 1.2$	$0.6 \pm 0.3$	$0.3 \pm 0.2$	$0.3 \pm 0.2$	$1.1 \pm 0.6$	$0.6 \pm 0.3$
VVV	$12.4 \pm 0.4$	$0.9 \pm 0.1$	$0.4 \pm 0.1$	$0.13 \pm 0.02$	$0.14 \pm 0.03$	$0.02 \pm 0.01$
VH	$40 \pm 6$	$2.6 \pm 1.4$	$0.9 \pm 0.8$	$0.7 \pm 0.8$	$0.4 \pm 0.6$	$0.01 \pm 0.01$
t̄t	$12.1 \pm 1.6$	$2.9 \pm 0.6$	$2.5 \pm 0.5$	$2.8 \pm 0.5$	$11.2 \pm 1.5$	$10.9 \pm 1.4$
t̄tH	$0.24 \pm 0.03$	$0.05 \pm 0.01$	$0.04 \pm 0.01$	$0.06 \pm 0.01$	$0.20 \pm 0.03$	$0.13 \pm 0.02$
Total	$5100 \pm 110$	$227 \pm 12$	$87 \pm 6$	$56.7 \pm 4.4$	$76 \pm 9$	$52.5 \pm 4.2$

Table 14: Post-fit yields in each of the 1-jet fit regions.

488 As described in Section 7, there are 226 systematic uncertainties that are considered as NPs in  
 489 the fit. These NPs are constrained by Gaussian or log-normal probability density functions. The  
 490 latter are used for normalisation factors to ensure that they are always positive. The expected  
 491 number of signal and background events are functions of the likelihood. The prior for each NP is  
 492 added as a penalty term, decreasing the likelihood as it is shifted away from its nominal value.

493 The impact of each NP is calculated by performing the fit with the parameter of interest held  
 494 fixed, varied from its fitted value by its uncertainty, and calculating  $\Delta\mu$  relative to the baseline  
 495 fit. The impact of the most significant sources of systematic uncertainties is summarized in Table  
 496 15.

Uncertainty Source	$\Delta\mu$	
WZ + 1-jet light XS	0.13	-0.18
WZ + charm cross-section	-0.10	0.12
Jet Energy Scale	0.1	-0.13
tZ cross-section	-0.10	0.10
WZ 1-jet/2-jet Migration	0.08	-0.07
Jet Energy Resolution	-0.10	0.10
Luminosity	-0.08	0.09
Other Diboson + b cross-section	-0.07	0.07
Flavor tagging	0.05	0.05
t <bar>t} cross-section</bar>	-0.05	0.05
Total Systematic Uncertainty	0.29	0.34

Table 15: Summary of the most significant sources of systematic uncertainty on the measurement of WZ + b with exactly one associated jet.

<sup>497</sup> The ranking and impact of those nuisance parameters with the largest contribution to the overall  
<sup>498</sup> uncertainty is shown in Figure 32.

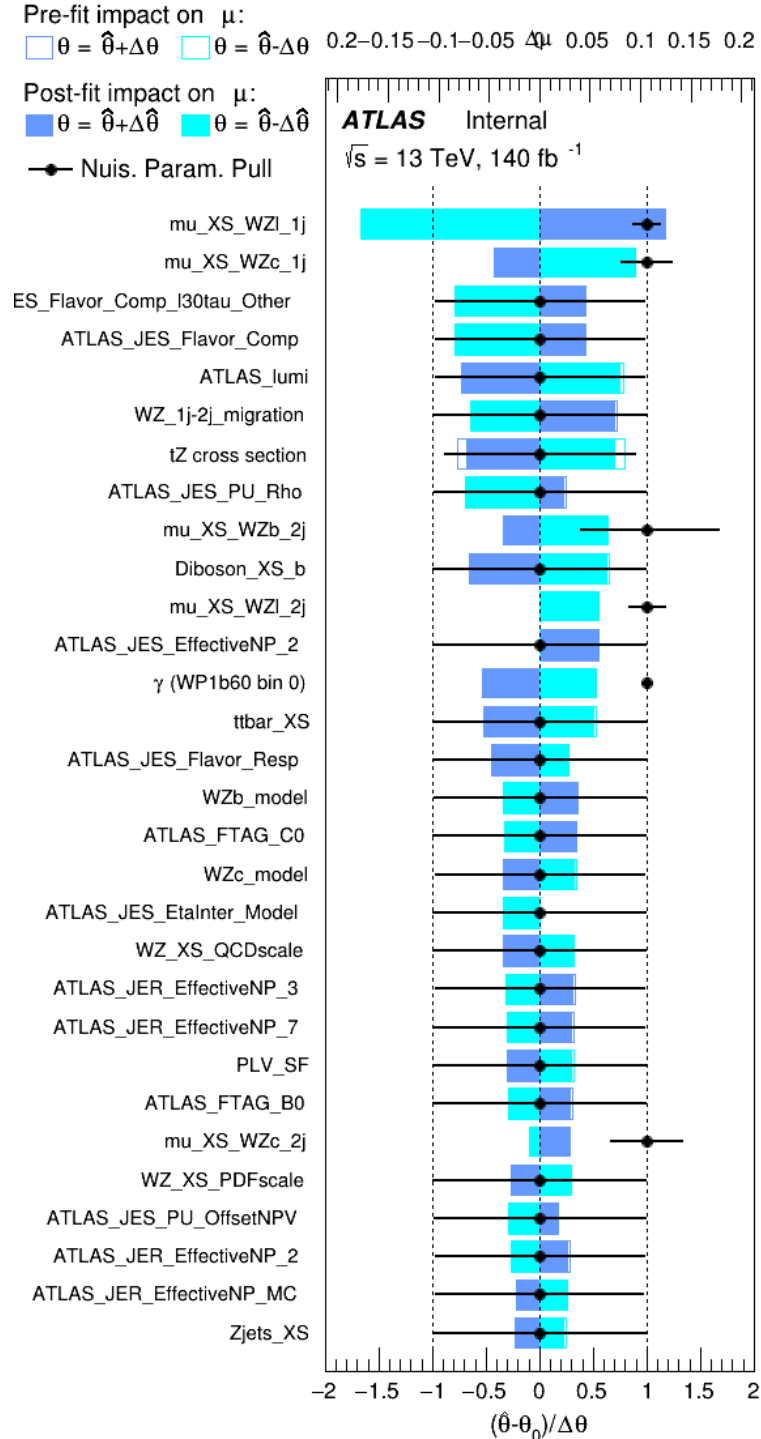


Figure 32: Impact of systematic uncertainties on the signal-strength of  $WZ + b$  for events with exactly one jet

<sup>499</sup> The large impact of the Jet Energy Scale and Jet Flavor Tagging is unsurprising, as the shape of  
<sup>500</sup> the fit regions depends heavily on the modeling of the jets. The other major sources of uncertainty  
<sup>501</sup> come from background modelling and cross-section uncertainty.

502 The correlations between these nuisance parameters are summarized in Figure 33.

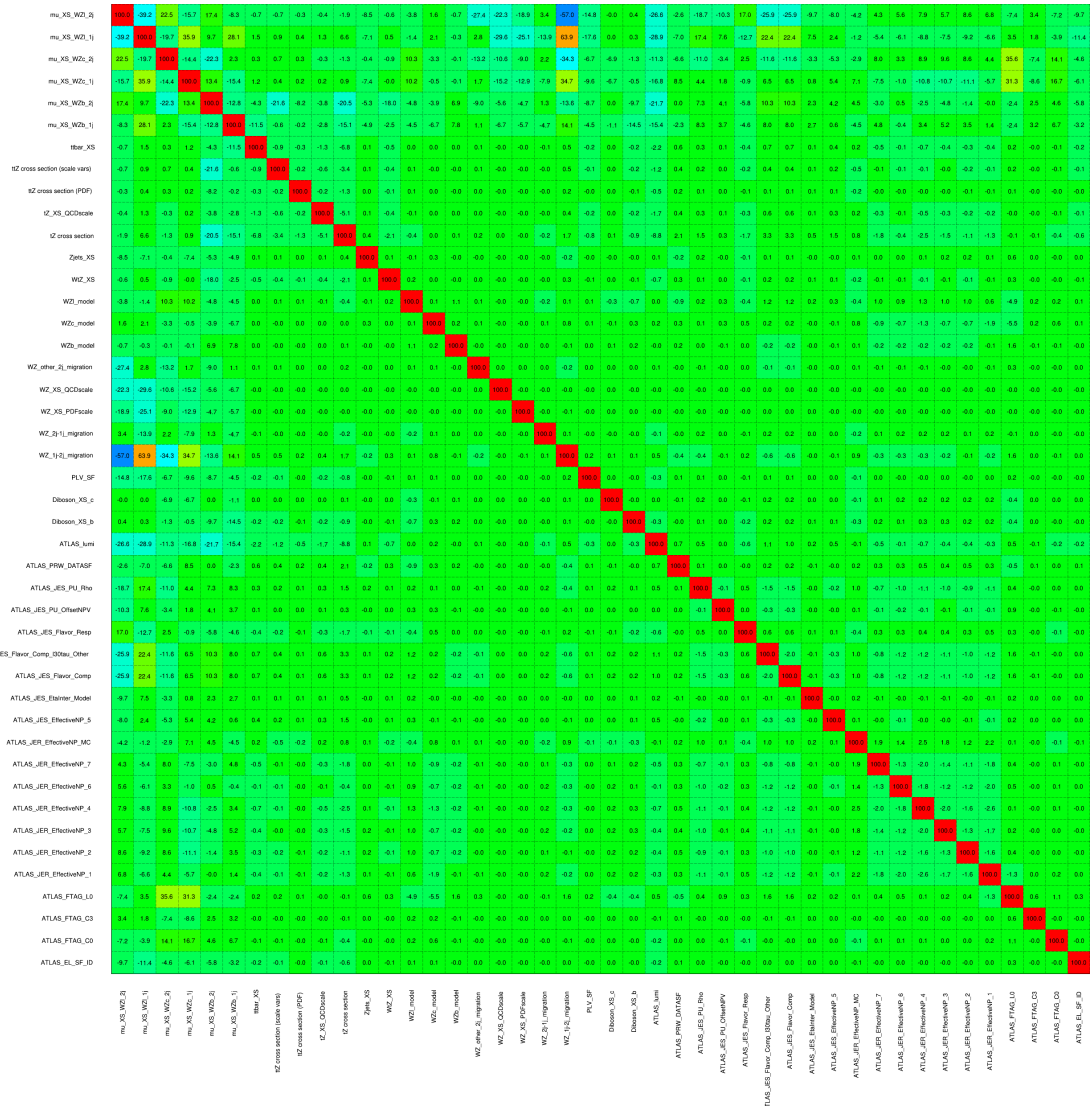


Figure 33: Correlations between nuisance parameters

503 The negative correlations between  $\mu_{WZ+charm}$  and  $\mu_{WZ+b}$  and  $\mu_{WZ+light}$  are expected: WZ +  
 504 charm is present in both the WZ + b and WZ + light enriched regions, therefore increasing the

fraction of charm requires increasing the fraction of  $WZ + b$  and  $WZ + \text{light}$ . This reasoning also explains the positive correlation between  $\mu_{WZ+b}$  and  $\mu_{WZ+\text{light}}$ .

Two of the major backgrounds in the region with the highest purity of  $WZ + b$  are  $tZ$  and Other VV + b, explaining the negative correlations between  $\mu_{WZ+b}$  and the  $tZ$  cross section, and the VV + b cross section.

The high correlation between the luminosity and  $\mu_{WZ+\text{light}}$  arises from the fact that the uncertainty on  $\mu_{WZ+\text{light}}$  is very low (around 4%). Small changes in luminosity cause a change in the yield of  $WZ + \text{light}$  that is large compared to its uncertainty, producing a large correlation between these two parameters.

## 8.2 2-jet Results

**The results of the fit are currently blinded.**

Pre-fit yields in each of the 2-jet fit regions are shown in Figure 8.2.

	2j, <85% WP	2j, 77%-85% WP	2j, 70%-77% WP	2j, 60%-70% WP	2j, >60% WP	tZ CR 2j
$WZ + b - 2j$	$3.1 \pm 1.6$	$6.7 \pm 0.5$	$5.6 \pm 0.4$	$8.0 \pm 0.6$	$31 \pm 2$	$14 \pm 1$
$WZ + c - 2j$	$180 \pm 20$	$54 \pm 6$	$41 \pm 3$	$24 \pm 3$	$11 \pm 2$	$4.8 \pm 0.6$
$WZ + l - 2j$	$1250 \pm 150$	$90 \pm 14$	$18 \pm 3$	$5.8 \pm 1.4$	$1.4 \pm 0.4$	$0.25 \pm 0.15$
$WZ + b - 1j$	$3.4 \pm 0.6$	$1.52 \pm 0.35$	$1.58 \pm 0.23$	$1.95 \pm 0.39$	$6.7 \pm 1.1$	$1.9 \pm 0.6$
$WZ + c - 1j$	$56 \pm 14$	$17.6 \pm 4.0$	$8.6 \pm 2.2$	$6.3 \pm 1.8$	$3.0 \pm 0.9$	$0.7 \pm 0.2$
$WZ + l - 1j$	$427 \pm 120$	$24 \pm 7$	$4.7 \pm 2.3$	$1.6 \pm 0.7$	$0.3 \pm 0.2$	$0.01 \pm 0.01$
$WZ - \text{Other}$	$129 \pm 29$	$6.1 \pm 4.6$	$1.2 \pm 0.3$	$0.3 \pm 0.2$	$2.9 \pm 0.5$	$3.6 \pm 0.6$
Other VV	$7.63 \pm 0.63$	$0.6 \pm 0.5$	$0.16 \pm 0.03$	$0.01 \pm 0.01$	$0.1 \pm 0.1$	$0.1 \pm 0.1$
$ZZ$	$135 \pm 20$	$14.1 \pm 3.2$	$4.7 \pm 0.8$	$4.0 \pm 0.6$	$4.1 \pm 0.7$	$3.1 \pm 0.5$
$t\bar{t}W$	$0.8 \pm 0.2$	$0.4 \pm 0.1$	$0.5 \pm 0.1$	$0.7 \pm 0.2$	$4.3 \pm 0.6$	$3.9 \pm 0.6$
$t\bar{t}Z$	$14.7 \pm 2.2$	$5.6 \pm 0.8$	$4.5 \pm 0.7$	$6.5 \pm 1.1$	$25.4 \pm 4.0$	$21.9 \pm 3.4$
rare Top	$0.14 \pm 0.04$	$0.07 \pm 0.03$	$0.03 \pm 0.02$	$0.09 \pm 0.03$	$0.37 \pm 0.07$	$0.6 \pm 0.1$
$t\bar{t}WW$	$0.04 \pm 0.03$	$0.02 \pm 0.02$	$0.01 \pm 0.01$	$0.01 \pm 0.00$	$0.03 \pm 0.03$	$0.01 \pm 0.01$
$Z + \text{jets}$	$110.0 \pm 22.9$	$9.6 \pm 2.0$	$2.1 \pm 0.50$	$1.6 \pm 0.4$	$5.1 \pm 1.1$	$1.5 \pm 0.3$
$W + \text{jets}$	$0.0 \pm 0.0$	$0.0 \pm 0.0$	$0.0 \pm 0.0$	$0.0 \pm 0.0$	$0.0 \pm 0.0$	$0.0 \pm 0.0$
$V + \gamma$	$25 \pm 18$	$0.5 \pm 0.2$	$0.1 \pm 0.1$	$0.1 \pm 0.1$	$0.0 \pm 0.02$	$0.05 \pm 0.07$
$tZ$	$15.9 \pm 2.9$	$6.9 \pm 1.3$	$5.1 \pm 1.0$	$8.0 \pm 1.5$	$18.7 \pm 3.2$	$36.4 \pm 6.1$
$tW$	$0.9 \pm 0.7$	$0.2 \pm 0.3$	$0.0 \pm 0.1$	$0.0 \pm 0.0$	$0.8 \pm 0.6$	$0.2 \pm 0.2$
$WtZ$	$4.9 \pm 2.5$	$1.5 \pm 0.8$	$1.1 \pm 0.6$	$1.3 \pm 0.7$	$4.6 \pm 2.4$	$3.3 \pm 1.7$
$VVV$	$7.4 \pm 0.3$	$1.0 \pm 0.1$	$0.4 \pm 0.1$	$0.2 \pm 0.1$	$0.13 \pm 0.03$	$0.04 \pm 0.01$
$VH$	$19.5 \pm 4.2$	$2.8 \pm 1.6$	$0.7 \pm 0.7$	$0.1 \pm 0.2$	$0.0 \pm 0.0$	$0.0 \pm 0.0$
$t\bar{t}$	$0.7 \pm 0.4$	$0.1 \pm 0.1$	$0.05 \pm 0.06$	$0.15 \pm 0.13$	$0.8 \pm 0.5$	$2.3 \pm 1.2$
$t\bar{t}$	$6.8 \pm 1.0$	$2.4 \pm 0.5$	$1.8 \pm 0.4$	$3.3 \pm 0.6$	$8.4 \pm 1.2$	$13.6 \pm 1.7$
$t\bar{t}H$	$0.4 \pm 0.1$	$0.2 \pm 0.1$	$0.16 \pm 0.02$	$0.23 \pm 0.03$	$0.94 \pm 0.11$	$1.03 \pm 0.12$
Total	$2580 \pm 160$	$229 \pm 24$	$89 \pm 13$	$69 \pm 11$	$120 \pm 15$	$108 \pm 11$

Table 16: Pre-fit yields in each of the 2-jet fit regions.

<sup>517</sup> The post-fit yields in each region are summarized in Figure 8.2.

	2j, <85% WP	2j, 77%-85% WP	2j, 70%-77% WP	2j, 60%-70% WP	2j, >60% WP	tZ CR 2j
WZ + b	$13 \pm 6$	$6.7 \pm 2.9$	$5.8 \pm 2.5$	$8.0 \pm 3.5$	$31 \pm 13$	$14 \pm 5$
WZ + c	$260 \pm 60$	$77 \pm 15$	$41 \pm 8$	$26 \pm 5$	$10.9 \pm 2.4$	$4.8 \pm 1.1$
WZ + l	$1860 \pm 90$	$90 \pm 12$	$17.6 \pm 2.8$	$5.8 \pm 1.3$	$1.4 \pm 0.4$	$0.3 \pm 0.2$
WZ + b - 1j	$3.4 \pm 0.6$	$1.52 \pm 0.35$	$1.58 \pm 0.23$	$1.95 \pm 0.39$	$6.7 \pm 1.1$	$1.9 \pm 0.6$
WZ + c - 1j	$56 \pm 14$	$17.6 \pm 4.0$	$8.6 \pm 2.2$	$6.3 \pm 1.8$	$3.0 \pm 0.9$	$0.7 \pm 0.2$
WZ + l - 1j	$427 \pm 120$	$24 \pm 7$	$4.7 \pm 2.3$	$1.6 \pm 0.7$	$0.3 \pm 0.2$	$0.01 \pm 0.01$
WZ - Other	$129 \pm 29$	$6.1 \pm 4.6$	$1.2 \pm 0.3$	$0.3 \pm 0.2$	$2.9 \pm 0.5$	$3.6 \pm 0.6$
Other VV	$7.6 \pm 0.6$	$0.3 \pm 0.3$	$0.3 \pm 0.1$	$0.1 \pm 0.06$	$0.03 \pm 0.02$	$0.1 \pm 0.1$
ZZ	$145 \pm 30$	$11.3 \pm 4.4$	$2.7 \pm 1.6$	$1.0 \pm 0.3$	$4.0 \pm 0.1$	$2.4 \pm 0.1$
t̄tW	$0.8 \pm 0.2$	$0.4 \pm 0.1$	$0.54 \pm 0.12$	$0.74 \pm 0.15$	$4.3 \pm 0.6$	$3.9 \pm 0.6$
t̄tZ	$14.7 \pm 2.2$	$5.6 \pm 0.8$	$4.5 \pm 0.7$	$6.5 \pm 1.0$	$25.4 \pm 3.9$	$21.9 \pm 3.3$
rare Top	$0.14 \pm 0.04$	$0.07 \pm 0.03$	$0.03 \pm 0.02$	$0.09 \pm 0.03$	$0.4 \pm 0.1$	$0.6 \pm 0.1$
t̄tWW	$0.04 \pm 0.03$	$0.02 \pm 0.02$	$0.01 \pm 0.01$	$0.01 \pm 0.01$	$0.03 \pm 0.03$	$0.01 \pm 0.01$
Z + jets	$110 \pm 23$	$9.6 \pm 2.0$	$2.1 \pm 0.5$	$1.6 \pm 0.4$	$5.1 \pm 1.1$	$1.5 \pm 0.3$
W + jets	$0.0 \pm 0.0$					
V + γ	$25 \pm 19$	$0.5 \pm 0.2$	$0.1 \pm 0.1$	$0.13 \pm 0.14$	$0.0 \pm 0.02$	$0.05 \pm 0.07$
tZ	$15.9 \pm 2.7$	$6.9 \pm 1.2$	$5.1 \pm 0.9$	$8.0 \pm 1.4$	$18.7 \pm 3.0$	$36 \pm 6$
tW	$0.1 \pm 0.7$	$0.2 \pm 0.3$	$0.0 \pm 0.1$	$0.0 \pm 0.0$	$0.8 \pm 0.6$	$0.2 \pm 0.2$
WtZ	$4.9 \pm 2.5$	$1.5 \pm 0.8$	$1.1 \pm 0.6$	$1.3 \pm 0.7$	$4.6 \pm 2.3$	$3.3 \pm 1.7$
VVV	$7.4 \pm 0.3$	$1.0 \pm 0.1$	$0.36 \pm 0.03$	$0.19 \pm 0.03$	$0.13 \pm 0.03$	$0.04 \pm 0.01$
VH	$19 \pm 4$	$2.8 \pm 1.6$	$0.7 \pm 0.7$	$0.1 \pm 0.2$	$0.0 \pm 0.0$	$0.0 \pm 0.0$
t̄t	$6.8 \pm 1.0$	$2.4 \pm 0.5$	$1.8 \pm 0.4$	$3.3 \pm 0.6$	$8.4 \pm 1.2$	$13.6 \pm 1.7$
t̄tH	$0.40 \pm 0.05$	$0.19 \pm 0.03$	$0.16 \pm 0.02$	$0.23 \pm 0.03$	$0.94 \pm 0.11$	$1.03 \pm 0.11$
Total	$2580 \pm 60$	$229 \pm 11$	$89 \pm 6$	$69.1 \pm 4.1$	$120 \pm 10$	$108 \pm 6$

Table 17: Post-fit yields in each of the 2-jet fit regions.

<sup>518</sup> The same set of systematic uncertainties consider for the 1-jet fit are included in the 2-jet fit as  
<sup>519</sup> well. The impact of the most significant systematic uncertainties is summarized in Table 18.

Uncertainty Source	$\Delta\mu$	
WZ + c 2-jet cross-section	0.19	0.15
WZ 0-jet, $>=3$ -jet cross-section	0.14	-0.14
Luminosity	-0.11	0.12
tZ cross-section	-0.11	0.11
Jet Energy Scale	-0.11	0.11
ttZ cross-section - QCD scale	-0.08	0.09
WZ + l cross-section	0.08	-0.07
WtZ cross-section	-0.07	0.07
Flavor tagging	0.05	0.05
Other VV + b cross-section	-0.05	0.05
Total	0.32	0.36

Table 18: Summary of the most significant sources of systematic uncertainty on the measurement of WZ + b 2-jet events.

520 The ranking and impact of those nuisance parameters with the largest contribution to the overall  
 521 uncertainty is shown in Figure 34.

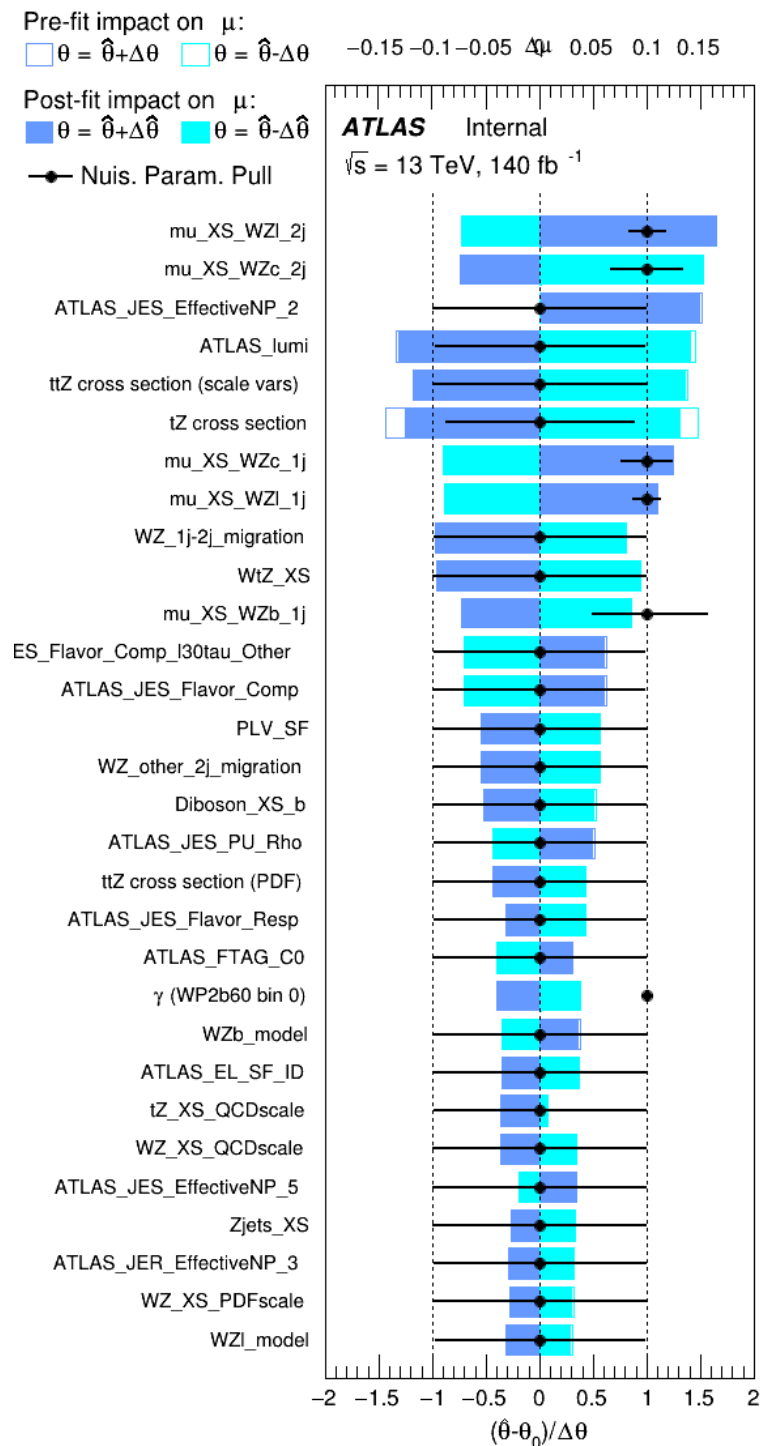


Figure 34: Impact of systematic uncertainties on the signal-strength of  $WZ + b$  in 2-jet events.

522 The large impact of the Jet Energy Scale and Jet Flavor Tagging is unsurprising, as the shape of  
523 the fit regions depends heavily on the modeling of the jets. The other major sources of uncertainty  
524 come from background modelling and cross-section uncertainty.

The correlations between these nuisance parameters are summarized in Figure 35.

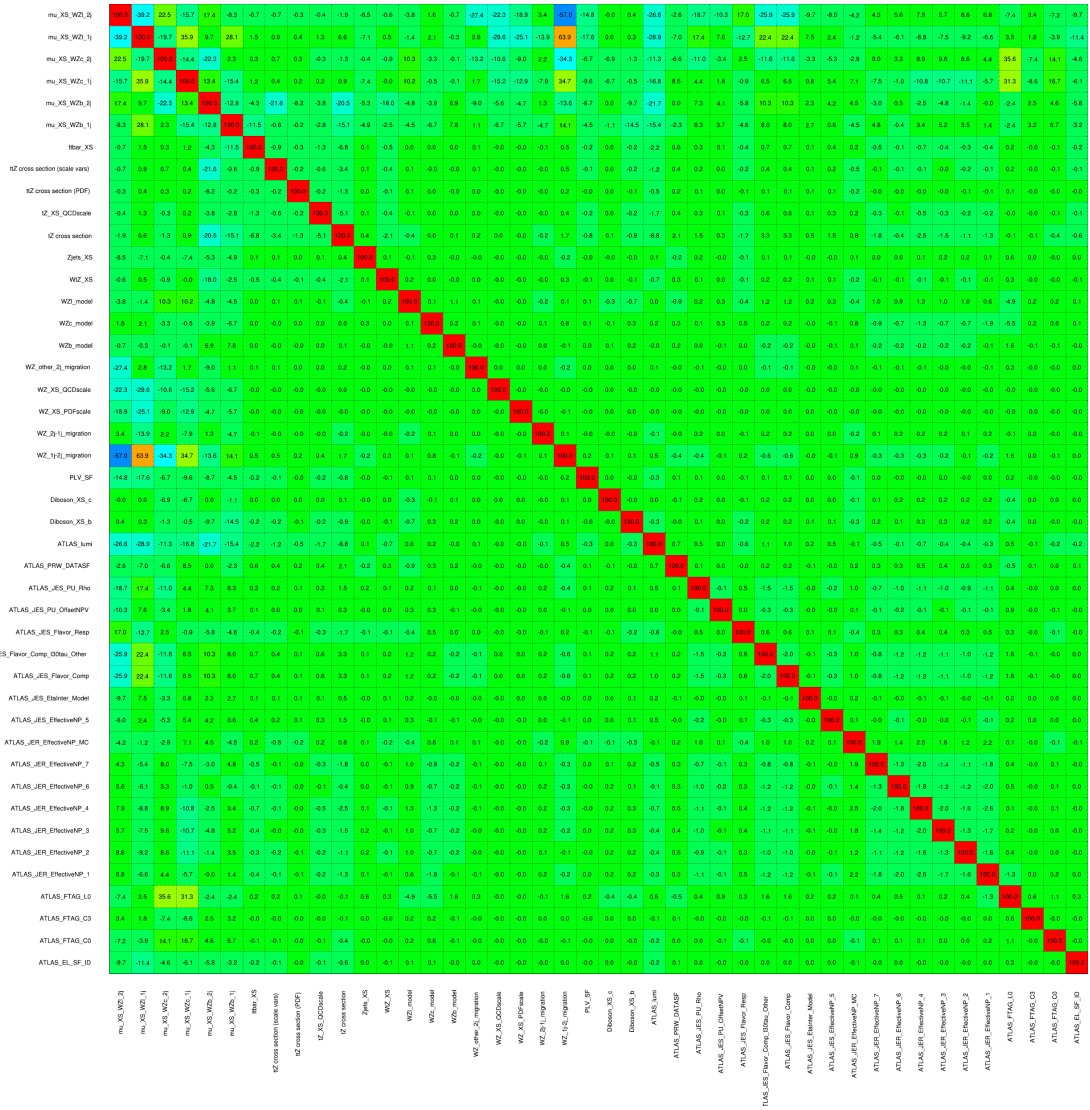


Figure 35: Correlations between nuisance parameters in the 2-jet fit

As in the 1-jet case, no significant, unexpected correlations are found between nuisance parameters.

528 **9 Conclusion**

529 A measurement of  $WZ +$  heavy flavor is performed using  $140 \text{ fb}^{-1}$  of  $\sqrt{s} = 13 \text{ TeV}$  proton-  
 530 proton collision data collected by the ATLAS detector at the LHC. The expected cross-section  
 531 of  $WZ+b$  with 1-jet is  $1.74^{+0.65}_{-0.61}(\text{stat})^{+0.42}_{-0.37}(\text{sys}) \text{ fb}$ , and  $14.6 \pm 2.5(\text{stat}) \pm 2.1(\text{sys}) \text{ fb}$  for  $WZ$   
 532 + charm, with a correlation of -0.23 between them. An expected significance of 2.2 is observed  
 533 for  $WZ + b$  in this region.

534 For the 2-jet regions, an expected significance of 2.6 is observed for  $WZ + b$ , with an expected  
 535 cross-section of  $2.46^{+0.83}_{-0.81}(\text{stat})^{+0.73}_{-0.68}(\text{sys}) \text{ fb}$ . For  $WZ +$  charm, a cross-section of  $12.7 \pm$   
 536  $2.2(\text{stat}) \pm 2.0(\text{sys}) \text{ fb}$  is expected for 2-jet events. A correlation of -0.26 is observed for  $WZ+b$   
 537 and  $WZ +$  charm.

538 **This section will be include final results once unblinded.**

539 **References**

- 540 [1] M. Aaboud et al. ‘Observation of electroweak  $W^\pm Z$  boson pair production in association  
 541 with two jets in  $\text{pp}$  collisions at  $\sqrt{s} = 13 \text{ TeV}$  with the ATLAS detector’. In: *Phys.  
 542 Lett.* B793 (2019), pp. 469–492. doi: [10.1016/j.physletb.2019.05.012](https://doi.org/10.1016/j.physletb.2019.05.012). arXiv:  
 543 [1812.09740 \[hep-ex\]](https://arxiv.org/abs/1812.09740).
- 544 [2] T. Gleisberg et al. ‘Event generation with SHERPA 1.1’. In: *JHEP* 02 (2009), p. 007. doi:  
 545 [10.1088/1126-6708/2009/02/007](https://doi.org/10.1088/1126-6708/2009/02/007). arXiv: [0811.4622 \[hep-ph\]](https://arxiv.org/abs/0811.4622).
- 546 [3] R. D. Ball et al. ‘Parton distributions for the LHC Run II’. In: *JHEP* 04 (2015), p. 040.  
 547 doi: [10.1007/JHEP04\(2015\)040](https://doi.org/10.1007/JHEP04(2015)040). arXiv: [1410.8849 \[hep-ph\]](https://arxiv.org/abs/1410.8849).
- 548 [4] H.-L. Lai et al. ‘New parton distributions for collider physics’. In: *Phys. Rev. D* 82 (2010),  
 549 p. 074024. doi: [10.1103/PhysRevD.82.074024](https://doi.org/10.1103/PhysRevD.82.074024). arXiv: [1007.2241 \[hep-ph\]](https://arxiv.org/abs/1007.2241).
- 550 [5] S. Frixione, G. Ridolfi and P. Nason. ‘A positive-weight next-to-leading-order Monte Carlo  
 551 for heavy flavour hadroproduction’. In: *JHEP* 09 (2007), p. 126. doi: [10.1088/1126-6708/2007/09/126](https://doi.org/10.1088/1126-<br/>
    552 6708/2007/09/126). arXiv: [0707.3088 \[hep-ph\]](https://arxiv.org/abs/0707.3088).
- 553 [6] E. Re. ‘Single-top Wt-channel production matched with parton showers using the POWHEG  
 554 method’. In: *Eur. Phys. J. C* 71 (2011), p. 1547. doi: [10.1140/epjc/s10052-011-1547-z](https://doi.org/10.1140/epjc/s10052-011-<br/>
    555 1547-z). arXiv: [1009.2450 \[hep-ph\]](https://arxiv.org/abs/1009.2450).
- 556 [7] ATLAS Collaboration. *Electron efficiency measurements with the ATLAS detector using  
 557 the 2015 LHC proton–proton collision data*. ATLAS-CONF-2016-024. 2016. URL: <https://cds.cern.ch/record/2157687>.
- 558 [8] ATLAS Collaboration. ‘Measurement of the muon reconstruction performance of the  
 559 ATLAS detector using 2011 and 2012 LHC proton–proton collision data’. In: *Eur. Phys.  
 560 J. C* 74 (2014), p. 3130. doi: [10.1140/epjc/s10052-014-3130-x](https://doi.org/10.1140/epjc/s10052-014-3130-x). arXiv: [1407.3935  
 561 \[hep-ex\]](https://arxiv.org/abs/1407.3935).

- 563 [9] *Evidence for the associated production of the Higgs boson and a top quark pair with the*  
 564 *ATLAS detector.* Tech. rep. ATLAS-CONF-2017-077. Geneva: CERN, Nov. 2017. URL:  
 565 <https://cds.cern.ch/record/2291405>.
- 566 [10] ATLAS Collaboration. *Jet Calibration and Systematic Uncertainties for Jets Reconstructed in the ATLAS Detector at  $\sqrt{s} = 13$  TeV.* ATL-PHYS-PUB-2015-015. 2015. URL:  
 567 <https://cds.cern.ch/record/2037613>.
- 569 [11] ATLAS Collaboration. *Selection of jets produced in 13 TeV proton–proton collisions with*  
 570 *the ATLAS detector.* ATLAS-CONF-2015-029. 2015. URL: <https://cds.cern.ch/record/2037702>.
- 572 [12] ATLAS Collaboration. ‘Performance of pile-up mitigation techniques for jets in pp col-  
 573 lisions at  $\sqrt{s} = 8$  TeV using the ATLAS detector’. In: *Eur. Phys. J. C* 76 (2016), p. 581.  
 574 DOI: [10.1140/epjc/s10052-016-4395-z](https://doi.org/10.1140/epjc/s10052-016-4395-z). arXiv: [1510.03823](https://arxiv.org/abs/1510.03823) [hep-ex].
- 575 [13] ATLAS Collaboration. *Performance of missing transverse momentum reconstruction with*  
 576 *the ATLAS detector in the first proton–proton collisions at  $\sqrt{s} = 13$  TeV.* ATL-PHYS-  
 577 PUB-2015-027. 2015. URL: <https://cds.cern.ch/record/2037904>.
- 578 [14] 2021. URL: [https://twiki.cern.ch/twiki/bin/view/AtlasProtected/BTagCalibrationRecommendationsRelease21#Tools\\_for\\_Flavor\\_Tagging\\_Calibra](https://twiki.cern.ch/twiki/bin/view/AtlasProtected/BTagCalibrationRecommendationsRelease21#Tools_for_Flavor_Tagging_Calibra).
- 581 [15] P. S. A. Hoecker. ‘TMVA 4 Toolkit for Multivariate Data Analysis with ROOT’. In:  
 582 *arXiv:physics/0703039* (2013).
- 583 [16] F. Cardillo et al. ‘Measurement of the fiducial and differential cross-section of a top quark  
 584 pair in association with a Z boson at 13 TeV with the ATLAS detector’. In: ATL-COM-  
 585 PHYS-2019-334 (Apr. 2019). URL: <https://cds.cern.ch/record/2672207>.
- 586 [17] T. Chen and C. Guestrin. ‘XGBoost: A Scalable Tree Boosting System’. In: *Proceedings*  
 587 *of the 22nd ACM SIGKDD International Conference on Knowledge Discovery and Data*  
 588 *Mining.* KDD ’16. San Francisco, California, USA: ACM, 2016, pp. 785–794. ISBN: 978-  
 589 1-4503-4232-2. DOI: [10.1145/2939672.2939785](https://doi.acm.org/10.1145/2939672.2939785). URL: <http://doi.acm.org/10.1145/2939672.2939785>.
- 591 [18] ATLAS Collaboration. ‘Luminosity determination in pp collisions at  $\sqrt{s} = 7$  TeV using  
 592 the ATLAS detector at the LHC’. In: *Eur. Phys. J. C* 71 (2011), p. 1630. DOI: [10.1140/epjc/s10052-011-1630-5](https://doi.org/10.1140/epjc/s10052-011-1630-5). arXiv: [1101.2185](https://arxiv.org/abs/1101.2185) [hep-ex].
- 594 [19] G. Avoni et al. ‘The new LUCID-2 detector for luminosity measurement and monitoring in  
 595 ATLAS’. In: *JINST* 13.07 (2018), P07017. DOI: [10.1088/1748-0221/13/07/P07017](https://doi.org/10.1088/1748-0221/13/07/P07017).
- 596 [20] G. Aad et al. ‘Jet energy resolution in proton-proton collisions at  $\sqrt{s} = 7$  TeV recorded  
 597 in 2010 with the ATLAS detector’. In: *The European Physical Journal C* 73.3 (Mar.  
 598 2013), p. 2306. ISSN: 1434-6052. DOI: [10.1140/epjc/s10052-013-2306-0](https://doi.org/10.1140/epjc/s10052-013-2306-0). URL:  
 599 <https://doi.org/10.1140/epjc/s10052-013-2306-0>.
- 600 [21] A. Collaboration. ‘Performance of b -jet identification in the ATLAS experiment’. In:  
 601 *Journal of Instrumentation* 11.04 (2016), P04008. URL: <http://stacks.iop.org/1748-0221/11/i=04/a=P04008>.

- 603 [22] ‘Observation of the associated production of a top quark and a Z boson at 13 TeV with  
604 ATLAS’. In: (July 2020). URL: <https://cds.cern.ch/record/2722504>.

605 **Appendices**

606 **.1 tZ Interference Studies**

607 Because it includes an on-shell Z boson as well as a b-jet and W from the top decay, tZ  
608 production represents an identical final state to WZ + b-jet. This implies the possibility of matrix  
609 level interference between these two processes not accounted for in the Monte Carlo simulations,  
610 which consider the two processes independently. Truth level studies are performed in order to  
611 estimate the impact of these interference effects.

612 In order to estimate the matrix level interference effects between tZ and WZ + b-jet, two different  
613 sets of simulations are produced using MadGraph 5 [**Madgraph**] - one which simulates these  
614 two processes independently, and another where they are produced simultaneously, such that  
615 interference effects are present. These two sets of samples are then compared, and the difference  
616 between them can be taken to represent any interference effects.

617 MadGraph simulations of 10,000 tZ and 10,000 WZ + b-jet events are produced, along with  
618 20,000 events where both are present, in the fiducial region where three leptons and at least one  
619 jet are produced.

620 A selection mimicking the preselection used in the main analysis is applied to the samples: The  
621 SS leptons are required to have  $p_T > 20$  GeV, and  $> 10$  GeV is required for the OS lepton. The  
622 associated b-jet is required to have  $p_T > 25$  GeV, and all physics objects are required to fall in a  
623 range of  $|\eta| < 2.5$ .

624 The kinematics of these samples after the selection has been applied are shown below:

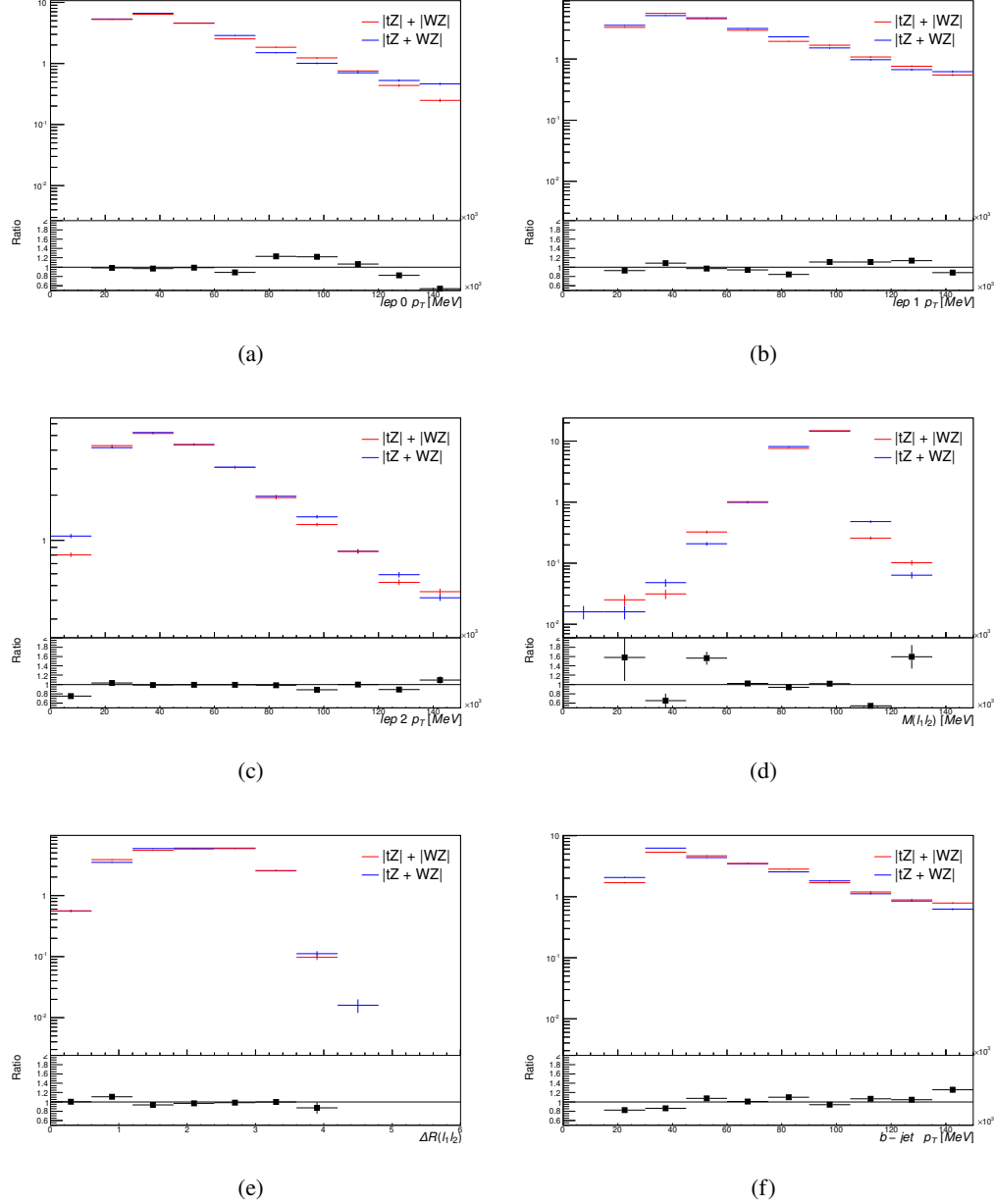


Figure 36: Comparisons between (a) the  $p_T$  of the lepton from the W, (b) and (c) show the  $p_T$  of the lepton from the Z, (d) the invariant mass of the Z-candidate, (e)  $\Delta R$  of the leptons from the Z, and (f) the  $p_T$  of the b-jet, for WZ and tZ events generated with interference effects (blue) and without interference effects (red).

625 The overall cross-section of the two methods agree within error, and no significant differences  
626 in the kinematic distributions are seen. It is therefore concluded that interference effects do not

627 significantly impact the results.

628 **.2 Alternate tZ Inclusive Fit**

629 While tZ is often considered as a distinct process from WZ + b, this could also be considered part  
 630 of the signal. Alternate studies are performed where, using the same framework as the nominal  
 631 analysis, a measurement of WZ + b is performed that includes tZ as part of WZ+b.

632 Because of this change, the tZ CR is no longer necessary, and only the five pseudo-continuous  
 633 b-tag regions are used in the fit. Further, systematics related to the tZ cross-section are removed  
 634 from the fit, as they are now encompassed by the normalization measurement of WZ + b. All  
 635 other systematic uncertainties are carried over from the nominal analysis.

636 A post-fit summary of the 1-jet regions used in the fit are shown in Figure 37.

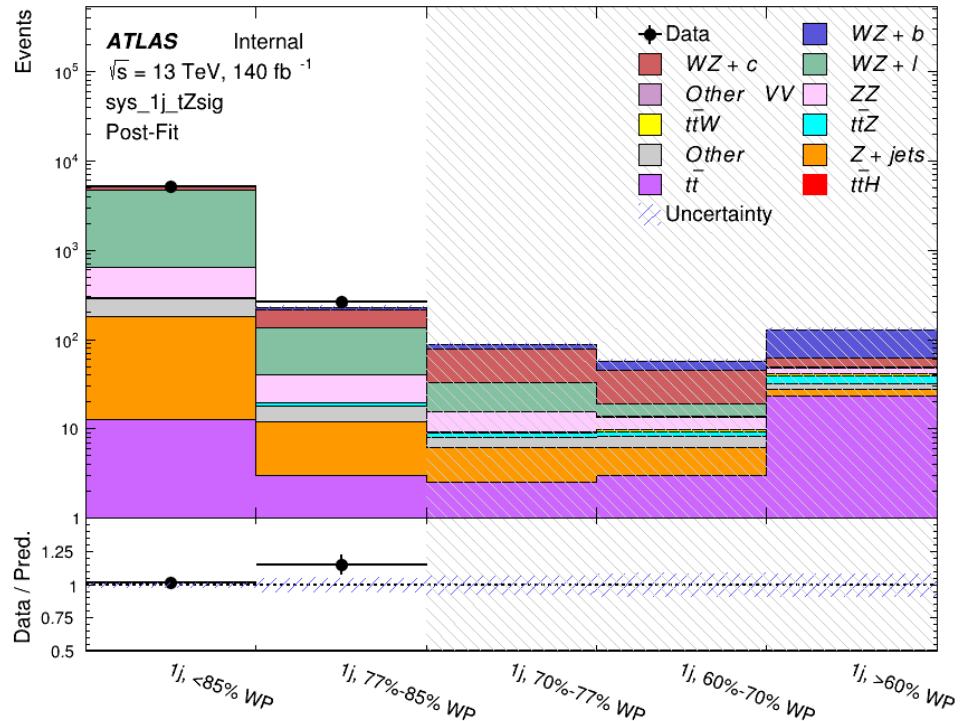


Figure 37: Post-fit summary of the 1-jet fit regions.

637 An expected WZ + b cross-section of  $4.1^{+0.78}_{-0.74}(\text{stat})^{+0.53}_{-0.52}(\text{sys}) \text{ fb}$  is extracted from the fit, with  
 638 an expected significance of  $4.0\sigma$ .

639 The impact of the predominate systematics are summarized in Table 19.

Uncertainty Source	$\Delta\mu$	
WZ + light cross-section	0.08	-0.08
Jet Energy Scale	-0.06	0.08
Luminosity	-0.05	0.06
WZ + charm cross-section	-0.04	0.05
Other Diboson + b cross-section	-0.04	0.04
WZ cross-section - QCD scale	-0.04	0.03
t <bar>t</bar>	-0.03	0.03
Jet Energy Resolution	-0.03	0.03
Flavor tagging	-0.03	0.03
Z+jets cross section	-0.02	0.02
Total Systematic Uncertainty	-0.15	0.16

Table 19: Summary of the most significant sources of systematic uncertainty on the measurement of WZ + b with exactly one associated jet.

640 A post-fit summary of the 2-jet regions used in the fit are shown in Figure 38.

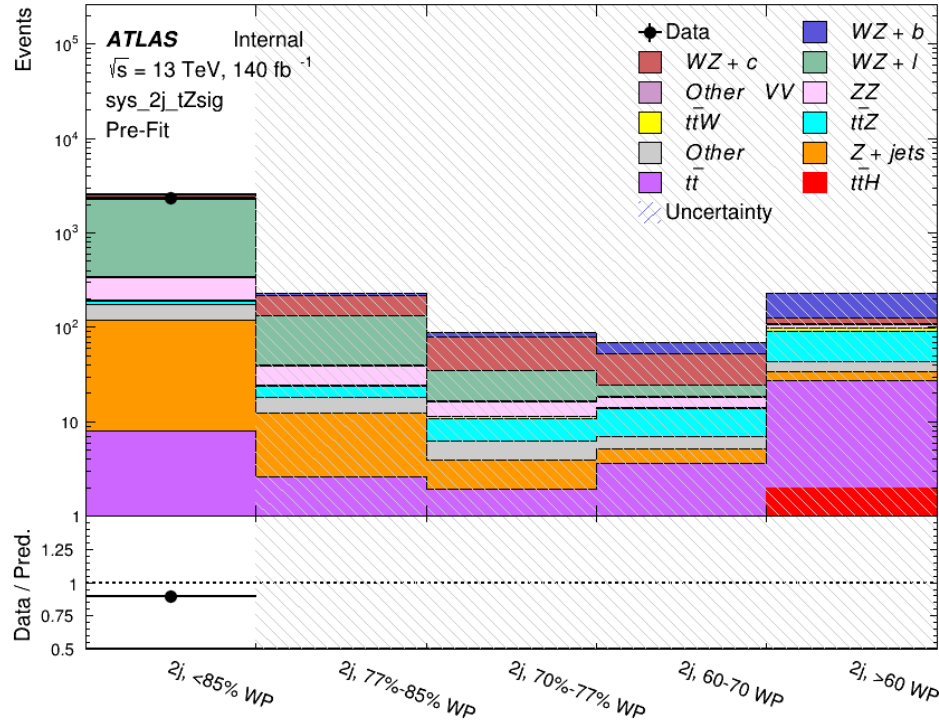


Figure 38: Post-fit summary of the 2-jet fit regions.

641 An expected WZ + b cross-section of  $5.9^{+0.9}_{-0.9}(\text{stat})^{+0.9}_{-0.8}(\text{sys}) \text{ fb}$  is extracted from the fit, with an

<sup>642</sup> expected significance of  $5.3\sigma$ .

<sup>643</sup> The impact of the predominate systematics are summarized in Table 20.

Uncertainty Source	$\Delta\mu$	
Luminosity	-0.07	0.07
Jet Energy Scale	0.06	0.05
ttZ cross-section - QCD scale	-0.05	0.05
WZ+l cross-section	0.05	-0.05
WZ+c cross-section	-0.03	0.05
WtZ cross-section	-0.03	0.03
WZ cross-section QCDscale	-0.03	0.03
Diboson cross-section b	-0.03	0.03
WZ cross-section - PDF	-0.03	0.03
Flavor Tagging	0.03	0.02
Total Systematic Uncertainty	-0.14	0.16

Table 20: Summary of the most significant sources of systematic uncertainty on the measurement of WZ + b with exactly one associated jet.

644 .3 DSID list

Data:

```

data15_13TeV.AllYear.physics_Main.PhysCont.DAOD_HIGG8D1.grp15_v01_p4134
data16_13TeV.AllYear.physics_Main.PhysCont.DAOD_HIGG8D1.grp16_v01_p4134
data17_13TeV.AllYear.physics_Main.PhysCont.DAOD_HIGG8D1.grp17_v01_p4134
data18_13TeV.AllYear.physics_Main.PhysCont.DAOD_HIGG8D1.grp18_v01_p4134

mc16a:
mc16_13TeV.361603.PowhegPy8EG_CT10nloME_AZNLOCTEQ6L1_ZZllll_mll4.deriv.DAOD_HIGG8D1.e4475_s3126_r9364_r9315_p4133
mc16_13TeV.361602.PowhegPy8EG_CT10nloME_AZNLOCTEQ6L1_WZlvvv_mll4.deriv.DAOD_HIGG8D1.e4054_s3126_r9364_r9315_p4133
mc16_13TeV.361604.PowhegPy8EG_CT10nloME_AZNLOCTEQ6L1_ZZvvll_mll4.deriv.DAOD_HIGG8D1.e4475_s3126_r9364_r9315_p4133
mc16_13TeV.361600.PowhegPy8EG_CT10nloME_AZNLOCTEQ6L1_WWlqlv.deriv.DAOD_HIGG8D1.e4616_s3126_r9364_r9315_p4133
mc16_13TeV.361605.PowhegPy8EG_CT10nloME_AZNLOCTEQ6L1_ZZvvvv_mll4.deriv.DAOD_HIGG8D1.e4054_s3126_s3136_r9364_r9315_p4133
mc16_13TeV.361601.PowhegPy8EG_CT10nloME_AZNLOCTEQ6L1_WZlqlj_mll4.deriv.DAOD_HIGG8D1.e4475_s3126_r9364_r9315_p4133
mc16_13TeV.364286.Sherpa_222_NNPDF30NNLO_llvjj_ss_EW4.deriv.DAOD_HIGG8D1.e6055_e5984_s3126_r9364_r9315_p3983 mc16_13TeV.364285.Sherpa_222_NNPDF30NNLO_llvjj_ss_EW4.deriv.DAOD_HIGG8D1.e6055_e5984_s3126_r9364_r9315_p4133
mc16_13TeV.364740.MGPy8EG_NNPDF30NLO_A14NNPDF23LO_llvjj_EW6_OFPlus.deriv.DAOD_HIGG8D1.e7421_e5984_s3126_r9364_r9315_p4133
mc16_13TeV.364742.MGPy8EG_NNPDF30NLO_A14NNPDF23LO_llvjj_EW6_SFPlus.deriv.DAOD_HIGG8D1.e7421_e5984_s3126_r9364_r9315_p4133
mc16_13TeV.364253.Sherpa_222_NNPDF30NNLO_lllv.deriv.DAOD_HIGG8D1.e5916_s3126_r9364_r9315_p4133
mc16_13TeV.364250.Sherpa_222_NNPDF30NNLO_llll.deriv.DAOD_HIGG8D1.e5894_s3126_r9364_r9315_p4133
mc16_13TeV.364254.Sherpa_222_NNPDF30NNLO_llvv.deriv.DAOD_HIGG8D1.e5916_s3126_r9364_r9315_p4133
mc16_13TeV.364255.Sherpa_222_NNPDF30NNLO_llvvv.deriv.DAOD_HIGG8D1.e5916_s3126_r9364_r9315_p4133
mc16_13TeV.410155.aMcAtNloPythia8EvtGen_MEN30NLO_A14N23LO_ttW.deriv.DAOD_HIGG8D1.e5070_s3126_r9364_r9315_p4133
mc16_13TeV.410156.aMcAtNloPythia8EvtGen_MEN30NLO_A14N23LO_ttZnunu.deriv.DAOD_HIGG8D1.e5070_s3126_r9364_r9315_p4133
mc16_13TeV.410157.aMcAtNloPythia8EvtGen_MEN30NLO_A14N23LO_ttZqq.deriv.DAOD_HIGG8D1.e5070_s3126_r9364_r9315_p4133
mc16_13TeV.410218.aMcAtNloPythia8EvtGen_MEN30NLO_A14N23LO_ttee.deriv.DAOD_HIGG8D1.e5070_s3126_r9364_r9315_p4133
mc16_13TeV.410219.aMcAtNloPythia8EvtGen_MEN30NLO_A14N23LO_ttmumu.deriv.DAOD_HIGG8D1.e5070_s3126_r9364_r9315_p4133
mc16_13TeV.410220.aMcAtNloPythia8EvtGen_MEN30NLO_A14N23LO_ttautau.deriv.DAOD_HIGG8D1.e5070_s3126_r9364_r9315_p4133
mc16_13TeV.410276.aMcAtNloPythia8EvtGen_MEN30NLO_A14N23LO_ttee_mll_1_5.deriv.DAOD_HIGG8D1.e6087_e5984_s3126_r9364_r9315_p4133
mc16_13TeV.410277.aMcAtNloPythia8EvtGen_MEN30NLO_A14N23LO_ttmumu_mll_1_5.deriv.DAOD_HIGG8D1.e6087_e5984_s3126_r9364_r9315_p4133
mc16_13TeV.410278.aMcAtNloPythia8EvtGen_MEN30NLO_A14N23LO_ttautau_mll_1_5.deriv.DAOD_HIGG8D1.e6087_e5984_s3126_r9364_r9315_p4133
mc16_13TeV.410397.MadGraphPythia8EvtGen_ttbar_wbee_MEN30LO_A14N23LO.deriv.DAOD_HIGG8D1.e6086_e5984_s3126_r9364_r9315_p4133
mc16_13TeV.410398.MadGraphPythia8EvtGen_ttbar_wbmumu_MEN30LO_A14N23LO.deriv.DAOD_HIGG8D1.e6086_e5984_s3126_r9364_r9315_p4133
mc16_13TeV.410399.MadGraphPythia8EvtGen_ttbar_wbtautau_MEN30LO_A14N23LO.deriv.DAOD_HIGG8D1.e6086_e5984_s3126_r9364_r9315_p4133
mc16_13TeV.410658.PhPy8EG_A14_tchan_BW50_lept_top.deriv.DAOD_HIGG8D1.e6671_e5984_s3126_r9364_r9315_p4133
mc16_13TeV.410659.PhPy8EG_A14_tchan_BW50_lept_antitop.deriv.DAOD_HIGG8D1.e6671_e5984_s3126_r9364_r9315_p4133
mc16_13TeV.410644.PowhegPythia8EvtGen_A14_singletop_schan_lept_top.deriv.DAOD_HIGG8D1.e65271_e5984_s3126_r9364_r9315_p4133
mc16_13TeV.410645.PowhegPythia8EvtGen_A14_singletop_schan_lept_antitop.deriv.DAOD_HIGG8D1.e65271_e5984_s3126_r9364_r9315_p4133
mc16_13TeV.304014.MadGraphPythia8EvtGen_A14NNPDF23_3top_SM.deriv.DAOD_HIGG8D1.e4324_s3126_r9364_r9315_p4133
mc16_13TeV.410080.MadGraphPythia8EvtGen_A14NNPDF23_4topSM.deriv.DAOD_HIGG8D1.e4111_s3126_r9364_r9315_p4133
mc16_13TeV.410081.MadGraphPythia8EvtGen_A14NNPDF23_ttbarWW.deriv.DAOD_HIGG8D1.e4111_s3126_r9364_r9315_p4133
mc16_13TeV.364100.Sherpa_221_NNPDF30NNLO_Zmmumu_MAXHTPTV0_70_CVetoBVeto.deriv.DAOD_HIGG8D1.e5271_s3126_r9364_r9315_p4133
mc16_13TeV.364101.Sherpa_221_NNPDF30NNLO_Zmmumu_MAXHTPTV0_70_CFilterBVeto.deriv.DAOD_HIGG8D1.e5271_s3126_r9364_r9315_p4133
mc16_13TeV.364102.Sherpa_221_NNPDF30NNLO_Zmmumu_MAXHTPTV0_70_BFilter.deriv.DAOD_HIGG8D1.e5271_s3126_r9364_r9315_p4133
mc16_13TeV.364103.Sherpa_221_NNPDF30NNLO_Zmmumu_MAXHTPTV0_140_CVetoBVeto.deriv.DAOD_HIGG8D1.e5271_s3126_r9364_r9315_p4133
mc16_13TeV.364104.Sherpa_221_NNPDF30NNLO_Zmmumu_MAXHTPTV0_140_CFilterBVeto.deriv.DAOD_HIGG8D1.e5271_s3126_r9364_r9315_p4133
mc16_13TeV.364106.Sherpa_221_NNPDF30NNLO_Zmmumu_MAXHTPTV140_280_CVetoBVeto.deriv.DAOD_HIGG8D1.e5271_s3126_r9364_r9315_p4133
mc16_13TeV.364107.Sherpa_221_NNPDF30NNLO_Zmmumu_MAXHTPTV140_280_CFilterBVeto.deriv.DAOD_HIGG8D1.e5271_s3126_r9364_r9315_p4133
mc16_13TeV.364108.Sherpa_221_NNPDF30NNLO_Zmmumu_MAXHTPTV140_280_BFilter.deriv.DAOD_HIGG8D1.e5271_s3126_r9364_r9315_p4133
mc16_13TeV.364109.Sherpa_221_NNPDF30NNLO_Zmmumu_MAXHTPTV280_500_CVetoBVeto.deriv.DAOD_HIGG8D1.e5271_s3126_r9364_r9315_p4133
mc16_13TeV.364110.Sherpa_221_NNPDF30NNLO_Zmmumu_MAXHTPTV280_500_CFilterBVeto.deriv.DAOD_HIGG8D1.e5271_s3126_r9364_r9315_p4133
mc16_13TeV.364111.Sherpa_221_NNPDF30NNLO_Zmmumu_MAXHTPTV280_500_BFilter.deriv.DAOD_HIGG8D1.e5271_s3126_r9364_r9315_p4133
mc16_13TeV.364111.Sherpa_221_NNPDF30NNLO_Zmmumu_MAXHTPTV280_500_BFilter.deriv.DAOD_HIGG8D1.e5271_s3126_r9364_r9315_p4133
mc16_13TeV.364112.Sherpa_221_NNPDF30NNLO_Zmmumu_MAXHTPTV500_1000.deriv.DAOD_HIGG8D1.e5271_s3126_r9364_r9315_p4133
mc16_13TeV.364113.Sherpa_221_NNPDF30NNLO_Zmmumu_MAXHTPTV1000_E_CMS.deriv.DAOD_HIGG8D1.e5271_s3126_r9364_r9315_p4133
mc16_13TeV.364114.Sherpa_221_NNPDF30NNLO_Zee_MAXHTPTV0_70_CVetoBVeto.deriv.DAOD_HIGG8D1.e5299_s3126_r9364_r9315_p4133
mc16_13TeV.364115.Sherpa_221_NNPDF30NNLO_Zee_MAXHTPTV0_70_CFilterBVeto.deriv.DAOD_HIGG8D1.e5299_s3126_r9364_r9315_p4133
mc16_13TeV.364116.Sherpa_221_NNPDF30NNLO_Zee_MAXHTPTV0_70_BFilter.deriv.DAOD_HIGG8D1.e5299_s3126_r9364_r9315_p4133
mc16_13TeV.364117.Sherpa_221_NNPDF30NNLO_Zee_MAXHTPTV70_140_CVetoBVeto.deriv.DAOD_HIGG8D1.e5299_s3126_r9364_r9315_p4133
mc16_13TeV.364118.Sherpa_221_NNPDF30NNLO_Zee_MAXHTPTV70_140_CFilterBVeto.deriv.DAOD_HIGG8D1.e5299_s3126_r9364_r9315_p4133
mc16_13TeV.364119.Sherpa_221_NNPDF30NNLO_Zee_MAXHTPTV70_140_BFilter.deriv.DAOD_HIGG8D1.e5299_s3126_r9364_r9315_p4133
mc16_13TeV.364120.Sherpa_221_NNPDF30NNLO_Zee_MAXHTPTV140_280_CVetoBVeto.deriv.DAOD_HIGG8D1.e5299_s3126_r9364_r9315_p4133
mc16_13TeV.364121.Sherpa_221_NNPDF30NNLO_Zee_MAXHTPTV140_280_CFilterBVeto.deriv.DAOD_HIGG8D1.e5299_s3126_r9364_r9315_p4133
mc16_13TeV.364122.Sherpa_221_NNPDF30NNLO_Zee_MAXHTPTV140_280_BFilter.deriv.DAOD_HIGG8D1.e5299_s3126_r9364_r9315_p4133

```





mc16\_13TeV.364535.Sherpa\_222\_NNPDF30NNLO\_taunugamma\_pty\_140\_E\_CMS.deriv.DAOD\_HIGG8D1.e5928\_s3126\_r9364\_r9315\_p4133  
 mc16\_13TeV.364535.Sherpa\_222\_NNPDF30NNLO\_taunugamma\_pty\_140\_E\_CMS.deriv.DAOD\_HIGG8D1.e5928\_e5984\_s3126\_r9364\_r9315\_p4133  
 mc16\_13TeV.410560.MadGraphPythia8EvtGen\_A14\_Z\_4fl\_tchan\_noAllHad.deriv.DAOD\_HIGG8D1.e5803\_s3126\_r9364\_r9315\_p4133  
 mc16\_13TeV.410013.PowhegPythiaEvtGen\_P2012\_Wt\_inclusive\_top.deriv.DAOD\_HIGG8D1.e3753\_s3126\_r9364\_r9315\_p4133  
 mc16\_13TeV.410014.PowhegPythiaEvtGen\_P2012\_Wt\_inclusive\_antitop.deriv.DAOD\_HIGG8D1.e3753\_s3126\_r9364\_r9315\_p4133  
 mc16\_13TeV.410408.aMcAtNloPythia8EvtGen\_tWZ\_Ztoll\_minDR1.deriv.DAOD\_HIGG8D1.e6423\_e5984\_s3126\_r9364\_r9315\_p4133  
 mc16\_13TeV.364242.Sherpa\_222\_NNPDF30NNLO\_WWW\_3l3v\_EW6.deriv.DAOD\_HIGG8D1.e5887\_s3126\_r9364\_r9315\_p4133  
 mc16\_13TeV.364243.Sherpa\_222\_NNPDF30NNLO\_WWZ\_4l2v\_EW6.deriv.DAOD\_HIGG8D1.e5887\_s3126\_r9364\_r9315\_p4133  
 mc16\_13TeV.364244.Sherpa\_222\_NNPDF30NNLO\_WWZ\_2l4v\_EW6.deriv.DAOD\_HIGG8D1.e5887\_s3126\_r9364\_r9315\_p4133  
 mc16\_13TeV.364245.Sherpa\_222\_NNPDF30NNLO\_WZZ\_5l1v\_EW6.deriv.DAOD\_HIGG8D1.e5887\_s3126\_r9364\_r9315\_p4133  
 mc16\_13TeV.364246.Sherpa\_222\_NNPDF30NNLO\_WZZ\_3l3v\_EW6.deriv.DAOD\_HIGG8D1.e5887\_s3126\_r9364\_r9315\_p4133  
 mc16\_13TeV.364247.Sherpa\_222\_NNPDF30NNLO\_ZZZ\_6l0v\_EW6.deriv.DAOD\_HIGG8D1.e5887\_s3126\_r9364\_r9315\_p4133  
 mc16\_13TeV.364248.Sherpa\_222\_NNPDF30NNLO\_ZZZ\_4l2v\_EW6.deriv.DAOD\_HIGG8D1.e5887\_s3126\_r9364\_r9315\_p4133  
 mc16\_13TeV.364249.Sherpa\_222\_NNPDF30NNLO\_ZZZ\_2l4v\_EW6.deriv.DAOD\_HIGG8D1.e5887\_s3126\_r9364\_r9315\_p4133  
 mc16\_13TeV.342284.Pythia8EvtGen\_A14NNPDF23LO\_WH125\_inc.deriv.DAOD\_HIGG8D1.e4246\_s3126\_r9364\_r9315\_p4133  
 mc16\_13TeV.342285.Pythia8EvtGen\_A14NNPDF23LO\_ZH125\_inc.deriv.DAOD\_HIGG8D1.e4246\_s3126\_r9364\_r9315\_p4133  
 mc16\_13TeV.341998.aMcAtNloHppEG\_UEEE5\_CTEQ6L1\_CT10ME\_tWH125\_gamgam\_yt\_plus1.deriv.DAOD\_HIGG8D1.e4394\_e5984\_s3126\_r9364\_r9315\_p4133  
 mc16\_13TeV.410389.MadGraphPythia8EvtGen\_A14NNPDF23\_tgamma\_nonallhadronic.deriv.DAOD\_HIGG8D1.e6155\_e5984\_s3126\_r9364\_r9315\_p4133  
 mc16\_13TeV.410470.PhPy8EG\_A14\_ttbar\_hdamp258p75\_nonallhad.deriv.DAOD\_HIGG8D1.e6337\_e5984\_s3126\_r9364\_r9315\_p4133  
 mc16\_13TeV.410472.PhPy8EG\_A14\_ttbar\_hdamp258p75\_dil.deriv.DAOD\_HIGG8D1.e6348\_e5984\_s3126\_r9364\_r9315\_p4133  
 mc16\_13TeV.346343.PhPy8EG\_A14NNPDF23\_NNPDF30ME\_ttH125\_allhad.deriv.DAOD\_HIGG8D1.e7148\_e5984\_s3126\_r9364\_r9315\_p4133  
 mc16\_13TeV.346344.PhPy8EG\_A14NNPDF23\_NNPDF30ME\_ttH125\_semilep.deriv.DAOD\_HIGG8D1.e7148\_e5984\_s3126\_r9364\_r9315\_p4133  
 mc16\_13TeV.346345.PhPy8EG\_A14NNPDF23\_NNPDF30ME\_ttH125\_dilep.deriv.DAOD\_HIGG8D1.e7148\_e5984\_s3126\_r9364\_r9315\_p4133  
  
 mc16d:  
 mc16\_13TeV.364253.Sherpa\_222\_NNPDF30NNLO\_lllv.deriv.DAOD\_HIGG8D1.e5916\_e5984\_s3126\_r10201\_r10210\_p4133  
 mc16\_13TeV.364250.Sherpa\_222\_NNPDF30NNLO\_llll.deriv.DAOD\_HIGG8D1.e5894\_e5984\_s3126\_r10201\_r10210\_p4133  
 mc16\_13TeV.364254.Sherpa\_222\_NNPDF30NNLO\_llvv.deriv.DAOD\_HIGG8D1.e5916\_e5984\_s3126\_r10201\_r10210\_p4133  
 mc16\_13TeV.364255.Sherpa\_222\_NNPDF30NNLO\_lvvv.deriv.DAOD\_HIGG8D1.e5916\_e5984\_s3126\_r10201\_r10210\_p4133  
 mc16\_13TeV.410155.aMcAtNloPythia8EvtGen\_MEN30NLO\_A14N23LO\_ttW.deriv.DAOD\_HIGG8D1.e5070\_e5984\_s3126\_r10201\_r10210\_p4133  
 mc16\_13TeV.410156.aMcAtNloPythia8EvtGen\_MEN30NLO\_A14N23LO\_ttZnunu.deriv.DAOD\_HIGG8D1.e5070\_e5984\_s3126\_r10201\_r10210\_p4133  
 mc16\_13TeV.410157.aMcAtNloPythia8EvtGen\_MEN30NLO\_A14N23LO\_ttZqq.deriv.DAOD\_HIGG8D1.e5070\_e5984\_s3126\_r10201\_r10210\_p4133  
 mc16\_13TeV.410218.aMcAtNloPythia8EvtGen\_MEN30NLO\_A14N23LO\_ttee.deriv.DAOD\_HIGG8D1.e5070\_e5984\_s3126\_r10201\_r10210\_p4133  
 mc16\_13TeV.410219.aMcAtNloPythia8EvtGen\_MEN30NLO\_A14N23LO\_ttmumu.deriv.DAOD\_HIGG8D1.e5070\_e5984\_s3126\_r10201\_r10210\_p4133  
 mc16\_13TeV.410220.aMcAtNloPythia8EvtGen\_MEN30NLO\_A14N23LO\_ttautau.deriv.DAOD\_HIGG8D1.e5070\_e5984\_s3126\_r10201\_r10210\_p4133  
 mc16\_13TeV.410276.aMcAtNloPythia8EvtGen\_MEN30NLO\_A14N23LO\_ttee\_mll\_1\_5.deriv.DAOD\_HIGG8D1.e6087\_e5984\_s3126\_r10201\_r10210\_p4133  
 mc16\_13TeV.410277.aMcAtNloPythia8EvtGen\_MEN30NLO\_A14N23LO\_ttmumu\_mll\_1\_5.deriv.DAOD\_HIGG8D1.e6087\_e5984\_s3126\_r10201\_r10210\_p4133  
 mc16\_13TeV.410278.aMcAtNloPythia8EvtGen\_MEN30NLO\_A14N23LO\_ttautau\_mll\_1\_5.deriv.DAOD\_HIGG8D1.e6087\_e5984\_s3126\_r10201\_r10210\_p4133  
 mc16\_13TeV.410397.MadGraphPythia8EvtGen\_ttbar\_wbee\_MEN30LO\_A14N23LO.deriv.DAOD\_HIGG8D1.e6086\_e5984\_s3126\_r10201\_r10210\_p4133  
 mc16\_13TeV.410398.MadGraphPythia8EvtGen\_ttbar\_wbmumu\_MEN30LO\_A14N23LO.deriv.DAOD\_HIGG8D1.e6086\_e5984\_s3126\_r10201\_r10210\_p4133  
 mc16\_13TeV.410399.MadGraphPythia8EvtGen\_ttbar\_wbtautau\_MEN30LO\_A14N23LO.deriv.DAOD\_HIGG8D1.e6086\_e5984\_s3126\_r10201\_r10210\_p4133  
 mc16\_13TeV.410658.PhPy8EG\_A14\_ttchan\_BW50\_lept\_top.deriv.DAOD\_HIGG8D1.e6671\_e5984\_s3126\_r10201\_r10210\_p4133  
 mc16\_13TeV.410659.PhPy8EG\_A14\_ttchan\_BW50\_lept\_antitop.deriv.DAOD\_HIGG8D1.e6671\_e5984\_s3126\_r10201\_r10210\_p4133  
 mc16\_13TeV.410644.PowhegPythia8EvtGen\_A14\_singletop\_schan\_lept\_top.deriv.DAOD\_HIGG8D1.e6527\_e5984\_s3126\_r10201\_r10210\_p4133  
 mc16\_13TeV.410645.PowhegPythia8EvtGen\_A14\_singletop\_schan\_lept\_antitop.deriv.DAOD\_HIGG8D1.e6527\_s3126\_r10201\_r10210\_p4133  
 mc16\_13TeV.304014.MadGraphPythia8EvtGen\_A14NNPDF23\_3top\_SM.deriv.DAOD\_HIGG8D1.e4324\_e5984\_s3126\_r10201\_r10210\_p4133  
 mc16\_13TeV.410080.MadGraphPythia8EvtGen\_A14NNPDF23\_4topSM.deriv.DAOD\_HIGG8D1.e4111\_e5984\_s3126\_r10201\_r10210\_p4133  
 mc16\_13TeV.410081.MadGraphPythia8EvtGen\_A14NNPDF23\_ttbarWW.deriv.DAOD\_HIGG8D1.e4111\_e5984\_s3126\_r10201\_r10210\_p4133  
 mc16\_13TeV.364100.Sherpa\_221\_NNPDF30NNLO\_Zmmumu\_MAXHTPTV0\_70\_CVetoBVeto.deriv.DAOD\_HIGG8D1.e5271\_s3126\_r10201\_r10210\_p4133  
 mc16\_13TeV.364101.Sherpa\_221\_NNPDF30NNLO\_Zmmumu\_MAXHTPTV0\_70\_CFilterBVeto.deriv.DAOD\_HIGG8D1.e5271\_s3126\_r10201\_r10210\_p4133  
 mc16\_13TeV.364101.Sherpa\_221\_NNPDF30NNLO\_Zmmumu\_MAXHTPTV0\_70\_CFilterBVeto.deriv.DAOD\_HIGG8D1.e5271\_e5984\_s3126\_r10201\_r10210\_p4133  
 mc16\_13TeV.364102.Sherpa\_221\_NNPDF30NNLO\_Zmmumu\_MAXHTPTV0\_70\_BFilter.deriv.DAOD\_HIGG8D1.e5271\_s3126\_r10201\_r10210\_p4133  
 mc16\_13TeV.364103.Sherpa\_221\_NNPDF30NNLO\_Zmmumu\_MAXHTPTV70\_140\_CVetoBVeto.deriv.DAOD\_HIGG8D1.e5271\_s3126\_r10201\_r10210\_p4133  
 mc16\_13TeV.364104.Sherpa\_221\_NNPDF30NNLO\_Zmmumu\_MAXHTPTV70\_140\_CFilterBVeto.deriv.DAOD\_HIGG8D1.e5271\_s3126\_r10201\_r10210\_p4133  
 mc16\_13TeV.364106.Sherpa\_221\_NNPDF30NNLO\_Zmmumu\_MAXHTPTV140\_280\_CVetoBVeto.deriv.DAOD\_HIGG8D1.e5271\_s3126\_r10201\_r10210\_p4133  
 mc16\_13TeV.364107.Sherpa\_221\_NNPDF30NNLO\_Zmmumu\_MAXHTPTV140\_280\_CFilterBVeto.deriv.DAOD\_HIGG8D1.e5271\_s3126\_r10201\_r10210\_p4133  
 mc16\_13TeV.364108.Sherpa\_221\_NNPDF30NNLO\_Zmmumu\_MAXHTPTV140\_280\_BFilter.deriv.DAOD\_HIGG8D1.e5271\_e5984\_s3126\_r10201\_r10210\_p4133  
 mc16\_13TeV.364108.Sherpa\_221\_NNPDF30NNLO\_Zmmumu\_MAXHTPTV140\_280\_BFilter.deriv.DAOD\_HIGG8D1.e5271\_s3126\_r10201\_r10210\_p4133  
 mc16\_13TeV.364109.Sherpa\_221\_NNPDF30NNLO\_Zmmumu\_MAXHTPTV280\_500\_CVetoBVeto.deriv.DAOD\_HIGG8D1.e5271\_e5984\_s3126\_r10201\_r10210\_p4133  
 mc16\_13TeV.364109.Sherpa\_221\_NNPDF30NNLO\_Zmmumu\_MAXHTPTV280\_500\_CFilterBVeto.deriv.DAOD\_HIGG8D1.e5271\_s3126\_r10201\_r10210\_p4133  
 mc16\_13TeV.364110.Sherpa\_221\_NNPDF30NNLO\_Zmmumu\_MAXHTPTV280\_500\_BFilter.deriv.DAOD\_HIGG8D1.e5271\_s3126\_r10201\_r10210\_p4133  
 mc16\_13TeV.364111.Sherpa\_221\_NNPDF30NNLO\_Zmmumu\_MAXHTPTV280\_500\_BFilter.deriv.DAOD\_HIGG8D1.e5271\_e5984\_s3126\_r10201\_r10210\_p4133





mc16\_13TeV.364192.Sherpa\_221\_NNPDF30NNLO\_Wtaunu\_MAXHTPTV140\_280\_BFilter.deriv.DAOD\_HIGG8D1.e5340\_e5984\_s3126\_r10201\_r10210\_p4133  
 mc16\_13TeV.364193.Sherpa\_221\_NNPDF30NNLO\_Wtaunu\_MAXHTPTV280\_500\_CVetoBVeto.deriv.DAOD\_HIGG8D1.e5340\_e5984\_s3126\_r10201\_r10210\_p4133  
 mc16\_13TeV.364193.Sherpa\_221\_NNPDF30NNLO\_Wtaunu\_MAXHTPTV280\_500\_CVetoBVeto.deriv.DAOD\_HIGG8D1.e5340\_e5984\_s3126\_s3136\_r10201\_r10210\_p4133  
 mc16\_13TeV.364194.Sherpa\_221\_NNPDF30NNLO\_Wtaunu\_MAXHTPTV280\_500\_CFilterBVeto.deriv.DAOD\_HIGG8D1.e5340\_e5984\_s3126\_r10201\_r10210\_p4133  
 mc16\_13TeV.364194.Sherpa\_221\_NNPDF30NNLO\_Wtaunu\_MAXHTPTV280\_500\_CFilterBVeto.deriv.DAOD\_HIGG8D1.e5340\_s3126\_r10201\_r10210\_p4133  
 mc16\_13TeV.364194.Sherpa\_221\_NNPDF30NNLO\_Wtaunu\_MAXHTPTV280\_500\_CFilterBVeto.deriv.DAOD\_HIGG8D1.e5340\_e5984\_s3126\_s3136\_r10201\_r10210\_p4133  
 mc16\_13TeV.364195.Sherpa\_221\_NNPDF30NNLO\_Wtaunu\_MAXHTPTV280\_500\_BFilter.deriv.DAOD\_HIGG8D1.e5340\_e5984\_s3126\_r10201\_r10210\_p4133  
 mc16\_13TeV.364195.Sherpa\_221\_NNPDF30NNLO\_Wtaunu\_MAXHTPTV280\_500\_BFilter.deriv.DAOD\_HIGG8D1.e5340\_s3126\_r10201\_r10210\_p4133  
 mc16\_13TeV.364196.Sherpa\_221\_NNPDF30NNLO\_Wtaunu\_MAXHTPTV500\_1000.deriv.DAOD\_HIGG8D1.e5340\_e5984\_s3126\_s3136\_r10201\_r10210\_p4133  
 mc16\_13TeV.364196.Sherpa\_221\_NNPDF30NNLO\_Wtaunu\_MAXHTPTV500\_1000.deriv.DAOD\_HIGG8D1.e5340\_s3126\_r10201\_r10210\_p4133  
 mc16\_13TeV.364197.Sherpa\_221\_NNPDF30NNLO\_Wtaunu\_MAXHTPTV1000\_E\_CMS.deriv.DAOD\_HIGG8D1.e5340\_e5984\_s3126\_r10201\_r10210\_p4133  
 mc16\_13TeV.364500.Sherpa\_222\_NNPDF30NNLO\_eegamma\_pty\_7\_15.deriv.DAOD\_HIGG8D1.e5928\_e5984\_s3126\_r10201\_r10210\_p4133  
 mc16\_13TeV.364501.Sherpa\_222\_NNPDF30NNLO\_eegamma\_pty\_15\_35.deriv.DAOD\_HIGG8D1.e5928\_e5984\_s3126\_r10201\_r10210\_p4133  
 mc16\_13TeV.364502.Sherpa\_222\_NNPDF30NNLO\_eegamma\_pty\_35\_70.deriv.DAOD\_HIGG8D1.e5928\_e5984\_s3126\_r10201\_r10210\_p4133  
 mc16\_13TeV.364503.Sherpa\_222\_NNPDF30NNLO\_eegamma\_pty\_70\_140.deriv.DAOD\_HIGG8D1.e5928\_e5984\_s3126\_r10201\_r10210\_p4133  
 mc16\_13TeV.364504.Sherpa\_222\_NNPDF30NNLO\_eegamma\_pty\_140\_E\_CMS.deriv.DAOD\_HIGG8D1.e5928\_e5984\_s3126\_r10201\_r10210\_p4133  
 mc16\_13TeV.364505.Sherpa\_222\_NNPDF30NNLO\_mumugamma\_pty\_7\_15.deriv.DAOD\_HIGG8D1.e5928\_e5984\_s3126\_r10201\_r10210\_p4133  
 mc16\_13TeV.364506.Sherpa\_222\_NNPDF30NNLO\_mumugamma\_pty\_15\_35.deriv.DAOD\_HIGG8D1.e5928\_e5984\_s3126\_r10201\_r10210\_p4133  
 mc16\_13TeV.364507.Sherpa\_222\_NNPDF30NNLO\_mumugamma\_pty\_35\_70.deriv.DAOD\_HIGG8D1.e5928\_e5984\_s3126\_r10201\_r10210\_p4133  
 mc16\_13TeV.364508.Sherpa\_222\_NNPDF30NNLO\_mumugamma\_pty\_70\_140.deriv.DAOD\_HIGG8D1.e5928\_e5984\_s3126\_r10201\_r10210\_p4133  
 mc16\_13TeV.364509.Sherpa\_222\_NNPDF30NNLO\_mumugamma\_pty\_140\_E\_CMS.deriv.DAOD\_HIGG8D1.e5928\_e5984\_s3126\_r10201\_r10210\_p4133  
 mc16\_13TeV.364510.Sherpa\_222\_NNPDF30NNLO\_tautaugamma\_pty\_7\_15.deriv.DAOD\_HIGG8D1.e5928\_e5984\_s3126\_r10201\_r10210\_p4133  
 mc16\_13TeV.364511.Sherpa\_222\_NNPDF30NNLO\_tautaugamma\_pty\_15\_35.deriv.DAOD\_HIGG8D1.e5928\_e5984\_s3126\_r10201\_r10210\_p4133  
 mc16\_13TeV.364512.Sherpa\_222\_NNPDF30NNLO\_tautaugamma\_pty\_35\_70.deriv.DAOD\_HIGG8D1.e5928\_e5984\_s3126\_r10201\_r10210\_p4133  
 mc16\_13TeV.364513.Sherpa\_222\_NNPDF30NNLO\_tautaugamma\_pty\_70\_140.deriv.DAOD\_HIGG8D1.e5928\_e5984\_s3126\_r10201\_r10210\_p4133  
 mc16\_13TeV.364513.Sherpa\_222\_NNPDF30NNLO\_tautaugamma\_pty\_70\_140.deriv.DAOD\_HIGG8D1.e5928\_e5984\_s3126\_r10201\_r10210\_p4133  
 mc16\_13TeV.364514.Sherpa\_222\_NNPDF30NNLO\_tautaugamma\_pty\_140\_E\_CMS.deriv.DAOD\_HIGG8D1.e5928\_e5984\_s3126\_r10201\_r10210\_p4133  
 mc16\_13TeV.364521.Sherpa\_222\_NNPDF30NNLO\_enugamma\_pty\_7\_15.deriv.DAOD\_HIGG8D1.e5928\_e5984\_s3126\_r10201\_r10210\_p4133  
 mc16\_13TeV.364522.Sherpa\_222\_NNPDF30NNLO\_enugamma\_pty\_15\_35.deriv.DAOD\_HIGG8D1.e5928\_e5984\_s3126\_r10201\_r10210\_p4133  
 mc16\_13TeV.364523.Sherpa\_222\_NNPDF30NNLO\_enugamma\_pty\_35\_70.deriv.DAOD\_HIGG8D1.e5928\_e5984\_s3126\_r10201\_r10210\_p4133  
 mc16\_13TeV.364524.Sherpa\_222\_NNPDF30NNLO\_enugamma\_pty\_70\_140.deriv.DAOD\_HIGG8D1.e5928\_e5984\_s3126\_r10201\_r10210\_p4133  
 mc16\_13TeV.364525.Sherpa\_222\_NNPDF30NNLO\_enugamma\_pty\_140\_E\_CMS.deriv.DAOD\_HIGG8D1.e5928\_e5984\_s3126\_r10201\_r10210\_p4133  
 mc16\_13TeV.364526.Sherpa\_222\_NNPDF30NNLO\_munugamma\_pty\_7\_15.deriv.DAOD\_HIGG8D1.e5928\_e5984\_s3126\_r10201\_r10210\_p4133  
 mc16\_13TeV.364527.Sherpa\_222\_NNPDF30NNLO\_munugamma\_pty\_15\_35.deriv.DAOD\_HIGG8D1.e5928\_e5984\_s3126\_r10201\_r10210\_p4133  
 mc16\_13TeV.364528.Sherpa\_222\_NNPDF30NNLO\_munugamma\_pty\_35\_70.deriv.DAOD\_HIGG8D1.e5928\_e5984\_s3126\_r10201\_r10210\_p4133  
 mc16\_13TeV.364529.Sherpa\_222\_NNPDF30NNLO\_munugamma\_pty\_70\_140.deriv.DAOD\_HIGG8D1.e5928\_e5984\_s3126\_r10201\_r10210\_p4133  
 mc16\_13TeV.364530.Sherpa\_222\_NNPDF30NNLO\_munugamma\_pty\_140\_E\_CMS.deriv.DAOD\_HIGG8D1.e5928\_e5984\_s3126\_r10201\_r10210\_p4133  
 mc16\_13TeV.364531.Sherpa\_222\_NNPDF30NNLO\_taunugamma\_pty\_7\_15.deriv.DAOD\_HIGG8D1.e5928\_e5984\_s3126\_r10201\_r10210\_p4133  
 mc16\_13TeV.364532.Sherpa\_222\_NNPDF30NNLO\_taunugamma\_pty\_15\_35.deriv.DAOD\_HIGG8D1.e5928\_e5984\_s3126\_r10201\_r10210\_p4133  
 mc16\_13TeV.364533.Sherpa\_222\_NNPDF30NNLO\_taunugamma\_pty\_35\_70.deriv.DAOD\_HIGG8D1.e5928\_e5984\_s3126\_r10201\_r10210\_p4133  
 mc16\_13TeV.364534.Sherpa\_222\_NNPDF30NNLO\_taunugamma\_pty\_70\_140.deriv.DAOD\_HIGG8D1.e5928\_e5984\_s3126\_r10201\_r10210\_p4133  
 mc16\_13TeV.364535.Sherpa\_222\_NNPDF30NNLO\_taunugamma\_pty\_140\_E\_CMS.deriv.DAOD\_HIGG8D1.e5928\_e5984\_s3126\_r10201\_r10210\_p4133  
 mc16\_13TeV.410560.MadGraphPythia8EvtGen\_A14\_Z\_4fl\_tchan\_noAllHad.deriv.DAOD\_HIGG8D1.e5803\_e5984\_s3126\_r10201\_r10210\_p4133  
 mc16\_13TeV.410013.PowhegPythiaEvtGen\_P2012\_Wt\_inclusive\_top.deriv.DAOD\_HIGG8D1.e3753\_s3126\_r10201\_r10210\_p4133  
 mc16\_13TeV.410014.PowhegPythiaEvtGen\_P2012\_Wt\_inclusive\_antitop.deriv.DAOD\_HIGG8D1.e3753\_s3126\_r10201\_r10210\_p4133  
 mc16\_13TeV.410408.aMcAtNloPythia8EvtGen\_tWZ\_Ztoll\_minDR1.deriv.DAOD\_HIGG8D1.e6423\_e5984\_s3126\_r10201\_r10210\_p4133  
 mc16\_13TeV.364242.Sherpa\_222\_NNPDF30NNLO\_WWW\_3l3v\_EW6.deriv.DAOD\_HIGG8D1.e5887\_e5984\_s3126\_r10201\_r10210\_p4133  
 mc16\_13TeV.364243.Sherpa\_222\_NNPDF30NNLO\_WWZ\_4l2v\_EW6.deriv.DAOD\_HIGG8D1.e5887\_e5984\_s3126\_r10201\_r10210\_p4133  
 mc16\_13TeV.364244.Sherpa\_222\_NNPDF30NNLO\_WWZ\_2l4v\_EW6.deriv.DAOD\_HIGG8D1.e5887\_e5984\_s3126\_r10201\_r10210\_p4133  
 mc16\_13TeV.364245.Sherpa\_222\_NNPDF30NNLO\_WZZ\_5l1v\_EW6.deriv.DAOD\_HIGG8D1.e5887\_e5984\_s3126\_r10201\_r10210\_p4133  
 mc16\_13TeV.364246.Sherpa\_222\_NNPDF30NNLO\_WZZ\_3l3v\_EW6.deriv.DAOD\_HIGG8D1.e5887\_e5984\_s3126\_r10201\_r10210\_p4133  
 mc16\_13TeV.364247.Sherpa\_222\_NNPDF30NNLO\_ZZZ\_6lv\_EW6.deriv.DAOD\_HIGG8D1.e5887\_e5984\_s3126\_r10201\_r10210\_p4133  
 mc16\_13TeV.364248.Sherpa\_222\_NNPDF30NNLO\_ZZZ\_4l2v\_EW6.deriv.DAOD\_HIGG8D1.e5887\_e5984\_s3126\_r10201\_r10210\_p4133  
 mc16\_13TeV.364249.Sherpa\_222\_NNPDF30NNLO\_ZZZ\_2l4v\_EW6.deriv.DAOD\_HIGG8D1.e5887\_e5984\_s3126\_r10201\_r10210\_p4133  
 mc16\_13TeV.342284.Pythia8EvtGen\_A14NNPDF23LO\_WH125\_inc.deriv.DAOD\_HIGG8D1.e4246\_e5984\_s3126\_r10201\_r10210\_p4133  
 mc16\_13TeV.342285.Pythia8EvtGen\_A14NNPDF23LO\_ZH125\_inc.deriv.DAOD\_HIGG8D1.e4246\_e5984\_s3126\_r10201\_r10210\_p4133  
 mc16\_13TeV.341998.aMcAtNloHppEG\_UEEE5\_CTEQ6L1\_CT10ME\_tWH125\_gamgam\_yt\_plus1.deriv.DAOD\_HIGG8D1.e4394\_e5984\_s3126\_r10201\_r10210\_p4133  
 mc16\_13TeV.410470.PhPy8EG\_A14\_ttbar\_hdamp258p75\_nonallhad.deriv.DAOD\_HIGG8D1.e6337\_e5984\_s3126\_r10201\_r10210\_p4133  
 mc16\_13TeV.410472.PhPy8EG\_A14\_ttbar\_hdamp258p75\_dil.deriv.DAOD\_HIGG8D1.e6348\_e5984\_s3126\_r10201\_r10210\_p4133  
 mc16\_13TeV.346343.PhPy8EG\_A14NNPDF23\_NNPDF30ME\_ttH125\_allhad.deriv.DAOD\_HIGG8D1.e7148\_e5984\_s3126\_r10201\_r10210\_p4133  
 mc16\_13TeV.346344.PhPy8EG\_A14NNPDF23\_NNPDF30ME\_ttH125\_semilep.deriv.DAOD\_HIGG8D1.e7148\_e5984\_a875\_r10201\_r10210\_p4133  
 mc16\_13TeV.346345.PhPy8EG\_A14NNPDF23\_NNPDF30ME\_ttH125\_dilep.deriv.DAOD\_HIGG8D1.e7148\_e5984\_a875\_r10201\_r10210\_p4133

mc16e:  
 mc16\_13TeV.361605.PowhegPy8EG\_CT10nloME\_AZNLOCTEQ6L1\_ZZvvvv\_mll4.deriv.DAOD\_HIGG8D1.e4054\_e5984\_s3126\_r10724\_r10726\_p4133  
 mc16\_13TeV.361602.PowhegPy8EG\_CT10nloME\_AZNLOCTEQ6L1\_WZlvvv\_mll4.deriv.DAOD\_HIGG8D1.e4054\_e5984\_s3126\_r10724\_r10726\_p4133  
 mc16\_13TeV.361601.PowhegPy8EG\_CT10nloME\_AZNLOCTEQ6L1\_WZlvvv\_mll4.deriv.DAOD\_HIGG8D1.e4475\_e5984\_s3126\_r10724\_r10726\_p4133  
 mc16\_13TeV.361600.PowhegPy8EG\_CT10nloME\_AZNLOCTEQ6L1\_WWlvlv.deriv.DAOD\_HIGG8D1.e4616\_e5984\_s3126\_r10724\_r10726\_p4133  
 mc16\_13TeV.361603.PowhegPy8EG\_CT10nloME\_AZNLOCTEQ6L1\_ZZlIII\_mll4.deriv.DAOD\_HIGG8D1.e4475\_e5984\_s3126\_r10724\_r10726\_p4133  
 mc16\_13TeV.361604.PowhegPy8EG\_CT10nloME\_AZNLOCTEQ6L1\_ZZvvll\_mll4.deriv.DAOD\_HIGG8D1.e4475\_e5984\_s3126\_r10724\_r10726\_p4133  
 mc16\_13TeV.364288.Sherpa\_222\_NNPDF30NNLO\_llll\_lowMIPtComplement.deriv.DAOD\_HIGG8D1.e6096\_s3126\_r10724\_p3983 mc16\_13TeV.364287.Sherpa\_222\_NNPDF30NNLO\_llll\_lowMIPtComplement.deriv.DAOD\_HIGG8D1.e6096\_s3126\_r10724\_p3983  
 mc16\_13TeV.364285.Sherpa\_222\_NNPDF30NNLO\_llvvjj\_EW6.deriv.DAOD\_HIGG8D1.e6055\_e5984\_s3126\_r10724\_r10726\_p3983  
 mc16\_13TeV.364284.Sherpa\_222\_NNPDF30NNLO\_llvvjj\_EW6.deriv.DAOD\_HIGG8D1.e6055\_s3126\_r10724\_p3983  
 mc16\_13TeV.364283.Sherpa\_222\_NNPDF30NNLO\_lllljj\_EW6.deriv.DAOD\_HIGG8D1.e6055\_s3126\_r10724\_p3983  
 mc16\_13TeV.364739.MGPy8EG\_NNPDF30NLO\_A14NNPDF23LO\_lvlljjEW6\_OFMinus.deriv.DAOD\_HIGG8D1.e7421\_e5984\_s3126\_r10724\_r10726\_p4133  
 mc16\_13TeV.364742.MGPy8EG\_NNPDF30NLO\_A14NNPDF23LO\_lvlljjEW6\_SFPlus.deriv.DAOD\_HIGG8D1.e7421\_e5984\_s3126\_r10724\_r10726\_p4133  
 mc16\_13TeV.364740.MGPy8EG\_NNPDF30NLO\_A14NNPDF23LO\_lvlljjEW6\_OFPlus.deriv.DAOD\_HIGG8D1.e7421\_e5984\_s3126\_r10724\_r10726\_p4133  
 mc16\_13TeV.364741.MGPy8EG\_NNPDF30NLO\_A14NNPDF23LO\_lvlljjEW6\_SFMinus.deriv.DAOD\_HIGG8D1.e7421\_e5984\_s3126\_r10724\_r10726\_p4133  
 mc16\_13TeV.364253.Sherpa\_222\_NNPDF30NNLO\_llll.deriv.DAOD\_HIGG8D1.e5916\_e5984\_s3126\_r10724\_r10726\_p4133  
 mc16\_13TeV.364250.Sherpa\_222\_NNPDF30NNLO\_llll.deriv.DAOD\_HIGG8D1.e5894\_e5984\_s3126\_r10724\_r10726\_p4133  
 mc16\_13TeV.364254.Sherpa\_222\_NNPDF30NNLO\_llvv.deriv.DAOD\_HIGG8D1.e5916\_e5984\_s3126\_r10724\_r10726\_p4133  
 mc16\_13TeV.364255.Sherpa\_222\_NNPDF30NNLO\_llvv.deriv.DAOD\_HIGG8D1.e5916\_e5984\_s3126\_r10724\_r10726\_p4133  
 mc16\_13TeV.410155.aMcAtNloPythia8EvtGen\_MEN30NLO\_A14N23LO\_ttW.deriv.DAOD\_HIGG8D1.e5070\_e5984\_s3126\_r10724\_r10726\_p4133  
 mc16\_13TeV.410156.aMcAtNloPythia8EvtGen\_MEN30NLO\_A14N23LO\_ttZnunu.deriv.DAOD\_HIGG8D1.e5070\_e5984\_s3126\_r10724\_r10726\_p4133  
 mc16\_13TeV.410157.aMcAtNloPythia8EvtGen\_MEN30NLO\_A14N23LO\_ttZqq.deriv.DAOD\_HIGG8D1.e5070\_e5984\_s3126\_r10724\_r10726\_p4133  
 mc16\_13TeV.410218.aMcAtNloPythia8EvtGen\_MEN30NLO\_A14N23LO\_ttee.deriv.DAOD\_HIGG8D1.e5070\_e5984\_s3126\_r10724\_r10726\_p4133  
 mc16\_13TeV.410219.aMcAtNloPythia8EvtGen\_MEN30NLO\_A14N23LO\_ttmumu.deriv.DAOD\_HIGG8D1.e5070\_e5984\_s3126\_r10724\_r10726\_p4133  
 mc16\_13TeV.410220.aMcAtNloPythia8EvtGen\_MEN30NLO\_A14N23LO\_ttautau.deriv.DAOD\_HIGG8D1.e5070\_e5984\_s3126\_r10724\_r10726\_p4133  
 mc16\_13TeV.410276.aMcAtNloPythia8EvtGen\_MEN30NLO\_A14N23LO\_ttee\_mll\_1\_5.deriv.DAOD\_HIGG8D1.e6087\_e5984\_s3126\_r10724\_r10726\_p4133  
 mc16\_13TeV.410277.aMcAtNloPythia8EvtGen\_MEN30NLO\_A14N23LO\_ttmumu\_mll\_1\_5.deriv.DAOD\_HIGG8D1.e6087\_e5984\_s3126\_r10724\_r10726\_p4133  
 mc16\_13TeV.410278.aMcAtNloPythia8EvtGen\_MEN30NLO\_A14N23LO\_ttautau\_mll\_1\_5.deriv.DAOD\_HIGG8D1.e6087\_e5984\_s3126\_r10724\_r10726\_p4133  
 mc16\_13TeV.410397.MadGraphPythia8EvtGen\_ttbar\_wbee\_MEN30LO\_A14N23LO.deriv.DAOD\_HIGG8D1.e6086\_e5984\_s3126\_r10724\_r10726\_p4133  
 mc16\_13TeV.410398.MadGraphPythia8EvtGen\_ttbar\_wbmumu\_MEN30LO\_A14N23LO.deriv.DAOD\_HIGG8D1.e6086\_e5984\_s3126\_r10724\_r10726\_p4133  
 mc16\_13TeV.410399.MadGraphPythia8EvtGen\_ttbar\_wbtautau\_MEN30LO\_A14N23LO.deriv.DAOD\_HIGG8D1.e6086\_e5984\_s3126\_r10724\_r10726\_p4133  
 mc16\_13TeV.410658.PhPy8EG\_A14\_tchan\_BW50\_lept\_top.deriv.DAOD\_HIGG8D1.e6671\_e5984\_s3126\_s3136\_r10724\_r10726\_p4133  
 mc16\_13TeV.410659.PhPy8EG\_A14\_tchan\_BW50\_lept\_antitop.deriv.DAOD\_HIGG8D1.e6671\_e5984\_s3126\_s3136\_r10724\_r10726\_p4133  
 mc16\_13TeV.410644.PowhegPythia8EvtGen\_A14\_singletop\_schan\_lept\_top.deriv.DAOD\_HIGG8D1.e6527\_e5984\_s3126\_r10724\_r10726\_p4133  
 mc16\_13TeV.410645.PowhegPythia8EvtGen\_A14\_singletop\_schan\_lept\_antitop.deriv.DAOD\_HIGG8D1.e6527\_e5984\_s3126\_r10724\_r10726\_p4133  
 mc16\_13TeV.304014.MadGraphPythia8EvtGen\_A14NNPDF23\_3top\_SM.deriv.DAOD\_HIGG8D1.e4324\_e5984\_s3126\_r10724\_r10726\_p4133  
 mc16\_13TeV.410080.MadGraphPythia8EvtGen\_A14NNPDF23\_4topSM.deriv.DAOD\_HIGG8D1.e4111\_e5984\_s3126\_r10724\_r10726\_p4133  
 mc16\_13TeV.410081.MadGraphPythia8EvtGen\_A14NNPDF23\_ttbarWW.deriv.DAOD\_HIGG8D1.e4111\_e5984\_s3126\_r10724\_r10726\_p4133  
 mc16\_13TeV.364100.Sherpa\_221\_NNPDF30NNLO\_Zmmumu\_MAXHTPTV0\_70\_CVetoBVeto.deriv.DAOD\_HIGG8D1.e5271\_e5984\_s3126\_s3136\_r10724\_r10726\_p4133  
 mc16\_13TeV.364100.Sherpa\_221\_NNPDF30NNLO\_Zmmumu\_MAXHTPTV0\_70\_CVetoBVeto.deriv.DAOD\_HIGG8D1.e5271\_e5984\_s3126\_r10724\_r10726\_p4133  
 mc16\_13TeV.364101.Sherpa\_221\_NNPDF30NNLO\_Zmmumu\_MAXHTPTV0\_70\_CFilterBVeto.deriv.DAOD\_HIGG8D1.e5271\_e5984\_s3126\_r10724\_r10726\_p4133  
 mc16\_13TeV.364102.Sherpa\_221\_NNPDF30NNLO\_Zmmumu\_MAXHTPTV0\_70\_BFilter.deriv.DAOD\_HIGG8D1.e5271\_e5984\_s3126\_s3136\_r10724\_r10726\_p4133  
 mc16\_13TeV.364102.Sherpa\_221\_NNPDF30NNLO\_Zmmumu\_MAXHTPTV0\_70\_BFilter.deriv.DAOD\_HIGG8D1.e5271\_e5984\_s3126\_r10724\_r10726\_p4133  
 mc16\_13TeV.364103.Sherpa\_221\_NNPDF30NNLO\_Zmmumu\_MAXHTPTV70\_140\_CVetoBVeto.deriv.DAOD\_HIGG8D1.e5271\_e5984\_s3126\_r10724\_r10726\_p4133  
 mc16\_13TeV.364103.Sherpa\_221\_NNPDF30NNLO\_Zmmumu\_MAXHTPTV70\_140\_CVetoBVeto.deriv.DAOD\_HIGG8D1.e5271\_e5984\_s3126\_s3136\_r10724\_r10726\_p4133  
 mc16\_13TeV.364104.Sherpa\_221\_NNPDF30NNLO\_Zmmumu\_MAXHTPTV70\_140\_CFilterBVeto.deriv.DAOD\_HIGG8D1.e5271\_e5984\_s3126\_r10724\_r10726\_p4133  
 mc16\_13TeV.364104.Sherpa\_221\_NNPDF30NNLO\_Zmmumu\_MAXHTPTV70\_140\_CFilterBVeto.deriv.DAOD\_HIGG8D1.e5271\_e5984\_s3126\_s3136\_r10724\_r10726\_p4133  
 mc16\_13TeV.364104.Sherpa\_221\_NNPDF30NNLO\_Zmmumu\_MAXHTPTV70\_140\_CFilterBVeto.deriv.DAOD\_HIGG8D1.e5271\_e5984\_s3126\_r10724\_r10726\_p4133  
 mc16\_13TeV.364106.Sherpa\_221\_NNPDF30NNLO\_Zmmumu\_MAXHTPTV140\_280\_CVetoBVeto.deriv.DAOD\_HIGG8D1.e5271\_e5984\_s3126\_s3136\_r10724\_r10726\_p4133  
 mc16\_13TeV.364106.Sherpa\_221\_NNPDF30NNLO\_Zmmumu\_MAXHTPTV140\_280\_CVetoBVeto.deriv.DAOD\_HIGG8D1.e5271\_e5984\_s3126\_r10724\_r10726\_p4133  
 mc16\_13TeV.364107.Sherpa\_221\_NNPDF30NNLO\_Zmmumu\_MAXHTPTV140\_280\_CFilterBVeto.deriv.DAOD\_HIGG8D1.e5271\_e5984\_s3126\_r10724\_r10726\_p4133  
 mc16\_13TeV.364107.Sherpa\_221\_NNPDF30NNLO\_Zmmumu\_MAXHTPTV140\_280\_CFilterBVeto.deriv.DAOD\_HIGG8D1.e5271\_e5984\_s3126\_s3136\_r10724\_r10726\_p4133  
 mc16\_13TeV.364108.Sherpa\_221\_NNPDF30NNLO\_Zmmumu\_MAXHTPTV140\_280\_CFilterBVeto.deriv.DAOD\_HIGG8D1.e5271\_e5984\_s3126\_r10724\_r10726\_p4133  
 mc16\_13TeV.364109.Sherpa\_221\_NNPDF30NNLO\_Zmmumu\_MAXHTPTV280\_500\_CVetoBVeto.deriv.DAOD\_HIGG8D1.e5271\_e5984\_s3126\_r10724\_r10726\_p4133  
 mc16\_13TeV.364110.Sherpa\_221\_NNPDF30NNLO\_Zmmumu\_MAXHTPTV280\_500\_CFilterBVeto.deriv.DAOD\_HIGG8D1.e5271\_e5984\_s3126\_r10724\_r10726\_p4133  
 mc16\_13TeV.364110.Sherpa\_221\_NNPDF30NNLO\_Zmmumu\_MAXHTPTV280\_500\_CFilterBVeto.deriv.DAOD\_HIGG8D1.e5271\_e5984\_s3126\_s3136\_r10724\_r10726\_p4133  
 mc16\_13TeV.364111.Sherpa\_221\_NNPDF30NNLO\_Zmmumu\_MAXHTPTV280\_500\_BFilter.deriv.DAOD\_HIGG8D1.e5271\_e5984\_s3126\_s3136\_r10724\_r10726\_p4133  
 mc16\_13TeV.364111.Sherpa\_221\_NNPDF30NNLO\_Zmmumu\_MAXHTPTV280\_500\_BFilter.deriv.DAOD\_HIGG8D1.e5271\_e5984\_s3126\_r10724\_r10726\_p4133  
 mc16\_13TeV.364112.Sherpa\_221\_NNPDF30NNLO\_Zmmumu\_MAXHTPTV500\_1000.deriv.DAOD\_HIGG8D1.e5271\_e5984\_s3126\_r10724\_r10726\_p4133  
 mc16\_13TeV.364113.Sherpa\_221\_NNPDF30NNLO\_Zmmumu\_MAXHTPTV1000\_E\_CMS.deriv.DAOD\_HIGG8D1.e5271\_e5984\_s3126\_r10724\_r10726\_p4133  
 mc16\_13TeV.364113.Sherpa\_221\_NNPDF30NNLO\_Zmmumu\_MAXHTPTV1000\_E\_CMS.deriv.DAOD\_HIGG8D1.e5271\_e5984\_s3126\_s3136\_r10724\_r10726\_p4133  
 mc16\_13TeV.364114.Sherpa\_221\_NNPDF30NNLO\_Zee\_MAXHTPTV0\_70\_CVetoBVeto.deriv.DAOD\_HIGG8D1.e5299\_e5984\_s3126\_s3136\_r10724\_r10726\_p4133





mc16\_13TeV.364196.Sherpa\_221\_NNPDF30NNLO\_Wtaunu\_MAXHTPTV500\_1000.deriv.DAOD\_HIGG8D1.e5340\_e5984\_s3126\_s3136\_r10724\_r10726\_p4133  
 mc16\_13TeV.364196.Sherpa\_221\_NNPDF30NNLO\_Wtaunu\_MAXHTPTV500\_1000.deriv.DAOD\_HIGG8D1.e5340\_e5984\_s3126\_r10724\_r10726\_p4133  
 mc16\_13TeV.364197.Sherpa\_221\_NNPDF30NNLO\_Wtaunu\_MAXHTPTV1000\_E\_CMS.deriv.DAOD\_HIGG8D1.e5340\_e5984\_s3126\_s3136\_r10724\_r10726\_p4133  
 mc16\_13TeV.364197.Sherpa\_221\_NNPDF30NNLO\_Wtaunu\_MAXHTPTV1000\_E\_CMS.deriv.DAOD\_HIGG8D1.e5340\_e5984\_s3126\_r10724\_r10726\_p4133  
 mc16\_13TeV.364500.Sherpa\_222\_NNPDF30NNLO\_eegamma\_pty\_7\_15.deriv.DAOD\_HIGG8D1.e5928\_e5984\_s3126\_r10724\_r10726\_p4133  
 mc16\_13TeV.364501.Sherpa\_222\_NNPDF30NNLO\_eegamma\_pty\_15\_35.deriv.DAOD\_HIGG8D1.e5928\_e5984\_s3126\_r10724\_r10726\_p4133  
 mc16\_13TeV.364502.Sherpa\_222\_NNPDF30NNLO\_eegamma\_pty\_35\_70.deriv.DAOD\_HIGG8D1.e5928\_e5984\_s3126\_r10724\_r10726\_p4133  
 mc16\_13TeV.364503.Sherpa\_222\_NNPDF30NNLO\_eegamma\_pty\_70\_140.deriv.DAOD\_HIGG8D1.e5928\_e5984\_s3126\_r10724\_r10726\_p4133  
 mc16\_13TeV.364504.Sherpa\_222\_NNPDF30NNLO\_eegamma\_pty\_140\_E\_CMS.deriv.DAOD\_HIGG8D1.e5928\_e5984\_s3126\_r10724\_r10726\_p4133  
 mc16\_13TeV.364505.Sherpa\_222\_NNPDF30NNLO\_mumugamma\_pty\_7\_15.deriv.DAOD\_HIGG8D1.e5928\_e5984\_s3126\_r10724\_r10726\_p4133  
 mc16\_13TeV.364506.Sherpa\_222\_NNPDF30NNLO\_mumugamma\_pty\_15\_35.deriv.DAOD\_HIGG8D1.e5928\_e5984\_s3126\_r10724\_r10726\_p4133  
 mc16\_13TeV.364507.Sherpa\_222\_NNPDF30NNLO\_mumugamma\_pty\_35\_70.deriv.DAOD\_HIGG8D1.e5928\_e5984\_s3126\_r10724\_r10726\_p4133  
 mc16\_13TeV.364508.Sherpa\_222\_NNPDF30NNLO\_mumugamma\_pty\_70\_140.deriv.DAOD\_HIGG8D1.e5928\_e5984\_s3126\_r10724\_r10726\_p4133  
 mc16\_13TeV.364509.Sherpa\_222\_NNPDF30NNLO\_mumugamma\_pty\_140\_E\_CMS.deriv.DAOD\_HIGG8D1.e5928\_e5984\_s3126\_r10724\_r10726\_p4133  
 mc16\_13TeV.364511.Sherpa\_222\_NNPDF30NNLO\_tautaugamma\_pty\_15\_35.deriv.DAOD\_HIGG8D1.e5928\_e5984\_s3126\_r10724\_r10726\_p4133  
 mc16\_13TeV.364512.Sherpa\_222\_NNPDF30NNLO\_tautaugamma\_pty\_35\_70.deriv.DAOD\_HIGG8D1.e5928\_e5984\_s3126\_r10724\_r10726\_p4133  
 mc16\_13TeV.364513.Sherpa\_222\_NNPDF30NNLO\_tautaugamma\_pty\_70\_140.deriv.DAOD\_HIGG8D1.e5928\_e5984\_s3126\_r10724\_r10726\_p4133  
 mc16\_13TeV.364514.Sherpa\_222\_NNPDF30NNLO\_tautaugamma\_pty\_140\_E\_CMS.deriv.DAOD\_HIGG8D1.e5928\_e5984\_s3126\_r10724\_r10726\_p4133  
 mc16\_13TeV.364522.Sherpa\_222\_NNPDF30NNLO\_enugamma\_pty\_15\_35.deriv.DAOD\_HIGG8D1.e5928\_e5984\_s3126\_r10724\_r10726\_p4133  
 mc16\_13TeV.364523.Sherpa\_222\_NNPDF30NNLO\_enugamma\_pty\_35\_70.deriv.DAOD\_HIGG8D1.e5928\_e5984\_s3126\_r10724\_r10726\_p4133  
 mc16\_13TeV.364524.Sherpa\_222\_NNPDF30NNLO\_enugamma\_pty\_70\_140.deriv.DAOD\_HIGG8D1.e5928\_e5984\_s3126\_r10724\_r10726\_p4133  
 mc16\_13TeV.364525.Sherpa\_222\_NNPDF30NNLO\_enugamma\_pty\_140\_E\_CMS.deriv.DAOD\_HIGG8D1.e5928\_e5984\_s3126\_r10724\_r10726\_p4133  
 mc16\_13TeV.364527.Sherpa\_222\_NNPDF30NNLO\_munugamma\_pty\_15\_35.deriv.DAOD\_HIGG8D1.e5928\_e5984\_s3126\_r10724\_r10726\_p4133  
 mc16\_13TeV.364528.Sherpa\_222\_NNPDF30NNLO\_munugamma\_pty\_35\_70.deriv.DAOD\_HIGG8D1.e5928\_e5984\_s3126\_r10724\_r10726\_p4133  
 mc16\_13TeV.364529.Sherpa\_222\_NNPDF30NNLO\_munugamma\_pty\_70\_140.deriv.DAOD\_HIGG8D1.e5928\_e5984\_s3126\_r10724\_r10726\_p4133  
 mc16\_13TeV.364530.Sherpa\_222\_NNPDF30NNLO\_munugamma\_pty\_140\_E\_CMS.deriv.DAOD\_HIGG8D1.e5928\_e5984\_s3126\_r10724\_r10726\_p4133  
 mc16\_13TeV.364532.Sherpa\_222\_NNPDF30NNLO\_taunugamma\_pty\_15\_35.deriv.DAOD\_HIGG8D1.e5928\_e5984\_s3126\_r10724\_r10726\_p4133  
 mc16\_13TeV.364533.Sherpa\_222\_NNPDF30NNLO\_taunugamma\_pty\_35\_70.deriv.DAOD\_HIGG8D1.e5928\_e5984\_s3126\_r10724\_r10726\_p4133  
 mc16\_13TeV.364534.Sherpa\_222\_NNPDF30NNLO\_taunugamma\_pty\_70\_140.deriv.DAOD\_HIGG8D1.e5928\_e5984\_s3126\_r10724\_r10726\_p4133  
 mc16\_13TeV.364535.Sherpa\_222\_NNPDF30NNLO\_taunugamma\_pty\_140\_E\_CMS.deriv.DAOD\_HIGG8D1.e5928\_e5984\_s3126\_r10724\_r10726\_p4133  
 mc16\_13TeV.410560.MadGraphPythia8EvtGen\_A14\_iZ\_4fl\_tchan\_noAllHad.deriv.DAOD\_HIGG8D1.e5803\_e5984\_s3126\_r10724\_r10726\_p4133  
 mc16\_13TeV.410408.aMcAtNloPythia8EvtGen\_tWZ\_Ztoll\_minDR1.deriv.DAOD\_HIGG8D1.e6423\_e5984\_s3126\_r10724\_r10726\_p4133  
 mc16\_13TeV.364242.Sherpa\_222\_NNPDF30NNLO\_WWW\_3l3v\_EW6.deriv.DAOD\_HIGG8D1.e5887\_e5984\_s3126\_r10724\_r10726\_p4133  
 mc16\_13TeV.364243.Sherpa\_222\_NNPDF30NNLO\_WWZ\_4l2v\_EW6.deriv.DAOD\_HIGG8D1.e5887\_e5984\_s3126\_r10724\_r10726\_p4133  
 mc16\_13TeV.364244.Sherpa\_222\_NNPDF30NNLO\_WWZ\_2l4v\_EW6.deriv.DAOD\_HIGG8D1.e5887\_e5984\_s3126\_r10724\_r10726\_p4133  
 mc16\_13TeV.364245.Sherpa\_222\_NNPDF30NNLO\_WZZ\_5l1v\_EW6.deriv.DAOD\_HIGG8D1.e5887\_e5984\_s3126\_r10724\_r10726\_p4133  
 mc16\_13TeV.364246.Sherpa\_222\_NNPDF30NNLO\_WZZ\_3l3v\_EW6.deriv.DAOD\_HIGG8D1.e5887\_e5984\_s3126\_r10724\_r10726\_p4133  
 mc16\_13TeV.364247.Sherpa\_222\_NNPDF30NNLO\_ZZZ\_6l0v\_EW6.deriv.DAOD\_HIGG8D1.e5887\_e5984\_s3126\_r10724\_r10726\_p4133  
 mc16\_13TeV.364248.Sherpa\_222\_NNPDF30NNLO\_ZZZ\_4l2v\_EW6.deriv.DAOD\_HIGG8D1.e5887\_e5984\_s3126\_r10724\_r10726\_p4133  
 mc16\_13TeV.364249.Sherpa\_222\_NNPDF30NNLO\_ZZZ\_2l4v\_EW6.deriv.DAOD\_HIGG8D1.e5887\_e5984\_s3126\_r10724\_r10726\_p4133  
 mc16\_13TeV.342284.Pythia8EvtGen\_A14NNPDF23LO\_WH125\_inc.deriv.DAOD\_HIGG8D1.e4246\_e5984\_s3126\_r10724\_r10726\_p4133  
 mc16\_13TeV.342285.Pythia8EvtGen\_A14NNPDF23LO\_ZH125\_inc.deriv.DAOD\_HIGG8D1.e4246\_e5984\_s3126\_r10724\_r10726\_p4133  
 mc16\_13TeV.341998.aMcAtNloHppEG\_UEEEES\_CTEQ6L1\_CT10ME\_iWH125\_gamgam\_yt\_plus1.deriv.DAOD\_HIGG8D1.e4394\_e5984\_s3126\_r10724\_r10726\_p4133  
 mc16\_13TeV.410389.MadGraphPythia8EvtGen\_A14NNPDF23\_ttgamma\_nonallhadronic.deriv.DAOD\_HIGG8D1.e6155\_e5984\_s3126\_r10724\_r10726\_p4133  
 mc16\_13TeV.410470.PhPy8EG\_A14\_ttbar\_hdamp258p75\_nonallhad.deriv.DAOD\_HIGG8D1.e6337\_e5984\_s3126\_r10724\_r10726\_p4133  
 mc16\_13TeV.410472.PhPy8EG\_A14\_ttbar\_hdamp258p75\_dil.deriv.DAOD\_HIGG8D1.e6348\_e5984\_s3126\_r10724\_r10726\_p4133  
 mc16\_13TeV.346343.PhPy8EG\_A14NNPDF23\_NNPDF30ME\_ttH125\_allhad.deriv.DAOD\_HIGG8D1.e7148\_e5984\_s3126\_r10724\_r10726\_p4133  
 mc16\_13TeV.346343.PhPy8EG\_A14NNPDF23\_NNPDF30ME\_ttH125\_allhad.deriv.DAOD\_HIGG8D1.e7148\_e5984\_a875\_r10724\_r10726\_p4133  
 mc16\_13TeV.346344.PhPy8EG\_A14NNPDF23\_NNPDF30ME\_ttH125\_semilep.deriv.DAOD\_HIGG8D1.e7148\_e5984\_a875\_r10724\_r10726\_p4133  
 mc16\_13TeV.346344.PhPy8EG\_A14NNPDF23\_NNPDF30ME\_ttH125\_semilep.deriv.DAOD\_HIGG8D1.e7148\_e5984\_s3126\_r10724\_r10726\_p4133  
 mc16\_13TeV.346345.PhPy8EG\_A14NNPDF23\_NNPDF30ME\_ttH125\_dilep.deriv.DAOD\_HIGG8D1.e7148\_e5984\_a875\_r10724\_r10726\_p4133  
 mc16\_13TeV.346345.PhPy8EG\_A14NNPDF23\_NNPDF30ME\_ttH125\_dilep.deriv.DAOD\_HIGG8D1.e7148\_e5984\_s3126\_r10724\_r10726\_p4133